

TRIBOLOGICAL STUDIES  
OF  
ION-IMPLANTED STEEL CONSTITUENTS

Ronghua Wei  
Department of Mechanical Engineering

In partial fulfillment of the requirements  
for the Degree of Doctor of Philosophy  
Colorado State University  
Fort Collins, Colorado  
Summer, 1990




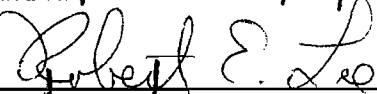
COLORADO STATE UNIVERSITY

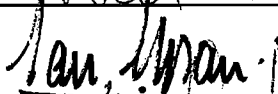
April 2, 1990

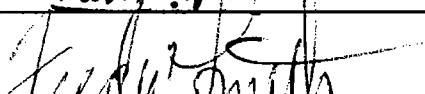
WE HEREBY RECOMMEND THAT THE DISSERTATION PREPARED UNDER OUR SUPERVISION BY RONGHUA WEI ENTITLED TRIBOLOGICAL STUDIES OF ION IMPLANTED STEEL CONSTITUENTS BE ACCEPTED AS FULFILLING IN PART REQUIREMENTS FOR THE DEGREE OF DOCTOR OF PHILOSOPHY.

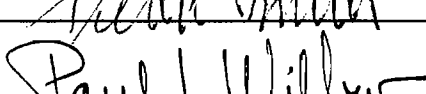
Committee on Graduate Work

  
\_\_\_\_\_

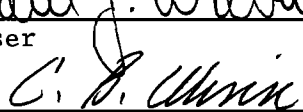
  
\_\_\_\_\_

  
\_\_\_\_\_

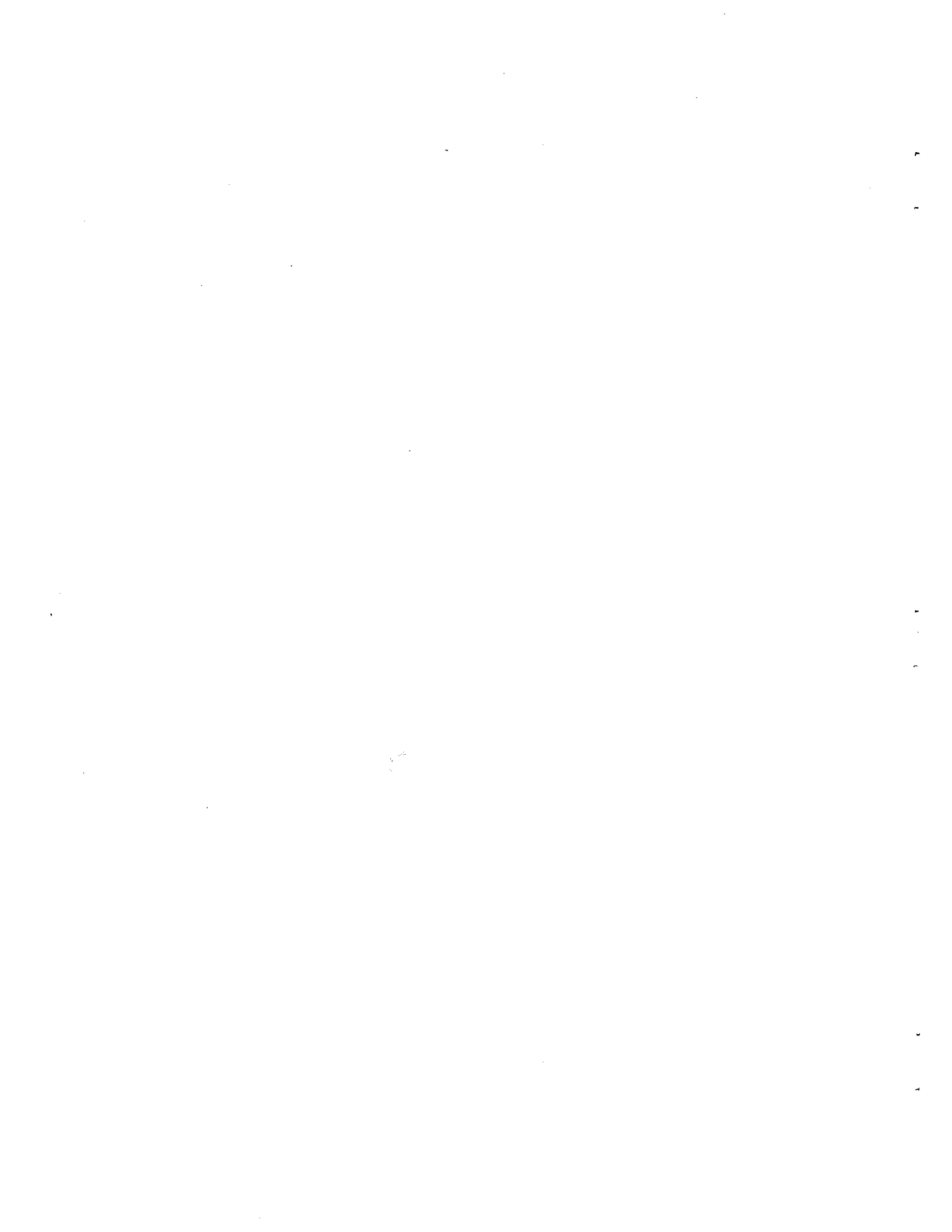
  
\_\_\_\_\_

  
\_\_\_\_\_

Adviser

  
\_\_\_\_\_

Department Head



## ABSTRACT OF DISSERTATION

### TRIBOLOGICAL STUDIES OF ION-IMPLANTED STEEL CONSTITUENTS

Tribological properties of ion-implanted ferrite and austenite were studied systematically using a unique oscillating pin-on-disc wear tester. The results show that nitrogen implantation at elevated temperatures to high doses dramatically improves the adhesive wear resistance of ferrite and the critical load at which the adhesive wear mechanism changes from mild to severe for austenite. The wear resistance of nitrogen-implanted ferrite is determined by the nitride formed. Ranked from most to least wear resistant the nitrides observed are  $\gamma'$ -Fe<sub>4</sub>N,  $\epsilon$ -Fe<sub>3</sub>N and  $\zeta$ -Fe<sub>2</sub>N. Extremely hard solid solutions of nitrogen develop on the implanted austenite surfaces and induce three orders of magnitude reductions in wear rates. The implantation conditions that should be used to produce deep, wear resistant layers for both steels are discussed in detail. Oscillating pin-on-disc wear tests demonstrate that nitrogen does not diffuse during the wearing process although tests conducted using conventional fixed pin-on-disc test equipment could erroneously suggest this occurs. Taken together, the results show that high dose rate implantation at low energies yields very high quality implanted surfaces at low cost.

Ronghua Wei  
Department of Mechanical Engineering  
Colorado State University  
Fort Collins, CO 80523  
Spring 1990

## ACKNOWLEDGMENTS

I gratefully acknowledge the contributions of my advisor, Dr. Paul J. Wilbur. Without his patience, help and instruction, the dissertation could not have been accomplished.

Special thanks are also given to the professors on my committee, Dr. F. W. Smith, Dr. I. L. Spain, Dr. R. E. Lee and Dr. W. S. Sampath, for the stimulating discussions and instruction they provided.

I express my thanks to my colleagues, John Anderson, Jeff Monheiser, John Williams and Verlin Friedly for technical and emotional support during the preparation of this dissertation.

Dr. D. L. Williamson and Ms. Li Wang of Colorado School of Mines, Golden, Colorado, Drs. G. Lux and I. Ivonov of Charles Evans and Associates, California, are also acknowledged for performing the Mössbauer spectroscopic, X-ray diffraction and Auger electron spectroscopic data used for stimulating discussions.

The National Science Foundation is also acknowledged for supporting of this work financially.

I am grateful for the support by my parents, my wife and my son. Without their encouragement and sacrifice, completing this dissertation would have been impossible.

## TABLE OF CONTENTS

<u>Title</u>	<u>Page</u>
INTRODUCTION.....	1
APPARATUS AND PROCEDURES.....	6
Ion Implantation.....	6
Sample Selection, Preparation and Wear Test.....	9
Mössbauer Spectroscopic and other Measurement Techniques....	14
RESULTS AND DISCUSSION - PURE IRON.....	18
Brief Summary.....	18
Overview.....	18
General Observations regarding Mössbauer and X-ray Diffraction Analyses.....	19
Mössbauer and X-ray Diffraction Analyses of Ferrite.....	20
Typical Distribution of Implanted Nitrogen in Ferrite.....	22
Wear Testing of Ferrite Discs.....	29
The Effects of Temperature and Dose on the Wear resistance.....	33
Morphological Studies on Ferrite.....	40
Comparison of Oscillating and Fixed Pin-on-Disc Wear Test.....	44
Wear Debris Study.....	51
Microhardness Testing of Ferrite Discs.....	54
RESULTS AND DISCUSSION - STAINLESS STEELS.....	59
Brief Summary.....	59
Overview.....	60
Nitrogen Concentration Profiles.....	61
Mössbauer and XRD Analyses.....	63
Oscillating Pin-on-Disc Wear Testing.....	68
Fixed Pin-on-Disc Tests.....	79
Frictional Effects.....	80
Microhardness Measurements.....	84
CONCLUSION.....	87
REFERENCES.....	89

## LIST OF FIGURES

<u>Figure No.</u>	<u>Title</u>	<u>Page</u>
1	Ion Implantation System Schematic.....	8
2	Oscillating Pin-on-Disc Sliding Wear Test Apparatus Schematic.....	11
3	Back Scatter Mössbauer Spectroscopy Schematic.....	16
4	Typical Conversion Electron Mössbauer Spectra of Ion-Implanted $\alpha$ -Fe Showing Various Nitrides as Indicted by Stick Diagrams.....	21
5	Typical Auger Profiles of Nitrogen Implanted $\alpha$ -Fe Discs.....	23
6a	AES Depth Profiles Showing the Effect of Temperature on the Nitrogen Distribution in Pure Iron ( $100 \mu\text{A}/\text{cm}^2$ ).....	26
6b	AES Depth Profiles Showing the Effect of Temperature on the Nitrogen Distribution in Pure Iron ( $750 \mu\text{A}/\text{cm}^2$ ).....	27
7	Typical Wear Histories of Pure Iron Discs.....	31
8	The Effect of Implantation Temperature on the Wear Resistance of $\alpha$ -Fe.....	35
9	The Effect of Implanted Nitrogen Dose on Wear Resistance of $\alpha$ -Fe.....	36
10	Correlation of Disc Mass Loss and Iron Nitride Fraction in a Nitrogen-Implanted Layer.....	39
11	Comparative Optical Micrographs of Unimplanted and Implanted Regions on a $\alpha$ -Fe Disc After a 5 h Wear Test.....	41
12	Scanning Electron Micrograph and Surface Roughness Histories During Oscillating Pin-on-Disc Wear Tests.....	42
12	(cont.) Scanning Electron Micrograph and Surface Roughness Histories During Oscillating Pin-on-Disc Wear Tests.....	43
13	Comparative Fixed Pin-on-Disc and Oscillating Pin-on-Disc Wear Test Results for $\alpha$ -Fe.....	45



**LIST OF FIGURES (continue)**

<u>Figure No.</u>	<u>Title</u>	<u>Page</u>
14	Typical Scanning Electron Micrographs of a Wear Groove in Nitrogen Implanted Iron.....	49
15	Scanning Electron Micrographs of Typical Wear Debris.....	52
15	(cont.) Scanning Electron Micrographs of Typical Wear Debris..	53
16	The Effect of Indenter Load on the Vickers Hardness of Ion Implanted $\alpha$ -Fe.....	56
17	The Effect of Indenter Load on the Vickers Hardness of Sputter-Coated Iron Nitride on $\alpha$ -Fe.....	57
18	Typical AES Profiles of Nitrogen Implanted 304 SS Discs.....	62
19	Typical Conversion Electron Mössbauer Spectra of Nitrogen-Implanted 304 Stainless Steel, (a)-(c).....	66
19	(cont.) Typical Conversion Electron Mössbauer Spectra of Nitrogen-Implanted 304 Stainless Steel, (d)-(f).....	67
20	Typical Sliding Wear Histories of Stainless Steel at 1 N Normal Load.....	69
21	Effect of Normal Load on Disc Mass Loss Rate (a) and Roughness (b).....	71
22	Effect of Normal Load on the Surface Morphology of an Unimplanted 304 Stainless Steel Disc (a) and Pin (b) Pair.....	72
23	Effect of Normal Load on the Surface Morphology of a Nitrogen-Implanted 304 Stainless Steel Disc (a) and Pin (b) Pair.....	73
24	Effects of Implanted Nitrogen Dose and Implantation Temperature on the Critical Loads for 304 Stainless Steel.....	77
25	Effect of Normal Load on Disc Mass Loss Rate - Fixed Pin Test.....	81
26	Effects of Normal Load, Pin Material and Lubrication on Friction Coefficient - Fixed Pin Test.....	82
27	Effects of Ion Implantation on the Microhardness for 304 Stainless Steel.....	85

## LIST OF TABLES

<u>Table No.</u>	<u>Title</u>	<u>Page</u>
1	The Composition of the Materials Used in this Study.....	9
2	Wear Test Parameters.....	12
3	Microstructural Data for 60 keV Nitrogen-Implanted Pure Iron Samples.....	24
4	Implantation Conditions for Pure $\alpha$ -Fe Discs.....	29
5	Results of Energy Dispersive X <sub>2</sub> ray Analysis of a Nitrogen Implanted Disc ( $4 \times 10^{17}$ N <sub>2</sub> /cm <sup>2</sup> ) after 3 hr of Wear Testing.....	50
6	Critical Loads for Stainless Steel Discs.....	76

## INTRODUCTION

Ion implantation is a process in which positively charged ions, produced in an ion source, are accelerated to a high speed and directed onto a solid substrate. After transferring their energy both elastically to the nuclei of the substrate atoms and inelastically to the electrons surrounding them, the ions eventually come to rest. In the course of slowing down by hitting substrate nuclei, the ions cause cascade collisions that generally disrupt the substrate structure and produce a variety of substrate defects (e.g. vacancies). The implanted element may form compounds with the substrate material and/or enter into a solid solution. As a consequence, the implanted layer generally differs both chemically and mechanically from the bulk material beneath it. Because the process can induce such changes, it is also called ion implantation metallurgy [1,2].

Although it is used most widely in the semiconductor industry, ion implantation has also come into use in the areas of material science and tribology over the last two decades [3-7]. Wear, the major tribological event, causes enormous waste in both industrial and personal life and any process that could reduce wear could have a great beneficial impact on the world economy. It has been shown that ion implantation can induce great improvements in a wide range of surface properties, including those related to wear, in a variety of materials [8-20]. Among these, steels are probably of greatest interest [21-82]. It has

been shown that ion implantation of light elements such as B, C and N, as well as heavier elements such as Ti, Sn, and Cr, into a variety of steel constituents (ferrite, austenite and martensite) can improve properties related to their wear resistance, friction coefficient, microhardness, fatigue life and corrosion resistance [21-25,32-41,48-58,64-75,80-82].

Compared to other surface modification techniques that induce improved wear performance (e.g. coatings or diffusion-processed surfaces), conventional ion implantation has been shown to have the following relative advantages:

1. Any element or combination of elements can be implanted into any solid base material. Since ion implantation is a non-equilibrium process, new alloys, which cannot be obtained in conventional ways, can be formed.
2. The ballistic range of implanted ions (and therefore the treated layer thickness) can be controlled readily by controlling the implantation energy, a parameter that can be adjusted readily over a substantial range in some implanters.
3. Ion implantation does not induce measurable changes in the dimensions, appearance or surface finish of a finished product. This can be important because cost savings are generally realized when a product can be finish machined in its softened state and then surface hardened.
4. Ion implantation need not induce changes in the properties of the bulk (subsurface) material because its temperature can be controlled independently. Consequently, implantation processing

enables one to avoid the use of more costly alloys, and still make a product with a high toughness and a hard surface.

5. Ion implanted layers do not have the adhesion problems induced by differential thermal expansion and/or interfacial corrosion that are typically associated with coatings, because the treated layer is integral with the base material rather than a coating.

Like any technique, however, ion implantation has short comings that limit its potential usefulness. In its early state of development, these short comings have been reflections of the following:

1. The ballistic range of implanted ions at typical implantation energies (~100 keV) is small and consequently implanted layers have been shallow (~ 0.1  $\mu\text{m}$  in typical materials). Shallow implanted layers limit the industrial acceptance of the technology because long lifetimes (deep implanted layers) are generally needed. Deeper implanted layers could be produced using higher energy (MeV level) implanters, but these units are much more costly and the task of heat removal from the product become more difficult when they are used.
2. The current density of most implanters, which were generally developed for the implantation of semiconductors, has typically been low ( $\leq 10 \mu\text{A}/\text{cm}^2$ ) and the area of the implantation zone on a surface has generally been small ( $\leq$  several square millimeters). In order to produce substantial tribological benefits in steels, both the ion doses that had to be delivered and the areas over which they had to be supplied, had to be increased to levels orders of magnitude greater than those associated with semiconductor implantation. As a result,

processing times have been long and costs have been high and the technique has not been applied widely.

3. Ion implantation has been a line-of-sight process. This means that products having interior surfaces are either difficult or in some situations impossible to implant.

This study identifies implantation procedures and process controls that facilitate rapid processing and the production of nitrogen-bearing layers that extend much deeper than the ballistic range of the implanted nitrogen. It was conducted using high current density equipment capable of delivering large ion doses rapidly over relatively large surfaces at low cost. While the difficulty associated with delivering doses to internal surfaces is not addressed here, it is noted that Conrad [83] has developed equipment and procedures that mitigate this problem.

Nitrogen ions have been used widely to change the tribological surface properties of steels because they are relatively easy to implant and they induce improved wear resistance. A variety of nitrides have been observed in nitrogen implanted steels [26,27,36,43,44,53,60-62,69,75-77], but which nitride should be sought in order to produce the most wear-resistant surface has not been identified. The question of how thick an implanted layer must be in order to produce a sufficiently wear-resistant surface also remains unanswered. In fact it has been claimed that a very thin (order 0.1  $\mu\text{m}$ ) implanted layer is adequate because nitrides formed in steels during implantation dissolve or dissociate and enable nitrogen diffusion deeper into a surface during the wearing process [55,56,71,72]. Hence, it has been argued that the beneficial effects of implantation persist long after a layer having the thickness of the implanted layer has been worn away. On the other hand,

others have claimed on the basis of their experiments that this tribo-enhanced diffusion process does not occur [49,50,57,65].

An objective of the work described herein is to obtain a better understanding of the physical mechanisms that control the thickness and wear resistant characteristics of nitrogen-implanted layers in two microstructural constituents of steels. Previous researchers working on this problem have used various steels selected because of their commercial usefulness. Unfortunately, these steels are compositionally complicated and it has been difficult to obtain basic understanding from the associated test results. In this work, only simple materials are used, namely, ferrite (pure  $\alpha$ -Fe) and austenite (AISI 304 and 310 stainless steels). It is argued that the results obtained using these simple microstructures will provide unequivocal evidence of the detailed mechanisms involved and that this understanding will eventually enable the prediction of the effects of implantation in the more complex and commercially more attractive steels. Although nitrogen is the primary implantant used in this work, some surfaces implanted with argon will also be examined to provide points of comparison.

## APPARATUS AND PROCEDURES

### Ion Implantation

The ion implanter used in this study has been designed specifically for the high dose level treatment that is required on mechanically active surfaces. The ion source used in the implanter is based on space-based ion thruster technology and it has ion beam current density and energy capabilities that range from 10 to 1500  $\mu\text{A}/\text{cm}^2$  and 10 to 80 keV, respectively. The diameter of the beam spot over which substantial implantation occurs on a target surface can be adjusted. For this work it was maintained at  $\sim 10$  cm and the current density was uniform to within 10% over a 5 cm diameter. A schematic diagram of the complete ion implantation system is shown in Fig. 1. As this figure suggests, the gas to be implanted (nitrogen or argon in this study) and electrical power are fed into a cylindrical chamber. Through a process of electron bombardment, these gaseous atoms are ionized and supplied to the optics subsystem where a steady stream of the positive ions produced are accelerated to a high kinetic energy (60 keV for this study). The highly collimated ion beam extracted through the optics subsystem is directed toward the target (sample) surface to be implanted. A portion of this beam is intercepted by the mask shown in Fig. 1 so only the sample will be implanted and unnecessary heating of the target-holding fixture by the high power beam will be minimized. In this study, all samples were implanted at an energy of 60 keV and current densities of



100, 500 and 750  $\mu\text{A}/\text{cm}^2$ . At these relatively high current densities, the samples could be processed very rapidly, thereby demonstrating the attractiveness of this implanter technology for low cost processing. Detailed descriptions of the implanter and its capabilities can be found elsewhere [84,85].

The high heat-capacity, copper fixture shown attached to the sample in Fig. 1 is designed so it can be cooled using either water or liquid nitrogen. It, therefore, serves as a sink into which the heat transported to the sample by the ion beam can be drawn. Since the temperature history of a steel can influence its tribological properties greatly, care was exercised to control the temperature on each sample being implanted. This was accomplished by monitoring its temperature using the thermocouple shown in Fig. 1 and then adjusting the mean input beam power to hold it in proper balance with the rate of heat removal to the fixture on which the sample was mounted. Gross temperature control in the desired range was achieved by installing a film with the proper thermal impedance between the sample and the water (or liquid nitrogen)-cooled fixture on which it was mounted. Initial heating of the sample was accomplished by aligning the mask shown in Fig. 1 so the beam would strike the sample. When its temperature, as sensed by the thermocouple, reached an upper limit; the mask was moved to interrupt the beam. The sample temperature was then allowed to drop until a low temperature set point was reached. The mask aperture was then aligned to again direct the beam onto the sample. This process of aperture positioning to achieve fine temperature control continued until the desired dose had been delivered. For these tests the temperature was generally controlled within  $\pm 50$  ( $\pm 25$  in some cases)  $^{\circ}\text{C}$  of the desired temperature

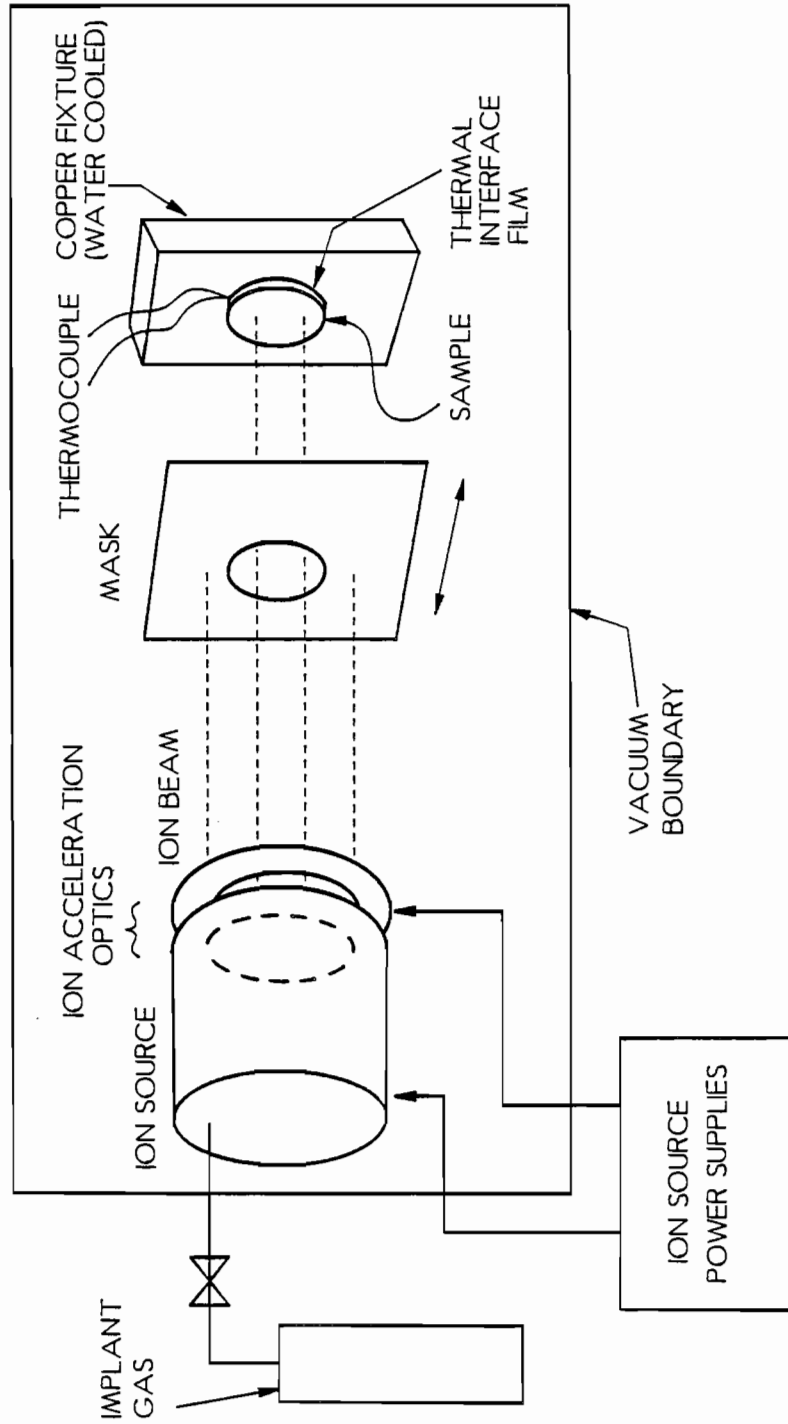


Fig. 1 Ion Implantation System Schematic

set point. In some cases where high sample temperatures were sought, the beam was directed onto the sample continuously until the desired dose had been implanted. In these cases only the final temperature (without a temperature range) will be cited.

### **Sample Selection, Preparation and Wear Testing**

In order to understand the basic phenomena that influence the quality of implanted layers produced on steels, two steel constituents having relatively simple microstructures were selected for study: ferrite (pure iron) and austenite (AISI type 304 stainless steel). Commercial quality AISI 304 stainless steel (SS) was used because it is a widely-used engineering material. Yang et al. and others [86-88] have pointed out, however, that this alloy is relatively unstable, a fact that is readily verified by the strain-induced transformation from austenite to martensite that occurs on the surfaces of samples being prepared (polished) for wear testing. In order to demonstrate that this transformation did not overwhelm the effects induced by ion implantation, some tests were also performed on a more stable austenitic stainless steel (AISI 310). The compositions of these three materials are listed in Table 1.

Because understanding the implantation conditions that would produce a wear-resistant surface was a goal of this work, non-destructive characterization of the tribological surfaces prior to and after implantation and prior to and during wear testing was required. This was accomplished in part using the back scatter Mössbauer spectroscopic technique known as conversion electron Mössbauer spectroscopy (CEMS) [89]. Since this technique requires a large sample

area ( $1-2 \text{ cm}^2$ ), a unique pin-on-disc wear tester, that can generate large ( $4.4 \text{ cm o.d. by } 2.1 \text{ cm i.d.}$ ), uniformly worn, flat surfaces was developed. The concept by which the wear tester operates is illustrated in Fig. 2. It involves simultaneous disc rotation at constant speed and radially inward and outward translation of a pin forced against the disc by a normal load  $F$ . Because the pin is moved in and then out at a

Table 1

The Composition of the Materials Used in this Study

Classification	Designation	Composition (wt%)
Ferrite	Fe	99.999% purity
Austenite	AISI type-304 SS	18-20 Cr, 8-10 Ni, 0.08 C, 2.0 Mn 1.0 Si, 0.045 P, 0.03 S, 0.1 N
Austenite	AISI type-310 SS	20-25 Cr, 18-20 Ni, 0.25 C, 2.0 Mn 1.5 S, 0.045 P, 0.03 S

constant radial speed and because the direction of pin motion is reversed essentially instantaneously, a uniformly worn region generally develops on the disc after it has been worn over a large number of disc revolutions. The frequency associated with the pin motion is small compared to the rotational frequency of the disc so the relative motion of the pin on the disc is essentially circumferential and therefore similar to the relative motion associated with a conventional (fixed pin-on-disc) tester.

The normal loads  $F$  and the frequencies of disc rotation and pin translation were selected at the values given in Table 2. For the disc dimensions used in these tests, the disc rotation frequency resulted in

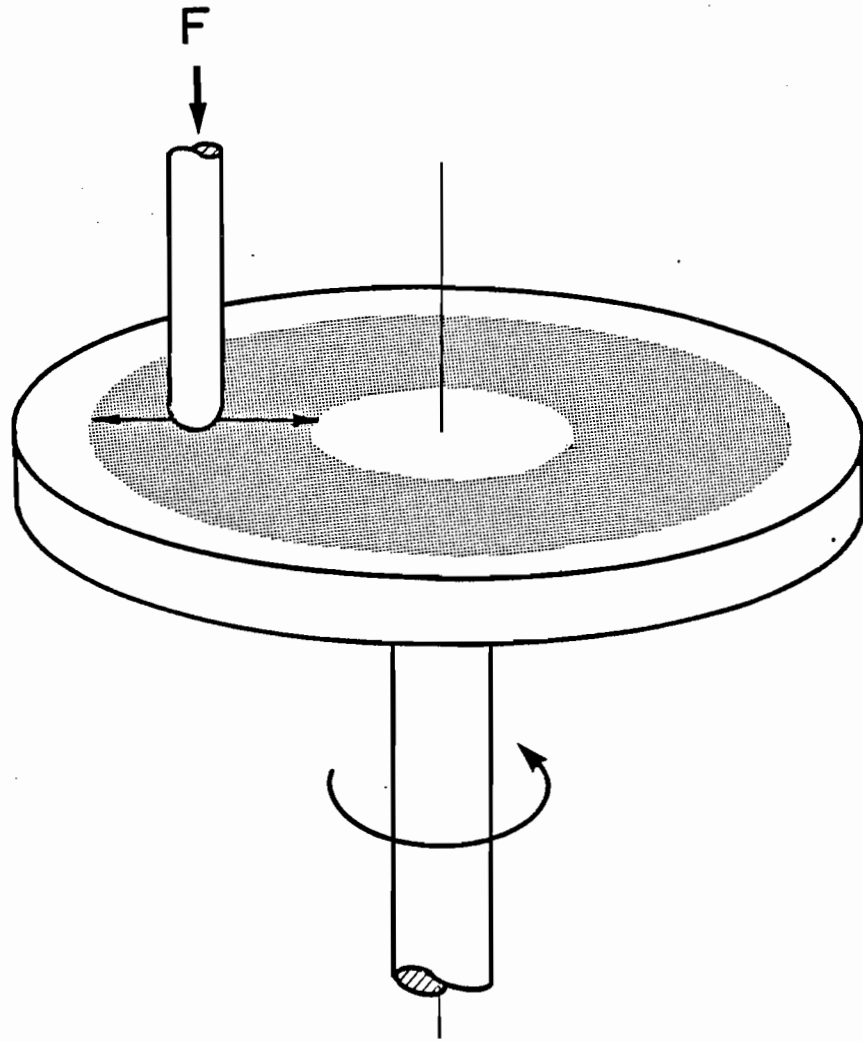


Fig. 2 Oscillating Pin-on-Disc Sliding Wear Test Apparatus Schematic

a relative sliding velocity between the pin and disc that varied between 9 and 18 cm/sec and had a mean value of 13 cm/s. This relatively low sliding velocity and the 5 N normal load were selected to produce a mild adhesive wear condition on the pure iron surfaces [90-93]. The normal load used on the SS samples was varied to determine the load that induced a transition from mild to severe adhesive wear.

Table 2  
Wear Test Parameters

Disc	Pin	Normal Load	Pin Translation Frequency	Disc Rotation Frequency
Pure Fe	Pure Fe	5 N	0.2 Hz	1.3 Hz
304 and 310 SS	304 SS or WC	Various	0.2 Hz	1.3 Hz

As suggested in Table 2, pure Fe and 304 SS pins were worn against the pure Fe and the 304 and 310 SS discs, respectively, to ensure the mild adhesive wear state that is typical of normal machine wear, but tungsten carbide (WC) pins were also used in some tests to minimize effects related to pin wear and the associated increase in pin contact area. All of the pins (except the WC ones) and discs used in the study were in an initial annealed state. The pins were cylindrical with a hemispherical contact surface (3.2 mm radius of curvature). The 5.0 cm dia by 0.18 cm thick discs, which were clamped to the rotating table of the test machine when they were being worn, could be removed periodically for measurement purposes and then reinstalled to be worn more. The normal Hertzian contact stresses achieved during wear testing

were initially 1.1 GPa in a ferrite disc and up to 4 GPa in a stainless steel one, but they dropped to a fraction of these values as the wear proceeded and the pin head flattened. The wear tester elements are sufficiently rigid to prevent undesirable deflection and vibration problems from developing. The pins and discs are also sufficiently small so wear rates determined from periodic disc mass loss measurements assure adequate accuracy (i.e. the  $\pm 11 \mu\text{g}$  accuracy achieved in disc mass loss measurements corresponding to a removed layer mean thickness [ $\pm 1.3 \text{ nm}$ ] is small compared to the implanted layer thickness [about 100 nm]).

The arm which supports the pin in the wear tester shown in Fig. 2 can also be held rigid and when this is done the apparatus operates as a conventional pin-on-disc wear tester. With the unit operating in this conventional way, the frictional force acting on the pin can be measured, but it cannot be measured accurately when the unit is operating in the oscillating pin mode.

The surface of each disc was prepared for implantation and/or wear testing by polishing it through 0.3  $\mu\text{m}$  grit to produce a mean roughness (i.e. mean amplitude of surface oscillations) that was less than 0.01  $\mu\text{m}$ . The hemispherical surfaces of the iron and SS pins were formed using a special tool before they were polished to a similar finish. After these elements had been cleaned and weighed, the disc was generally implanted and then wear tested against an unimplanted pin. Pins were not implanted because their contact surface areas changed as they wore. An implanted surface would have worn through the initial contact point quickly and the fraction of the wearing surfaces that bore nitrogen would have changed during the testing process. Changes in the

disc surface roughness induced by implantation were found to be insignificant.

During wear testing a mixture of 10 percent oleic acid in kerosene was supplied at a sufficiently high rate at the pin/disc interface so wear debris was flushed away from the wear zone and through a filter system as soon as it emerged from the contact region. Oleic acid (the highest molecular weight mono-unsaturated fatty acid that is liquid in the room temperature environment where the tests were conducted) was selected because it is a good boundary lubricant and it was mixed with kerosene to make it easier to pump and filter. The friction coefficient measured using this lubricant with pure iron pins and discs in the fixed pin-on-disc test configuration was  $0.13 \pm 0.01$  and that for stainless steels that had not undergone a transition to severe adhesive wear was 0.1-0.2. These friction coefficients are in good agreement with those measured by Shephard and Suh [90] and by Kiek, et al. [93] and they are considered indicative of mild adhesive wear.

### **Mössbauer Spectroscopic and other Measurement Techniques**

Measurement techniques used in support of the wear tests include optical and scanning electron microscopy (SEM) to determine surface morphologies of both the pin and disc surfaces and of the wear debris; profilometry to determine surface finish (and in the case of fixed pin wear tests, wear groove contours); depth profiling Auger electron spectroscopy (AES) to determine implanted ion concentrations as a function of depth; energy dispersive X-ray spectroscopy (EDS) using a KeVex Quantum detector that can detect X-rays from elements as low in atomic number as carbon to determine the surface concentrations of



implanted and impurity species on the pins, discs and wear debris; microhardness measurements to determine the hardness of the implanted layer and conversion electron Mössbauer spectroscopy (CEMS), conversion X-ray Mössbauer spectroscopy (CXMS) and X-Ray diffraction (XRD) to determine the relative concentrations and approximate depths of the nitride phases formed.

The Mössbauer spectroscopic technique [76,89,94-97] is a particularly appealing one for this study because it enables a researcher to measure mean concentrations of the implanted ions that are bonded to iron and to infer their bonding condition vis a vis the bulk material without introducing surface damage. The mechanism by which this is accomplished can be understood with the aid of Fig. 3. Here a specimen of interest (the disc used for wear testing in the present case) is exposed to a beam of 14.4 keV  $\gamma$ -rays from a moving source of excited  $^{57}\text{Fe}$  atoms. These  $\gamma$ -rays are resonantly absorbed by the  $^{57}\text{Fe}$  nuclei in the disc and in the subsequent spontaneous decay, electrons and X-rays are ejected from the  $^{57}\text{Fe}$  atom by the internal conversion process. This process results in the ejection of a 7.3 keV K-shell electron and either a second 5.6 keV L-shell electron or a 6.4 keV X-ray. Because the  $\gamma$ -ray resonance cross section is high only over a very narrow energy range and because the energy at which this peak occurs is affected by the bonding of the  $^{57}\text{Fe}$  atom to its nearest neighbors,  $^{57}\text{Fe}$  bonded in different ways yield electrons and X-rays at slightly different energies of the incident  $\gamma$ -ray. As a result, slight Doppler velocity-induced changes in the incident  $\gamma$ -ray energy make it possible to generate unique Mössbauer spectra associated with either the electrons or X-rays emitted by the atoms that depend on these bonding

# BACK SCATTER MÖSSBAUER SPECTROSCOPY

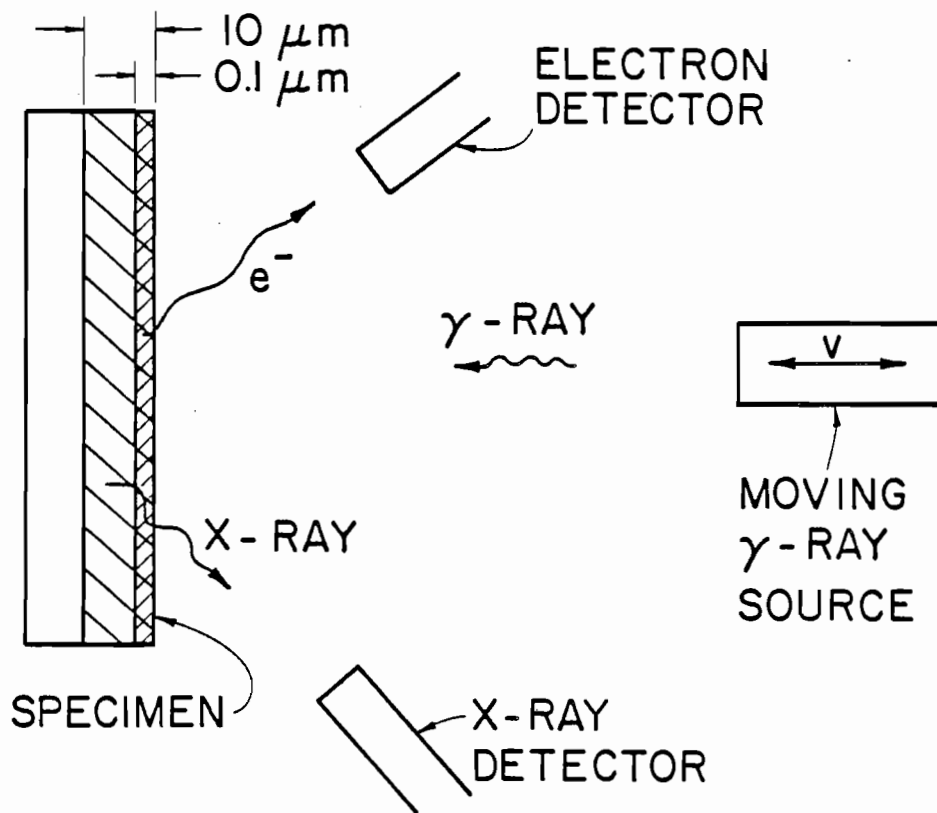


Fig. 3 Back Scatter Mössbauer Spectroscopy Schematic

arrangements. It is particularly important to note for the purposes of this study that the Mössbauer electron mean free paths are such that most can escape from the sample only if they are produced within about  $0.1 \mu\text{m}$  of the surface. Because typical implanted layers are also about  $0.1 \mu\text{m}$  deep, Mössbauer electrons produce signatures that describe the implanted layer. X-ray spectra, on the other hand, tend to describe the bulk material composition because they can escape through the surface from the depth of about  $10 \mu\text{m}$ .

## RESULTS AND DISCUSSION - PURE IRON

### Brief Summary

Wear tests of ferrite (pure  $\alpha$ -Fe) implanted with nitrogen were carried out on the oscillating pin-on-disc test machine. The results show that nitrogen implantation at elevated temperatures to high doses dramatically improves the adhesive wear resistance of ferrite. The wear resistance of nitrogen implanted ferrite is determined by the nitride formed. Ranked from most to least wear resistant the nitrides observed are  $\gamma'$ -Fe<sub>4</sub>N,  $\epsilon$ -Fe<sub>x</sub>N (where  $x \approx 3$ ), and  $\zeta$ -Fe<sub>2</sub>N. No evidence of nitride break-up and attendant nitrogen migration during wear testing is found. Nitrogen does diffuse into ferrite rapidly when it is implanted at an elevated temperature and this enhances its wear resistance.

### Overview

Ion implantation has been used to improve such steel properties as wear, fatigue and corrosion resistances, but it has been believed that these beneficial effects would not last long because treated layers have generally been thin (e.g. nitrogen implanted at 100 keV into steel was concentrated within 0.1  $\mu$ m of the surface). In order to increase the implanted layer depth and make the process more appealing for industrial applications, MeV implanters can be used [40] but they are expensive.

This work focuses on improving the durability of nitrogen-implanted surfaces by processing to high dose levels at moderate energies, high

current densities and elevated temperatures. Such processing can produce relatively thick implanted layers rapidly and inexpensively. Specific studies investigate 1) which steel-constituent nitrides are most wear resistant, 2) the extent to which nitrogen can be induced to migrate during implantation at elevated temperatures and dose levels and 3) the extent to which the beneficial effect of implantation persists after an implanted layer has been worn away. While the ultimate objective of the work will be to investigate these phenomena for the various constituents of steels (ferrite and austenite), this part of the dissertation will describe the results obtained with ferrite only. The oscillating pin-on-rotating disc wear tester will be shown to be better suited to the testing of implanted layers than conventional pin-on-disc machines. Finally, it will be shown that deep implantation of nitrogen can be realized using a low energy implanter provided the temperature of the surface being implanted is controlled in the proper range.

#### **General Observations Regarding Mössbauer and X-ray Diffraction Analyses**

Mössbauer spectroscopic and X-ray diffraction measurements were used in this study to determine the nitrogen bonding/microstructural features of the various implanted layers. These analyses are non-intrusive and they were conducted before and after implantation and periodically during wear testing. They, therefore, enable one to track the formation and transformation of nitrides and other phases after implantation and throughout the wearing process. Thus, they facilitate identification of preferred phases and the implantation conditions that encourage their production. Once a particular nitride or nitrogen-containing phase is formed during implantation, however, it has been

found to remain unchanged until it is removed as wear debris [82,96]. Hence the data presented here will be only those measured after implantation and prior to wear testing.

### Mössbauer and X-ray Diffraction Analyses of Ferrite

Figure 4 shows typical examples of CEMS plots for nitrogen-implanted ferrite. Each plot includes measured data points together with curves representing the subspectra required to obtain a good fit to the data points. Stick diagrams shown above each plot define the peaks associated with each subspectrum. The subspectra can be compared with those of known materials for identification. The stick diagrams for the upper plot suggest that both  $\alpha$ -Fe and orthorhombic iron nitride ( $\zeta$ -Fe<sub>2</sub>N) are present. The  $\alpha$ -Fe signal is present for all samples because  $\alpha$ -Fe is found both beneath the implanted layer and mixed with the nitrogen containing phases in the implantation-modified layer. The other plots in Fig. 4 show the spectra for hexagonal  $\epsilon$ -Fe<sub>x</sub>N ( $x \approx 3$ ) and face-centered-cubic (fcc)  $\gamma'$ -Fe<sub>4</sub>N. In some cases, a mixture of the nitrides is found in the implanted layer, but one nitride generally dominates. Knowledge of which nitride is formed under certain implantation conditions (dose and temperature in this study) is important because each nitride has been observed to exhibit different wear characteristics. By using CEMS and XRD the fractions of the various constituents can be determined and approximate layer thicknesses can be estimated under certain assumptions. Additional details concerning the procedures used to obtain quantitative information about the nitrogen that is bonded or in solid solution through Mössbauer and x-ray diffraction analyses are given elsewhere [96,97].

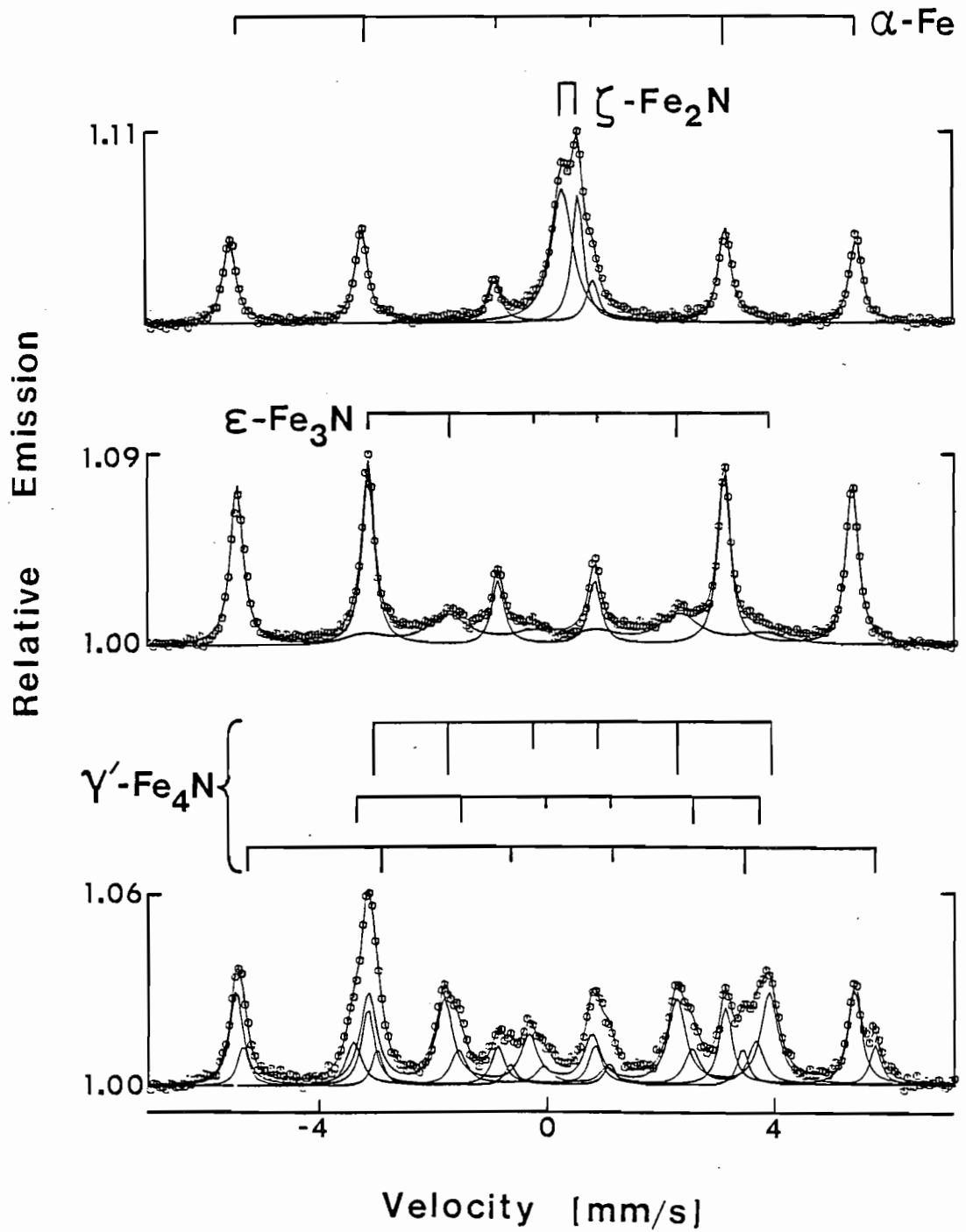


Fig. 4 Typical Conversion Electron Mössbauer Spectra of Ion-Implanted  $\alpha$ -Fe Showing Various Nitrides as Indicted by Stick Diagrams

### Typical Distribution of Implanted Nitrogen in Ferrite

AES data showing nitrogen concentration profiles in typical nitrogen-implanted iron discs prior to wear testing are shown in Fig. 5. These data indicate that 60 keV nitrogen ions (principally molecular ions- $N_2^+$ ) implanted to a dose of  $1 \times 10^{17} N_2/cm^2$  at low temperature (90 °C) tend to be concentrated in a layer that is less than 100 nm thick. In fact, most samples implanted below about 300 °C show the same profile, an near-gaussian distribution with the peak concentration around 30 percent. As the temperature increases to  $380 \pm 50$  °C nitrogen goes much deeper and the peak concentration drops to about 15 - 20 at.%. The deeper nitrogen penetration indicates the substrate temperature was elevated to the point where significant diffusion occurred. Increasing the temperature further to  $430 \pm 50$  °C seems not to induce deeper nitrogen diffusion, but it does induce lower nitrogen concentrations that suggest a loss of nitrogen possibly as a result of diffusion through the free surface. In fact, further increases in the temperature cause the nitrogen concentration to decrease until it approaches zero in a disc implanted at 600 °C. Data corresponding to the disc implanted to high dose ( $1 \times 10^{18} N_2/cm^2$ ) at the intermediate temperature (260 °C) is particularly noteworthy. They show that implantation to a dose an order of magnitude higher than that for the others does not induce significantly deeper penetration of the nitrogen. This suggests that high dose implantation at this temperature does not facilitate nitrogen diffusion. Rather, most of the implanted nitrogen is lost from the surface layer in which it is bound through the sputter-erosion mechanism. As a result of this process, the final nitrogen profile has a relatively broad peak like those observed by Terwagne et al. [99] but



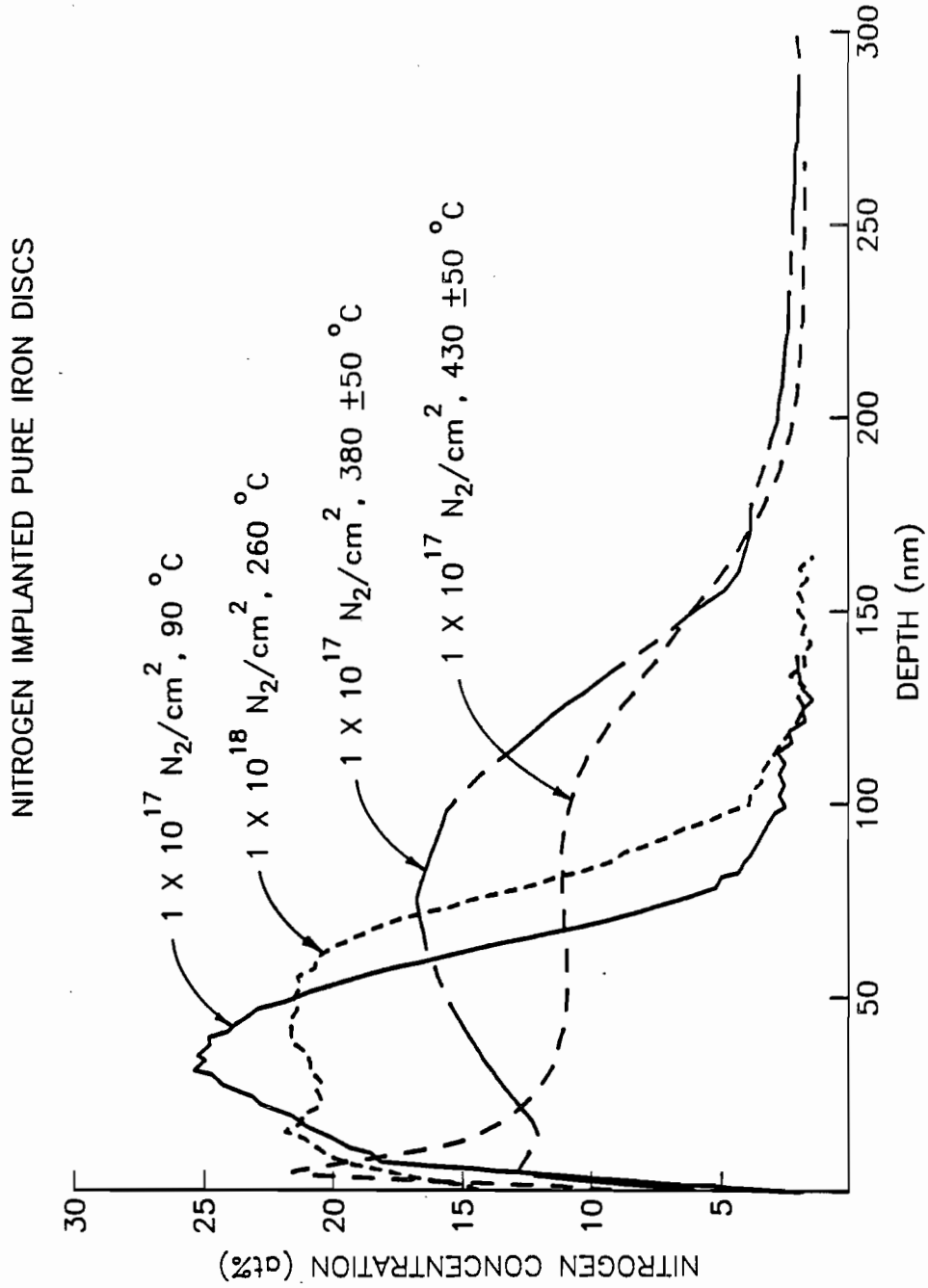


Fig. 5 Typical Auger Profiles of Nitrogen Implanted  $\alpha$ -Fe Discs

it is otherwise similar to the profiles observed at low doses. It is believed that both deep penetration and high retention of nitrogen are preferable for long wear lifetime. These results are important, therefore, because they suggest there is an implantation temperature at which nitrogen penetration and retention will be optimal.

A systematic study of the effects of temperature realized during implantation, dose rate and dose on the concentration profile and bonding state of nitrogen implanted into a series of pure iron samples was conducted. Table 3 identifies the dominant nitrides present after implantation as determined by CEMS and XRD at these different temperature, dose and dose rate conditions.

Table 3

## Microstructural Data for 60 keV Nitrogen-Implanted Pure Iron Samples

Sample No.	Implantation Conditions			Dominant Nitride(s)
	Dose Rate ( $\mu\text{A}/\text{cm}^2$ )	Dose ( $\times 10^{17} \text{N}_2/\text{cm}^2$ )	Temperature ( $^{\circ}\text{C}$ )	
1	100	0.25	50	$\alpha'$ -martensite
2	100	0.5	65	$\alpha'$ -martensite
3	100	1	80	$\epsilon$ -Fe <sub>x</sub> N (2.5<x<3.2)
4	100	1	200	$\epsilon$ -Fe <sub>x</sub> N (x $\approx$ 3)
5	100	4	100	$\zeta$ -Fe <sub>2</sub> N
6	100	4	$\approx$ 400	$\gamma'$ -Fe <sub>4</sub> N
7	750	1	$\approx$ 250	$\epsilon$ -Fe <sub>x</sub> N (2.02<x<2.5)
8	750	4	280	$\zeta$ -Fe <sub>2</sub> N
9	750	0.5	$\approx$ 400	$\gamma'$ -Fe <sub>2</sub> N
10	750	1	570	$\gamma'$ -Fe <sub>4</sub> N

Figure 6 shows subsurface profiles of nitrogen concentration (determined by AES) associated with these same pure iron samples. The samples for Fig. 6a were all implanted at the lower dose rate

( $100 \mu\text{A}/\text{cm}^2$  - Sample Nos. 1 thru 6) while those for Fig. 6b were implanted at the higher dose rate ( $750 \mu\text{A}/\text{cm}^2$  - Sample Nos. 7 thru 10). The dominant phases formed during implantation are also indicated for each profile.

The following observations regarding the data of Table 3 and Fig. 6 are offered:

1. Implantation to a low dose ( $\leq 5 \times 10^{16} \text{ N}_2/\text{cm}^2$ ) at a low temperature ( $\leq 65 \text{ }^\circ\text{C}$ ) [Sample Nos. 1 and 2 in Fig. 6a] induces the formation of  $\alpha'$ -phase iron (martensite containing nitrogen in solid solution) to a depth of  $\sim 100 \text{ nm}^*$ .
2. At higher doses ( $1 \times 10^{17} \text{ N}_2/\text{cm}^2$ ) and low temperatures ( $\leq 250 \text{ }^\circ\text{C}$ ), concentration levels increase, the depth of nitrogen penetration does not change significantly and the  $\epsilon\text{-Fe}_x\text{N}$  (hexagonal) phase is formed [Sample Nos. 3 and 4 in Fig. 6a and No. 7 in Fig. 6b].
3. At still higher doses ( $4 \times 10^{17} \text{ N}_2/\text{cm}^2$ ) and low to intermediate temperatures ( $100\text{-}280 \text{ }^\circ\text{C}$ ), concentrations increase until they reach a limit of  $\sim 35 \text{ at.}\%$ , substantial increases in the depth of nitrogen migration begin to be observed and the structure changes to the  $\zeta\text{-Fe}_2\text{N}$  (orthorhombic) phase [sample No. 5 in Fig. 6a and No. 8 in Fig. 6b]. When the temperature is increased to  $\sim 400 \text{ }^\circ\text{C}$  at the same dose ( $4 \times 10^{17} \text{ N}_2/\text{cm}^2$ ) the peak concentration drops to about  $20 \text{ at.}\%$ , the implantation depth

\*The concentration profile associated with Sample No. 2 is suggestive of substantial nitrogen migration. This result is inconsistent with all other results obtained in the study and is considered to be incorrect. It is considered likely that depth associated with each data point from Sample No. 2 is half of the value given in Fig. 6a.

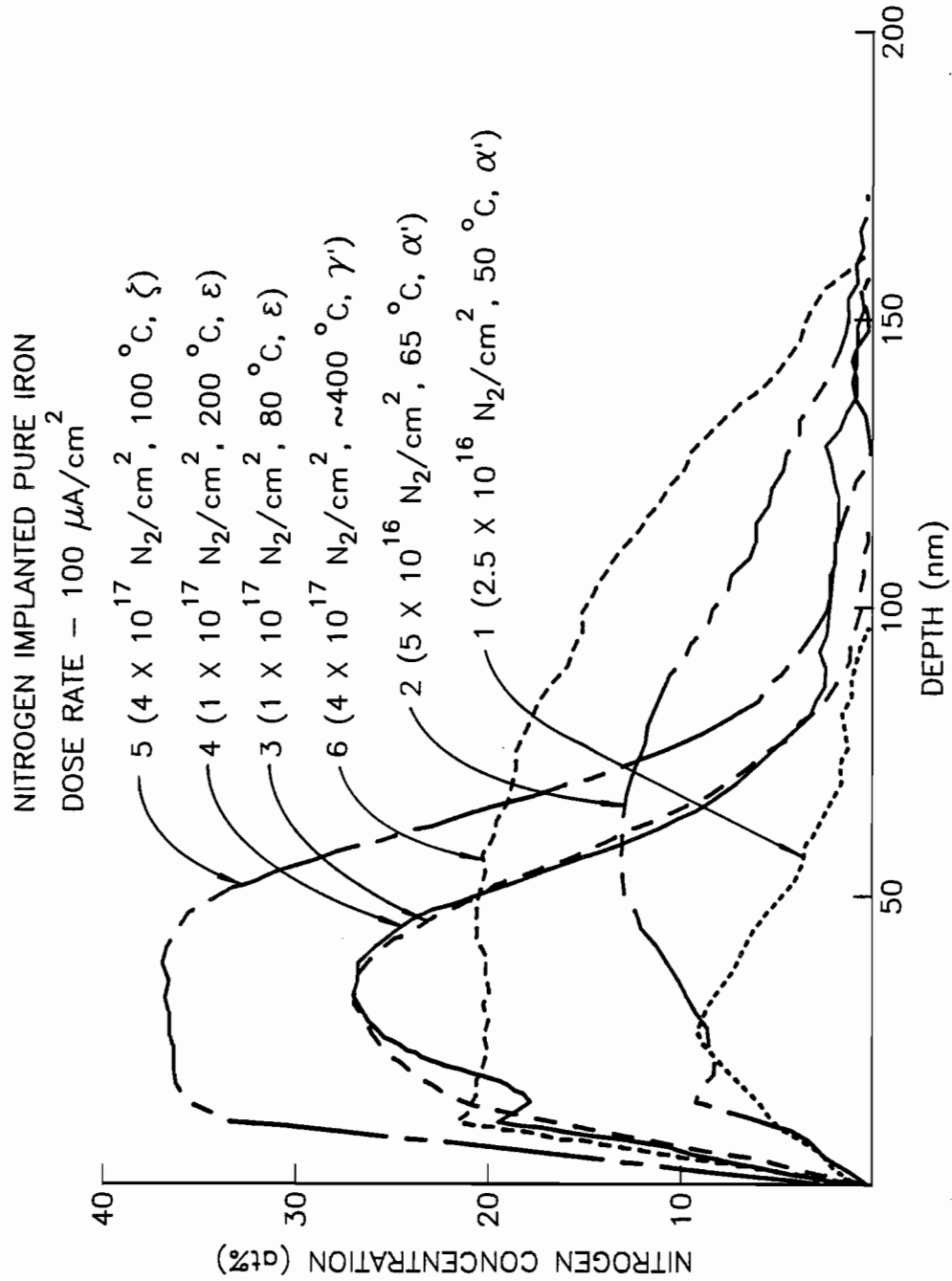


Fig. 6a AES Depth Profiles Showing the Effect of Temperature on the Nitrogen Distribution in Pure Iron ( $100 \mu\text{A}/\text{cm}^2$ )

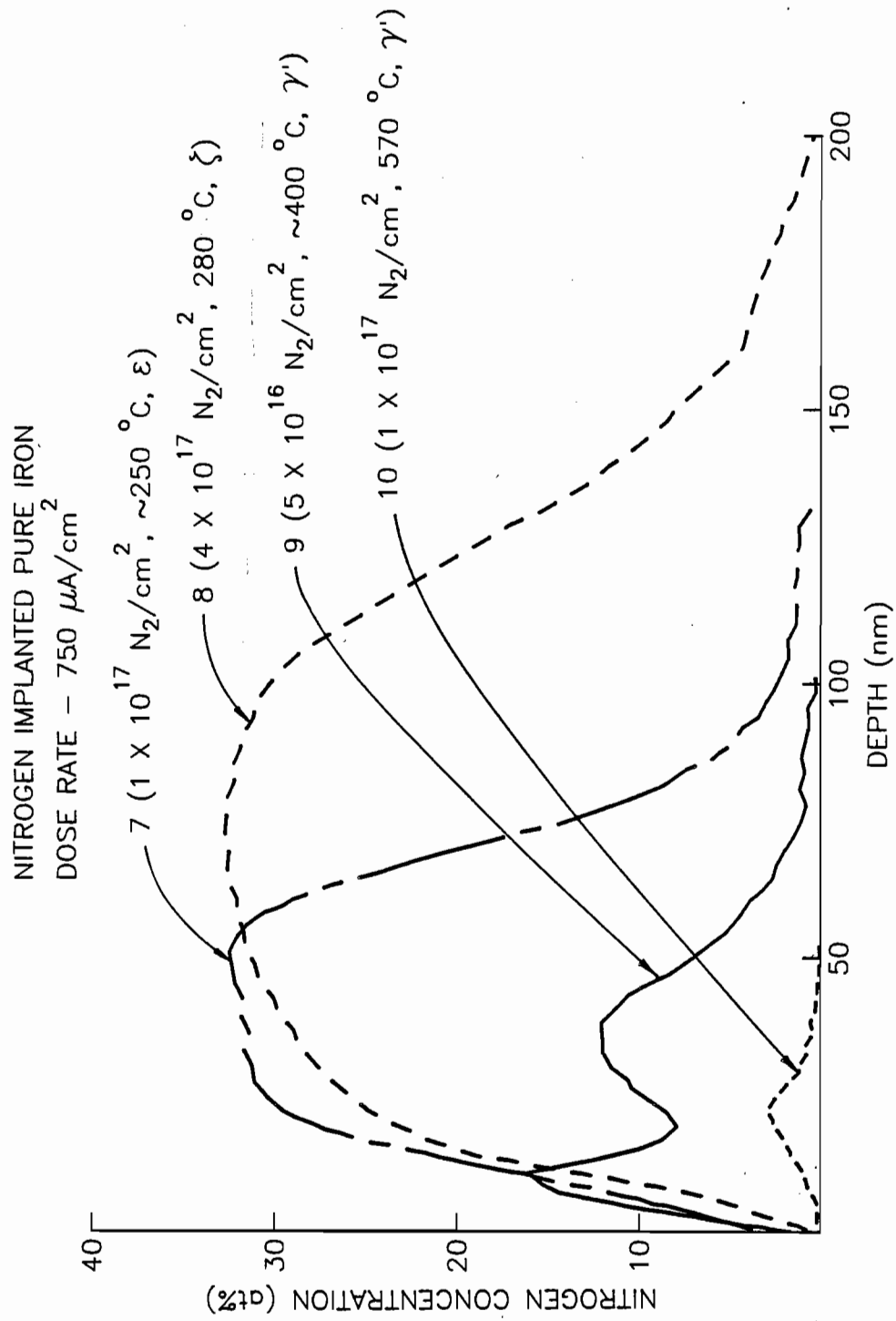


Fig. 6b AES Depth Profiles Showing the Effect of Temperature on the Nitrogen Distribution in Pure Iron ( $750 \mu\text{A}/\text{cm}^2$ )

increases and the  $\gamma'$ -Fe<sub>4</sub>N (fcc) phase forms [Sample No. 6 in Fig. 6a].

4. When sample temperature is held below 280 °C during implantation, the profiles exhibit the nearly gaussian shape predicted by LSS theory [98] if the dose is low ( $1 \times 10^{17}$  N<sub>2</sub>/cm<sup>2</sup>) but they become distorted (flat topped) if the dose is increased to  $4 \times 10^{17}$  N<sub>2</sub>/cm<sup>2</sup>. This trend was also observed by Terwagne, et al. who conducted tests at temperatures below 200 °C and doses less than  $5 \times 10^{17}$  ions /cm<sup>2</sup> [99].
5. Increases in temperature above ~400 C cause progressively higher rates of nitrogen diffusion that distort the profiles and eventually cause a substantial loss of nitrogen either into the bulk or out of the free surface [Sample Nos. 6, 9 and 10 in Figs. 6a and b].
6. The peak nitrogen concentrations correlate very well with the dominant iron nitride that forms. At concentrations below 20 at.%, Fe<sub>4</sub>N forms; near 25 at.% the nitride is Fe<sub>3</sub>N and near the maximum concentration (~33 at.%) Fe<sub>2</sub>N is formed. At concentrations of ~10 at.% or less,  $\alpha'$ -martensite develops provided the temperature is low, otherwise  $\gamma'$ -Fe<sub>4</sub>N forms at  $\lesssim 400$  °C.
7. The consistency of the trends observed at the two markedly different dose rates of Figs. 6a and 6b suggests that dose rate exerts a second order influence on the microstructure and depth over the dose and temperature ranges investigated.

### Wear Testing of Ferrite Discs

In order to study the tribological effects of the dose to which a disc is implanted and its temperature history during implantation, a number of discs were wear-tested against Fe pins using the oscillating pin-on-disc tester operating under the wear conditions listed in Table 2. The implantation conditions for all the  $\alpha$ -Fe discs tested in

Table 4

Implantation Conditions for Pure  $\alpha$ -Fe Discs

Sample No.	Dose Rate $\mu\text{A}/\text{cm}^2$	Dose $\times 10^{17} \text{ N}_2/\text{cm}^2$	Temperature $^{\circ}\text{C}$	Dominant Nitride(s)
Fe1	-	-	-	
Fe2	-	-	-	
Fe3	-	-	-	
Fe4	100	0.5	140	
Fe5	100	0.5	$\approx 200$	$\epsilon$
Fe6	100	1	-	
Fe7	100	1	10	$\zeta$ or $\epsilon$
Fe8	100	1	90	$\zeta$ or $\epsilon$
Fe9	100	1	130	$\epsilon$ or $\zeta$
Fe10	100	1	180	
Fe11	500	1	$300 \pm 50$	$\epsilon'$
Fe12	500	1	$380 \pm 50$	$\epsilon$
Fe13	100	1	$430 \pm 50$	$\gamma'$
Fe14	100	1	460	$\gamma'$
Fe15	100	1	$\approx 500$	$\gamma'$
Fe16	500	3	$380 \pm 50$	$\epsilon(+\gamma')$
Fe17	100	4	130	$\zeta$
Fe18	100	4	$\approx 400$	$\gamma'(+\epsilon+\zeta)$
Fe19	500	10	260	$\zeta$
Fe20	100	10	$380 \pm 50$	$\gamma'$
Fe21	500	100	400	$\zeta(+\epsilon)$
* Fe22	100	4	-	$\gamma'$
** Fe23	-	-	-	
** Fe24	100	1	110	
Fe25	100	1	80	(Ar implanted)

\* Half of Disc Implanted

\*\* Used in Fixed-Pin Wear Tests

this study are listed in Table 4. The phase(s) formed during implantation and listed in the table were determined using CEMS and confirmed using XRD. Typical wear test results obtained on discs implanted at dose rates of 100 and 500  $\mu\text{A}/\text{cm}^2$  to various doses at different temperatures are shown in Fig. 7. In addition to the implanted discs, three unimplanted discs were wear-tested to establish a reference wear curve. The data for the unimplanted discs shown in Fig. 7 represent the mean value of the three. The precision associated with the mass measurements is reflected in the fact that the standard deviation for these data is  $-0.05$  mg. The data for the unimplanted discs in Fig. 7 show that they experience rapid wear initially followed by a reduction in wear rate (presumably due to disc work-hardening that increases to a saturation level as the disc is worn).

When the implanted discs are subjected to the same wear test as the unimplanted ones, the data of Fig. 7 indicate they wear differently. Discs Fe17 (open squares) and Fe5 (open triangles), which were implanted at low temperatures (130 and 200  $^{\circ}\text{C}$  respectively) and wear tested for 40 hr, exhibit a wear rate that is low initially and then stabilizes at the same terminal wear rate as that exhibited by the unimplanted discs. It is argued in these cases that wear-resistant iron nitrides produced during the implantation process induce initial disc wear rates that are low. Once these implanted layers have been worn away (i.e. after 15 to 20 hr when a surface layer with a mean thickness of the order of the  $0.1 \mu\text{m}$  implanted layer thickness has been removed) the wear rate stabilizes at the same terminal value as that observed for the unimplanted discs. It is noted that all discs listed in Table 4 implanted at temperatures that were below  $-300$   $^{\circ}\text{C}$  or above  $-430$   $^{\circ}\text{C}$  exhibited this



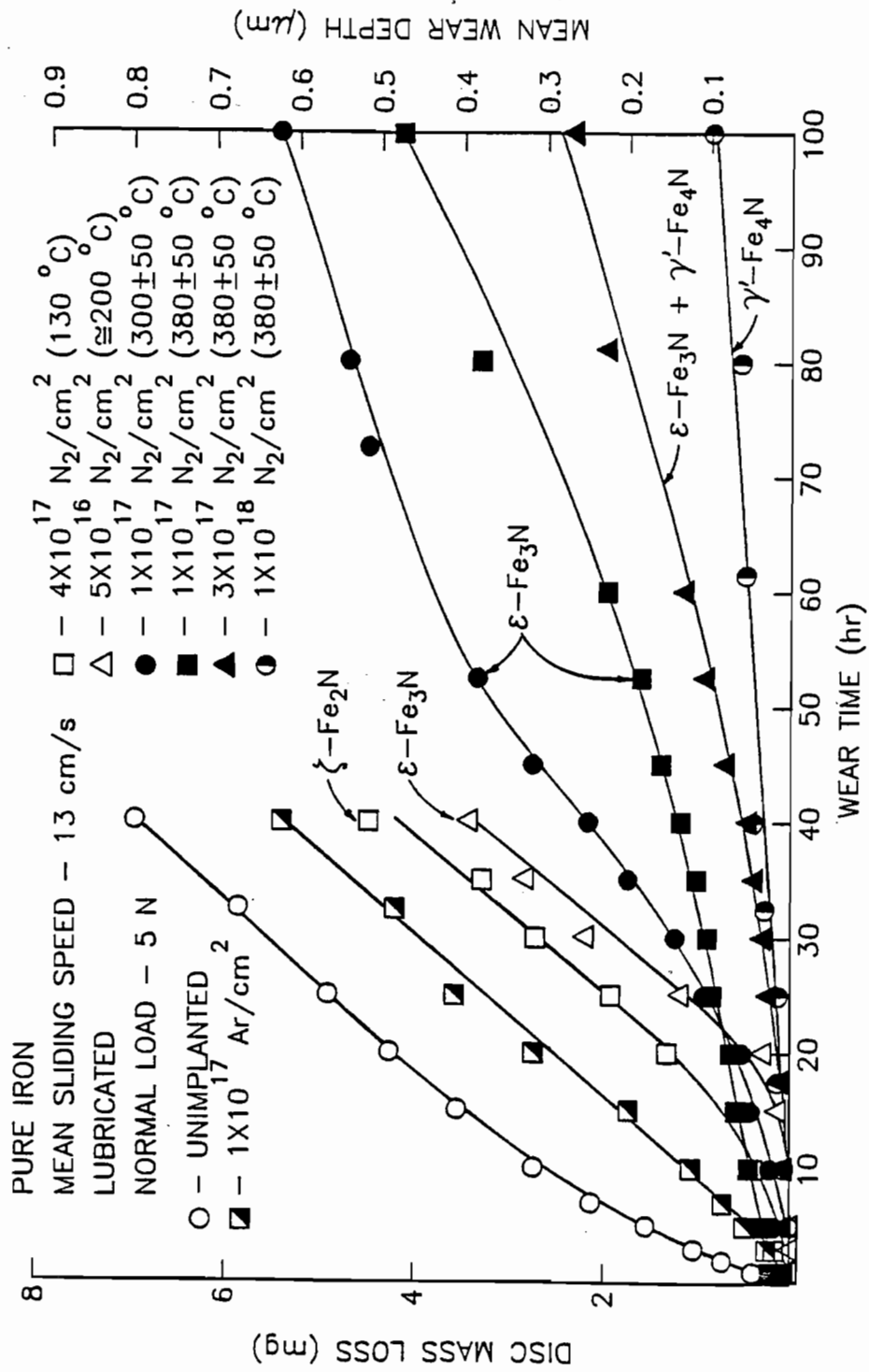


Fig. 7 Typical Wear Histories of Pure Iron Discs

same behavior. They all exhibited a low initial wear rate and then reverted to the terminal wear rate of the unimplanted discs when a layer roughly as thick as the implanted layer had been worn away.

On the other hand, discs that were maintained at temperatures in the range 300 - 400 °C during implantation (all solid symbols and the half-solid circles in Fig. 7) exhibited markedly different wear behavior. Even after these discs have been worn for 100 hr, they exhibit mass loss rates (slopes) that are much lower than the terminal rate for unimplanted ferrite. This implies that implanted nitrogen is still present. Indeed, SEM and CEMS data show nitrogen is still on or near the surfaces of each of these discs.

More careful examination of the data of Fig. 7 also show that the wear resistance realized at a dose of  $1 \times 10^{17} \text{ N}_2/\text{cm}^2$  is enhanced by increasing the temperature sustained during implantation from 300 to 380°C (compare the solid circle data to that for the solid squares). AES data indicate this occurs because the higher temperature facilitates deeper nitrogen diffusion. The notations by each of the curves in Fig. 7 indicate the dominant nitride (determined from Mössbauer data) for each of the implantation dose and temperature conditions. Consideration of this information reveals that  $\zeta\text{-Fe}_2\text{N}$  is formed at high dose/low temperature conditions ( $4 \times 10^{17} \text{ N}_2/\text{cm}^2$  @ 130 °C - Fe17 in Table 4),  $\epsilon\text{-Fe}_3\text{N}$  is formed at low dose/low temperature to moderate dose/elevated temperature conditions ( $0.5$  to  $3 \times 10^{17} \text{ N}_2/\text{cm}^2$  @ 200 to 380  $\pm 50$  °C - Fe5, Fe11, Fe12, and Fe16) and  $\gamma'\text{-Fe}_4\text{N}$  is formed at the high dose/elevated temperature condition ( $3 \times 10^{17}$  to  $1 \times 10^{18} \text{ N}_2/\text{cm}^2$  @ 380  $\pm 50$  °C - Fe16 and Fe20). Further, the discs implanted at 380  $\pm 50$  °C for an extended time so a high dose could be delivered (half solid circles -

Fe20) exhibit even thicker, more wear-resistant layers. In this particular case, the combination of a high dose and a properly maintained temperature assure sufficient diffusion time and adequate nitrogen so a thick layer of  $\gamma'$ -Fe<sub>4</sub>N can form. If this dose were delivered at a much lower temperature, adequate diffusion could not occur and  $\zeta$ -Fe<sub>2</sub>N or even nitrogen bubbles would form. These observations are also in agreement with AES data of Table 3 and Fig. 6. Finally, it is observed that the data of Fig. 7 suggest that the nitrides formed, ranked from most to least wear resistant are:  $\gamma'$ -Fe<sub>4</sub>N,  $\epsilon$ -Fe<sub>3</sub>N and  $\zeta$ -Fe<sub>2</sub>N. These test results indicate, therefore, that the nitrogen compound with the least nitrogen ( $\gamma'$ -Fe<sub>4</sub>N) is most resistant to sliding wear. This ordering is consistent with recent hardness measurements on N-implanted  $\alpha$ -Fe containing these same nitrides for which no wear tests were conducted [80].

Figure 7 also shows the wear data obtained from a disc that had been implanted with argon to a dose of  $1 \times 10^{17}$  N<sub>2</sub>/cm<sup>2</sup> (Fe25). In this case the wear rate stabilizes at the steady-state value from the beginning of the test. It is argued that this occurs because the argon ions, which do not enter into the microstructure chemically, do introduce substantial physical damage that has an effect similar to that induced by the work hardening that determines the terminal steady-state wear rate of unimplanted ferrite.

### **The Effects of Temperature and Dose on the Wear Resistance**

In order to study the tribological effects of the temperature history of a disc during implantation more carefully, a number of discs were implanted to the same dose ( $1 \times 10^{17}$  N<sub>2</sub>/cm<sup>2</sup>) while they were being

maintained at different temperatures. Results obtained from these tests are compared to the wear characteristics of the unimplanted discs in Fig. 8. It can be seen that all nitrogen-implanted discs have wear curves that lie below the one for the unimplanted discs and that the most wear-resistant surface is realized when the implantation is carried out near a temperature of 380 °C. These data also show quite clearly that the wear resistance drops from its peak value when the temperature is increased above 380 °C to 430 °C. This behavior can be understood by recognizing that nitrogen implanted at a low temperature is confined to a shallow region. If the temperature is too high and the dose is low ( $1 \times 10^{17} \text{ N}_2/\text{cm}^2$  in this case) the implanted nitrogen can diffuse so rapidly that an insufficient amount of the preferred nitride ( $\gamma'$ -Fe<sub>4</sub>N) is formed and the wear resistance is not as great as expected. This condition, which was observed in discs Fel4, Fel5 (Table 4) and is consistent with the observations of Fig. 5.

The dose of implanted nitrogen also affects the tribological durability of a surface. Figure 9 shows this effect for the case of pure  $\alpha$ -Fe discs implanted at  $380 \pm 50$  °C (the optimum temperature associated with the  $1 \times 10^{17} \text{ N}_2/\text{cm}^2$  dose data of Fig. 8). From the Fig. 9 data it is clear that increases in dose up to  $1 \times 10^{18} \text{ N}_2/\text{cm}^2$  induce reduced wear rates either directly because of the increased dose or indirectly because of the increase in the implantation time (and hence available diffusion time) required to deliver it. The Fig. 9 data also show that increases in dose induce changes in the dominant nitride present from  $\epsilon$ -Fe<sub>3</sub>N (corresponding to about 25 at.% nitrogen) to  $\gamma'$ -Fe<sub>4</sub>N (corresponding to about 20 at.% nitrogen). Initially, it may seem strange that increasing the amount of delivered nitrogen could cause the

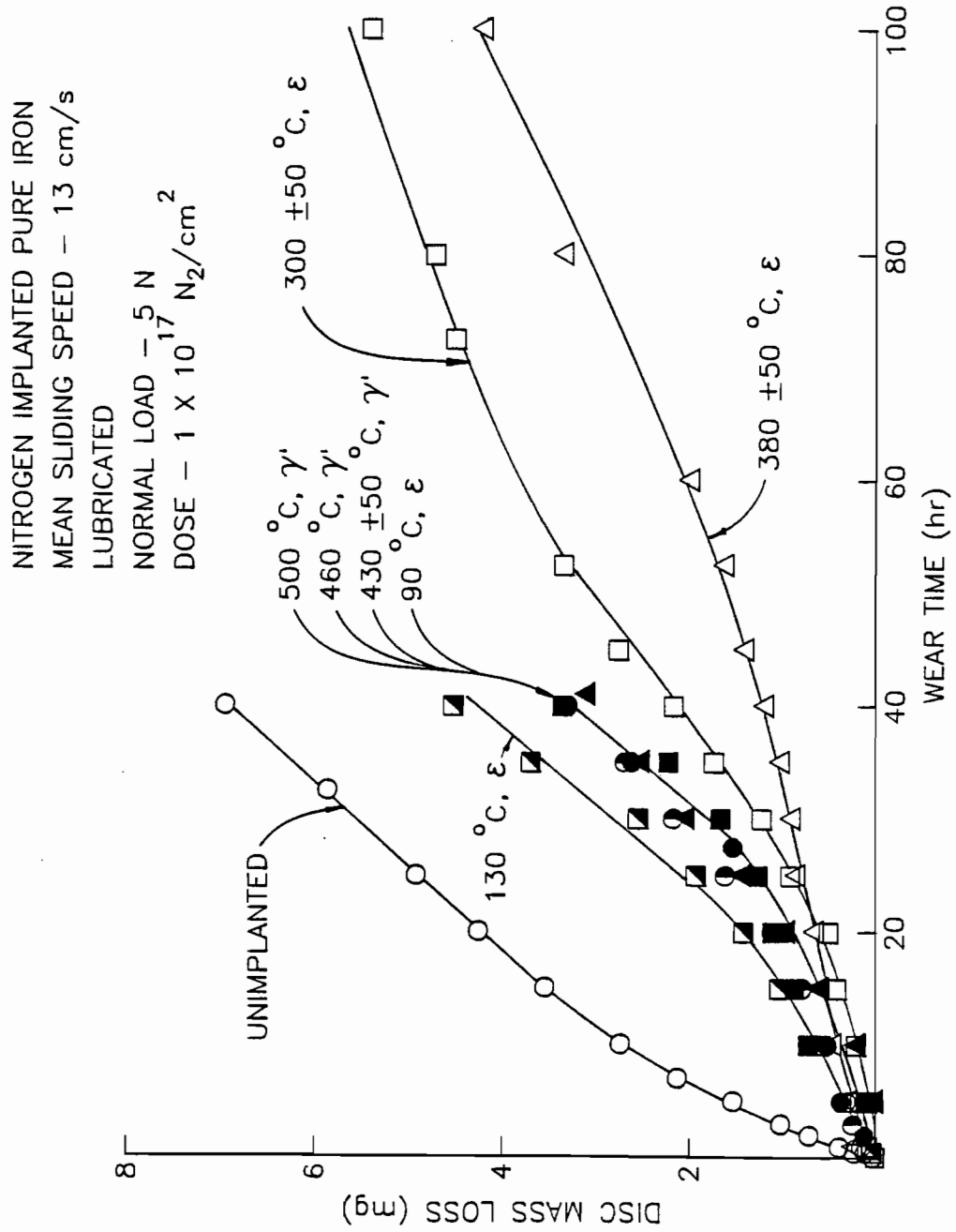


Fig. 8 The Effect of Implantation Temperature on the Wear Resistance of  $\alpha$ -Fe

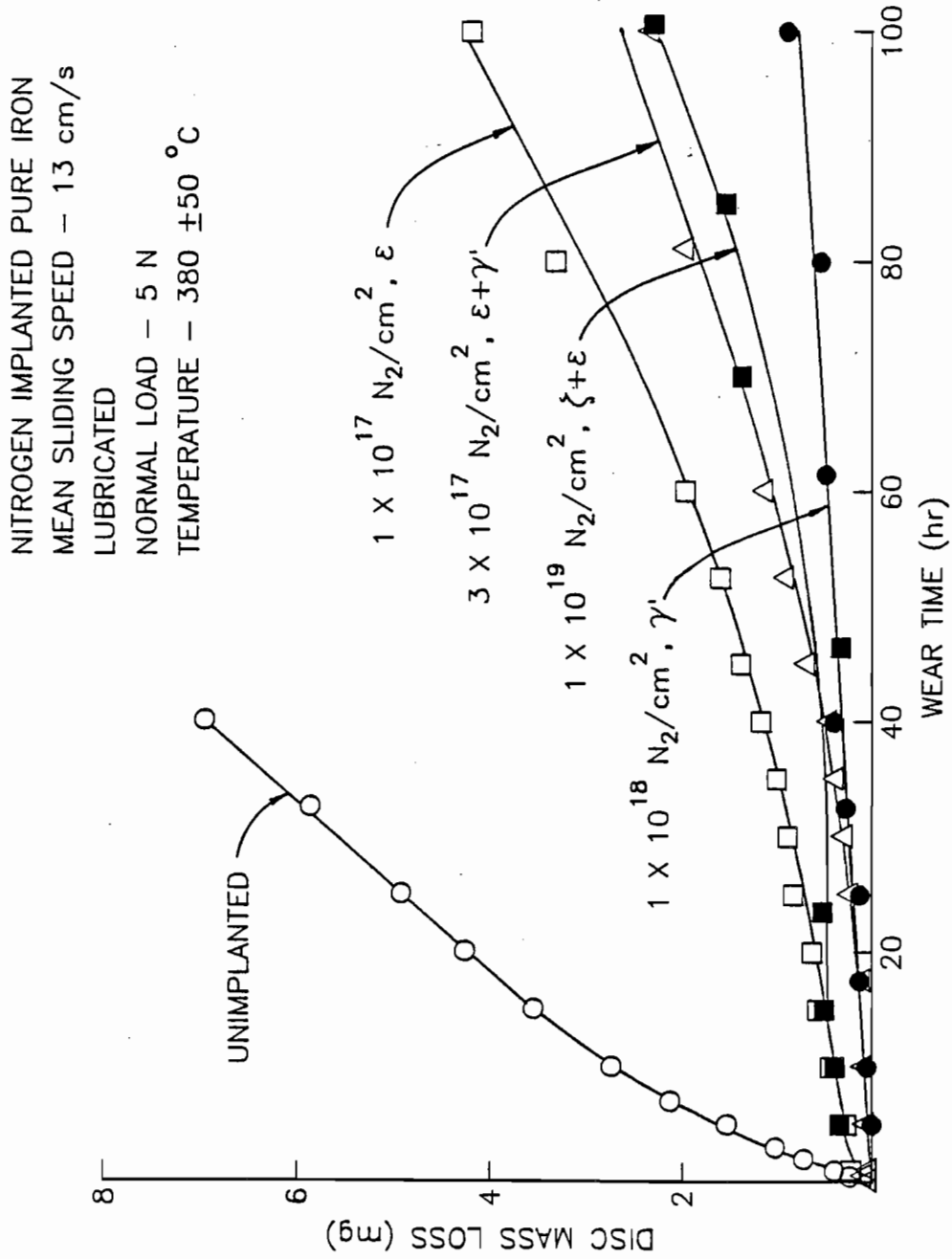


Fig. 9 The Effect of Implanted Nitrogen Dose on Wear Resistance of  $\alpha$ -Fe

concentrations to decrease. To understand this one must recognize that disproportionately longer times are generally required to maintain a prescribed disc temperature while delivering larger doses (the beam must be interrupted a greater fraction of the implantation time to assure temperatures are not exceeded). It is also possible to change the time a disc is at temperature during implantation by controlling the rate of heat removal from it. When this was done so a sample could be implanted to  $1 \times 10^{18} \text{ N}_2/\text{cm}^2$  at a lower temperature (260 °C) the wear curve (not shown in Figs. 8 or 9) fell back into the range of the solid and half-solid data points on Fig. 8, the depth of nitrogen was limited to about 100 nm and  $\zeta\text{-Fe}_2\text{N}$  was the nitride formed.

Figure 9 also includes data associated with a disc implanted to ( $1 \times 10^{19} \text{ N}_2/\text{cm}^2$ ) and it shows higher wear rates than the one implanted to  $1 \times 10^{18} \text{ N}_2/\text{cm}^2$ . This poorer performance is believed to be related to the fact that it was implanted at a higher current density ( $500 \mu\text{A}/\text{cm}^2$  rather than the  $100 \mu\text{A}/\text{cm}^2$ ). This caused higher nitrogen concentrations and resulted in the formation of some of the least wear-resistant ( $\zeta\text{-Fe}_2\text{N}$ ) nitride. Hence, even though implantation conditions favor a very deep implanted layer, the lowest wear rates were not realized. To obtain the deepest, most wear resistant layers under high dose rate, very high dose implantation conditions ( $500 \mu\text{A}/\text{cm}^2$  to  $\sim 1 \times 10^{19} \text{ N}_2/\text{cm}^2$ ), it is believed that temperatures above  $\sim 380$  °C are required to enable sufficiently rapid nitrogen diffusion and assure formation of the  $\gamma'$  nitride phase.

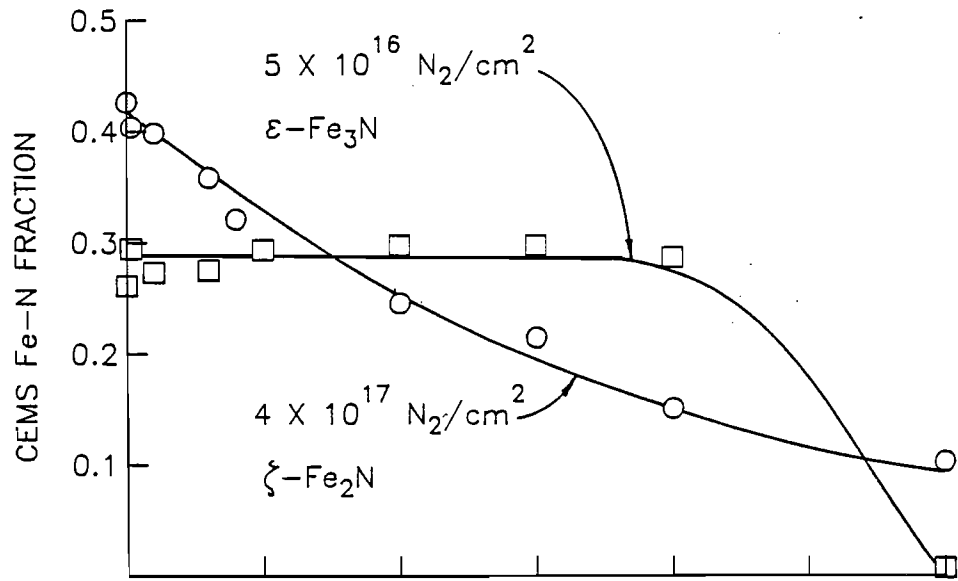
The data of Fig. 7, 8 and 9 also suggest that among discs having the same nitride (as in the cases where  $\epsilon\text{-Fe}_3\text{N}$  is formed) the disc implanted more deeply because it is at a temperature where rapid

nitrogen diffusion occurs (i.e. at  $380 \pm 50$  °C), exhibits greater wear resistant endurance than ones with thinner layers (i.e. ones implanted at  $300 \pm 50$  °C and 200 °C) as shown in Fig. 7. Finally, it should be pointed out that only the nitrogen compounds identified in this paragraph have been observed and that no evidence of interstitial nitrogen in  $\alpha$ -Fe ( $\alpha'$ -martensite) has been found in the nitrogen-implanted discs which were wear-tested. Additional details of the Mössbauer analysis and examples of quantitative determination of bonded nitrogen have been presented elsewhere [96,97].

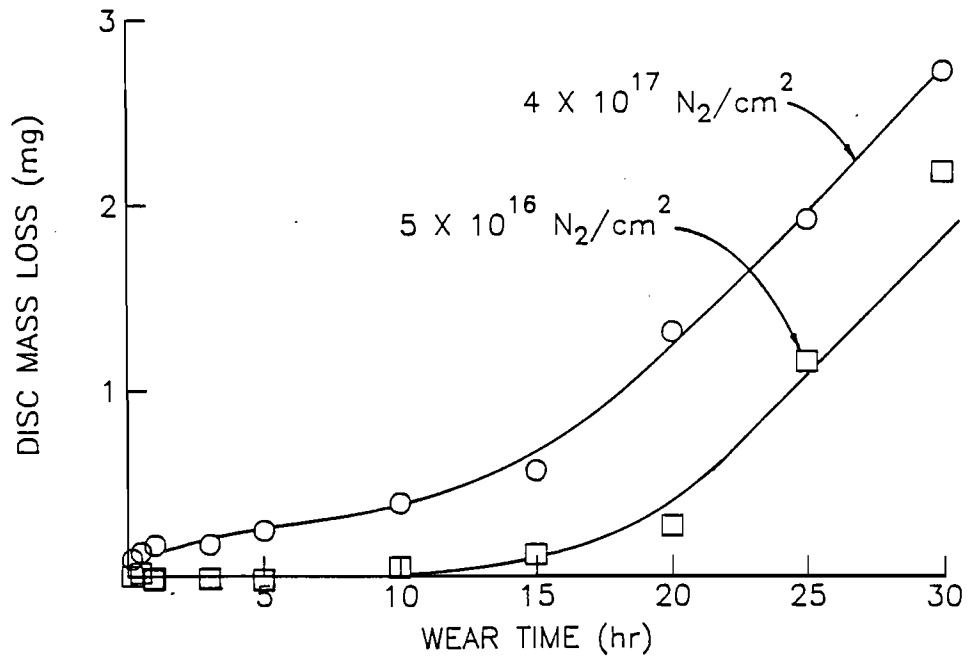
The data of Fig. 10 show the correlation between wear behavior and nitride concentration in the  $0.1 \mu\text{m}$  near-surface layer of discs implanted to different doses at low temperature to produce two different nitrides. The disc implanted to  $5 \times 10^{16} \text{ N}_2/\text{cm}^2$  is seen to exhibit a low wear rate and a nearly constant nitride ( $\epsilon\text{-Fe}_3\text{N}$ ) concentration during the first 20 hr of wear. After that, the wear rate increases rapidly to the same value associated with unimplanted discs (Fig. 7) as the nitride fraction drops rapidly to almost zero. On the other hand, the other disc exhibits more uniform wear and a more rapid decrease in its nitride ( $\zeta\text{-Fe}_2\text{N}$ ) concentration as its surface is being gradually worn away.

It is also important to note that Mossbauer data obtained for each data point indicated for the wear test data in Figs. 7, 8 and 9 show that the state into which the nitrogen is bound is established during the implantation process. Tests like those associated with the data of Fig. 10 show that this state does not change as the discs are worn. This is important because it indicates that the nitrides do not break up





(a)



(b)

Fig. 10 Correlation of Disc Mass Loss and Iron Nitride Fraction in a Nitrogen-Implanted Layer

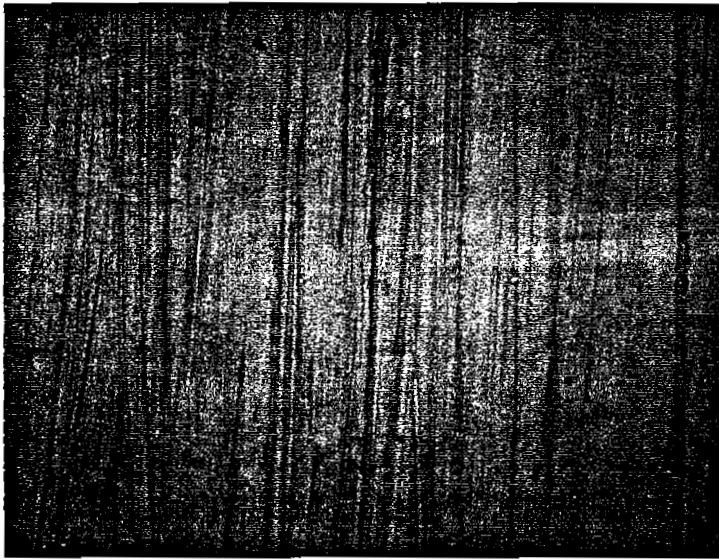
and substantial nitrogen diffusion during the wear process is therefore unlikely.

### **Morphological Studies on Ferrite**

When discs were removed periodically during the wearing process so they could be weighed, they were also examined under optical and scanning electron microscopes and their surface roughness was measured using a profilometer. The optical micrographs of Fig. 11 compare the surface of a region that had been implanted with one that had not on the same disc (Fe22). Because the two regions were on the same discs, they were both subjected to the same wear conditions. The micrographs clearly show that the density of the wear scratches is much higher in the unimplanted region than they are in the implanted one. This suggests that the implanted region is the harder of the two.

A more exhaustive study, this one carried out using a scanning electron microscope to record the time histories of the surfaces of two different discs during the wearing process, is shown in Fig. 12. The two discs compared in this figure are an implanted one (Fe17) and an unimplanted one (Fe2). In general the micrographs in this figure show the wear scars on both discs are long grooves initially and that these surfaces begin to take on a furrowed appearance after about 5 hr for the unimplanted disc and 25 hr for the implanted one. The appearance of this furrowed structure seems, therefore, to develop for both discs at about the times their wear rates stabilize at the steady-state value (Fig. 7).

Another important feature illustrating the differences in the wear behavior of the unimplanted and implanted discs, which can be seen in



(a) UNIMPLANTED



(b) IMPLANTED

Fig. 11 Comparative Optical Micrographs of Unimplanted and Implanted Regions on a  $\alpha$ -Fe Disc After a 5 h Wear Test

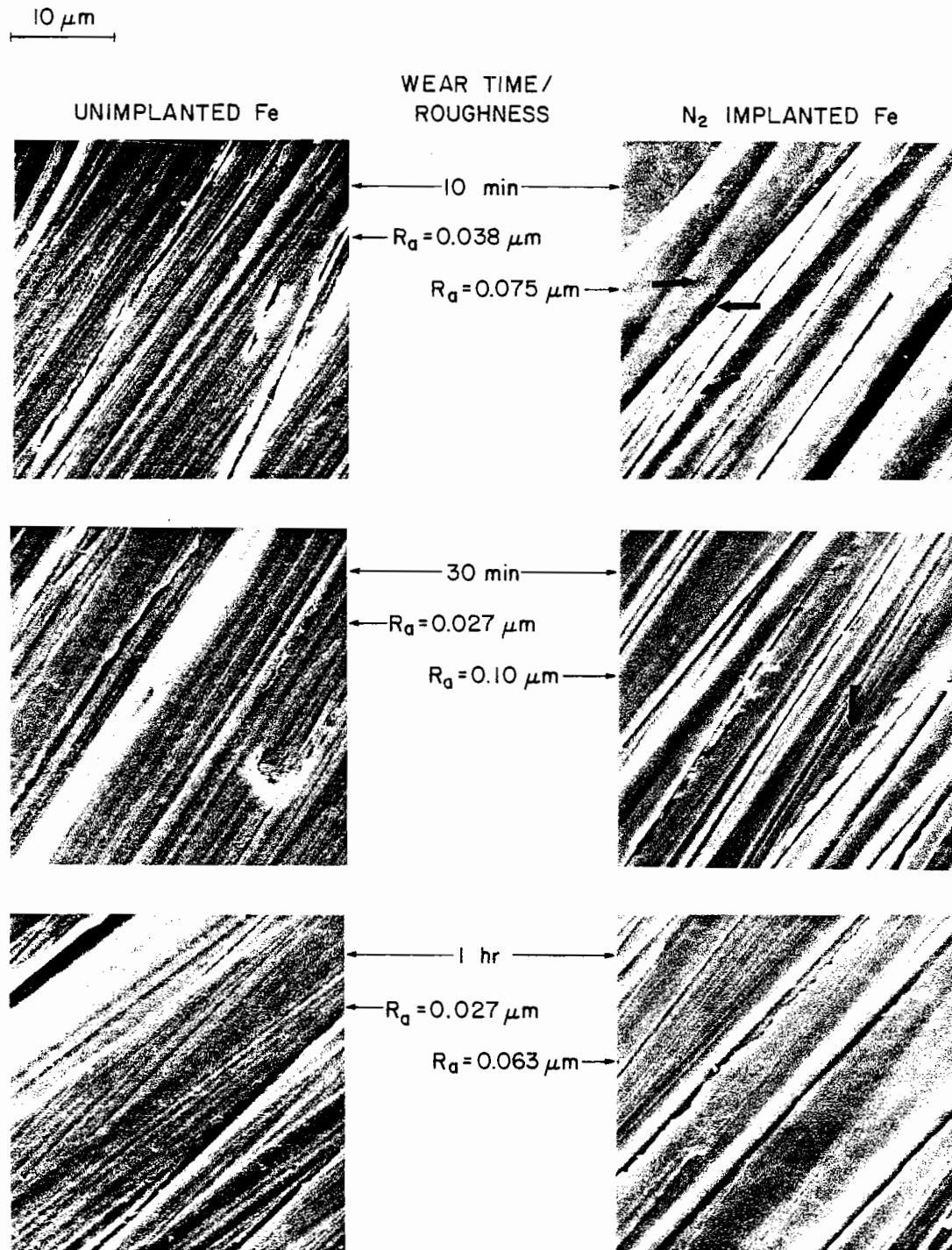


Fig. 12 Scanning Electron Micrograph and Surface Roughness Histories During Oscillating Pin-on-Disc Wear Tests

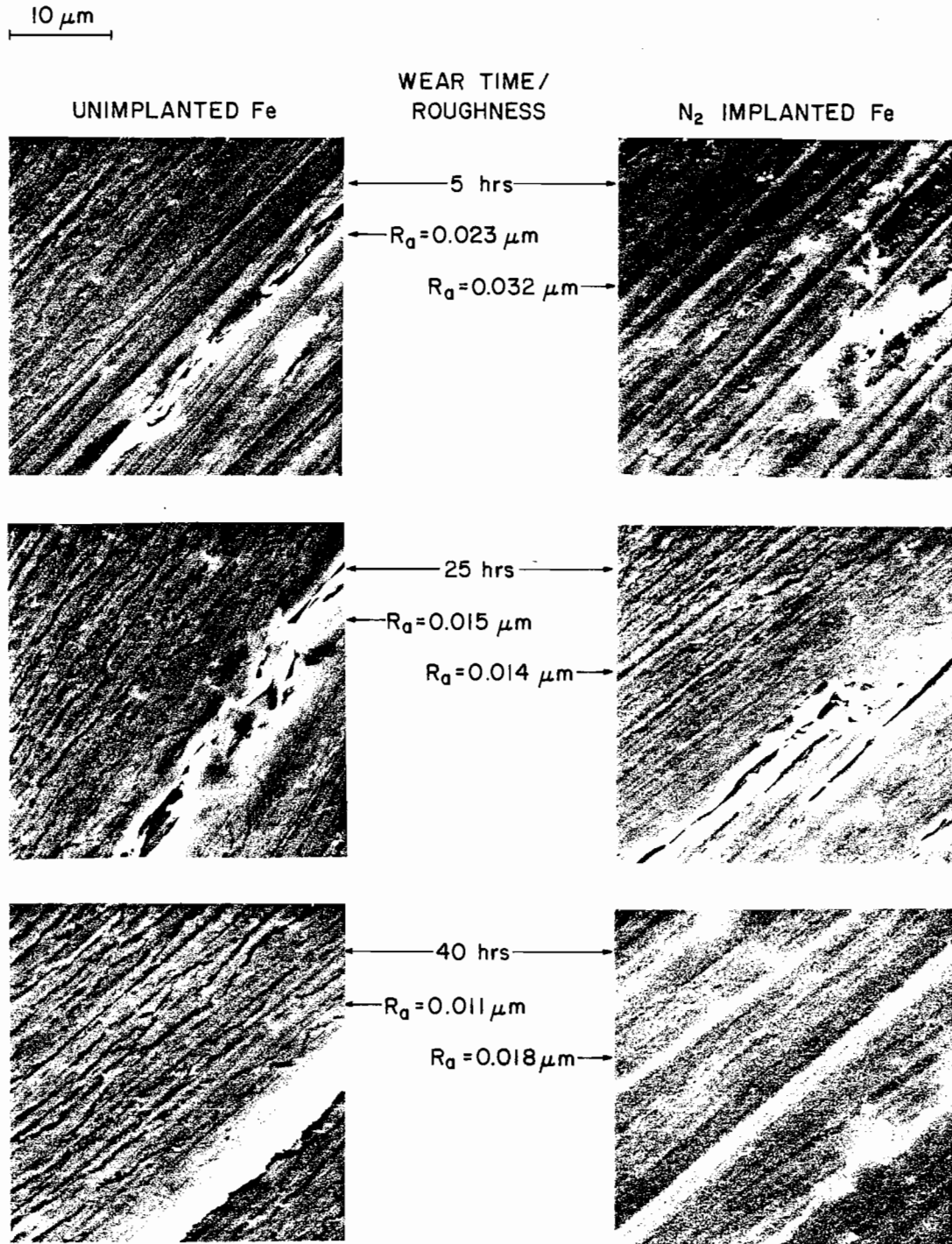


Fig. 12 (cont.) Scanning Electron Micrograph and Surface Roughness Histories During Oscillating Pin-on-Disc Wear Tests

the 10 min and to a lesser extent in the 30 min micrographs of Fig. 12, is that faint polishing marks running oblique to the wear grooves are visible on the implanted disc, as indicated by the arrows, while none are visible on the unimplanted one. Further, the roughness ( $R_a$ ) of the implanted disc develops until it is about three times that of the unimplanted disc during this early (~30 min) time interval. Taken together these two observations suggest that the implanted disc is being worn by hard particles (possibly nitrides) that embed in the pin and plow through the disc. On the other hand, contact occurs over much broader asperities that produce shallower and broader grooves in the unimplanted disc and cause more rapid wear. This is shown by more rapid mass loss, more rapid removal of the polishing marks and the greater roughness on the unimplanted disc. It is also noted that the data of Fig. 12 show the roughnesses of both the implanted and unimplanted surfaces, which were  $\sim 0.015 \mu\text{m}$  prior to the start of wear testing, rise dramatically and then fall gradually to values near the pre-test roughness at about the times for onset of steady-state wear for each disc.

#### **Comparison of Oscillating and Fixed Pin-on-Disc Wear Tests**

Because conventional sliding wear test machines usually involve fixed rather than oscillating pin configurations it was decided that wear data for implanted and unimplanted discs should be generated in the fixed-pin mode so they could be compared to data generated in the oscillating-pin mode. Figure 13 shows a typical comparison of such data with the fixed-pin data represented by the square symbols and the oscillating-pin data represented by the circular ones. Comparison of

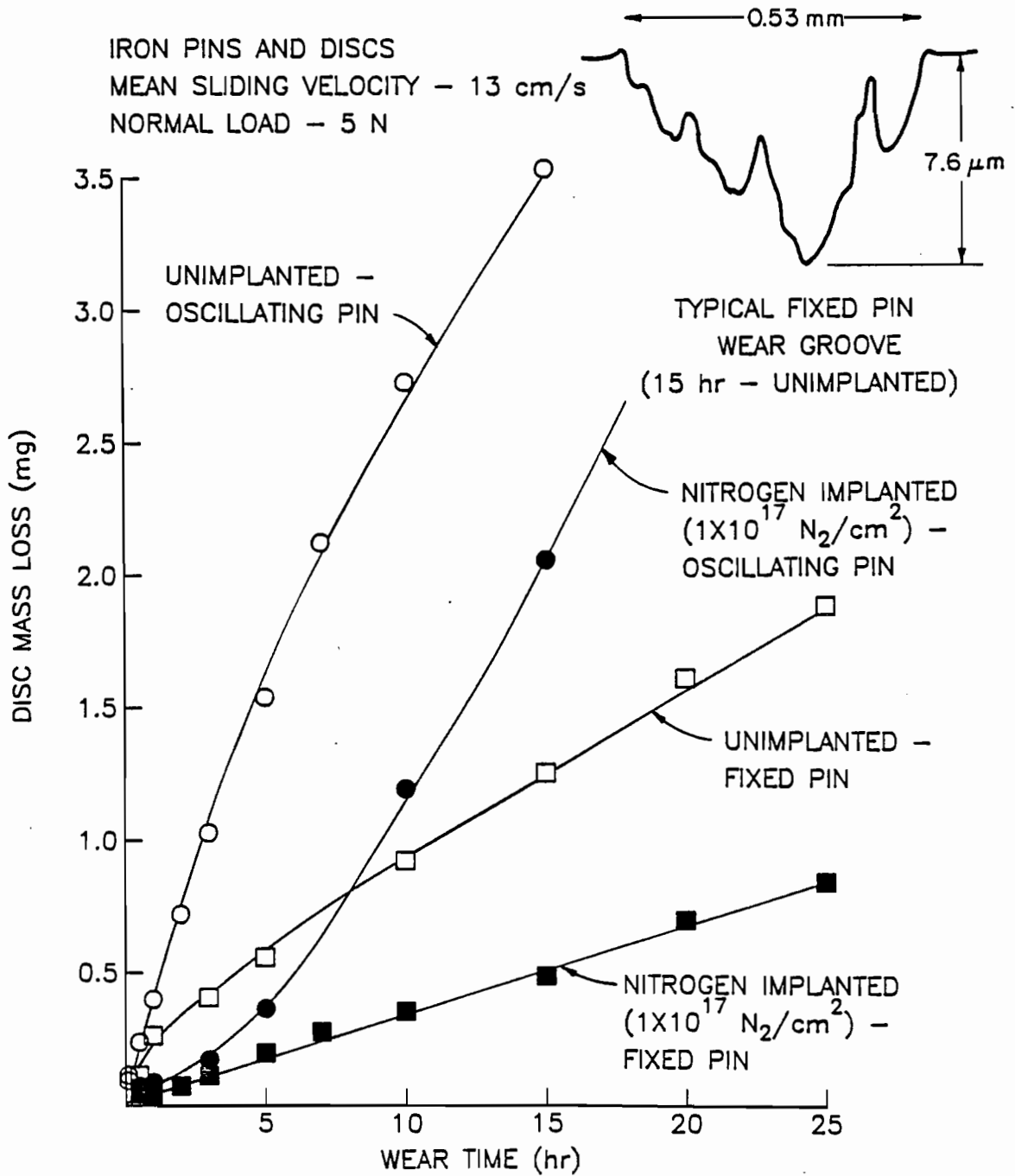


Fig. 13 Comparative Fixed Pin-on-Disc and Oscillating Pin-on Disc Wear Test Results for  $\alpha$ -Fe

the open data points (unimplanted cases) suggests that they both exhibit similar qualitative behavior, but the disc mass loss rate drops to a stable value in about 1 hr in the fixed-pin test while 10 hr is required in the oscillating-pin one. Further, the wear rates are higher in the oscillating-pin tests. It is argued that wear rates are greater in the oscillating mode (whether the surface is implanted or not) because plastic deformation causes shoulders to form on each side of a plowing track. In the oscillating pin mode, subsequent traverses by the pin cut across these shoulders and dislodge material from them with relative ease. In the fixed pin mode, on the other hand, the pin remains in one groove, the shoulders produced by plastic deformation are not traversed by the pin and the material removal rate is lower. In addition, it may be that wear debris is more easily flushed from the disc surface when the pin is oscillating.

The most significant effect shown by the data of Fig. 13 is the dramatically different nature of the fixed and oscillating-pin wear curves for the implanted discs (solid symbols). They show that disc wear rate increases abruptly for the oscillating-pin case after about 15 hr while that associated with the fixed-pin case shows no change throughout the test. It has been shown earlier (Fig. 7) that oscillating pin wear data increase rather abruptly to a steady-state wear rate as the implanted nitrogen layer wears away. The fact that the fixed-pin data show no such break suggests that sufficient nitrogen is available to sustain a low wear rate operating condition over the full duration of the test. The reason why this is the case can be understood by considering the fixed-pin wear groove cross-sectional profile at the top of Fig. 13. This profile pertains to an unimplanted disc, but



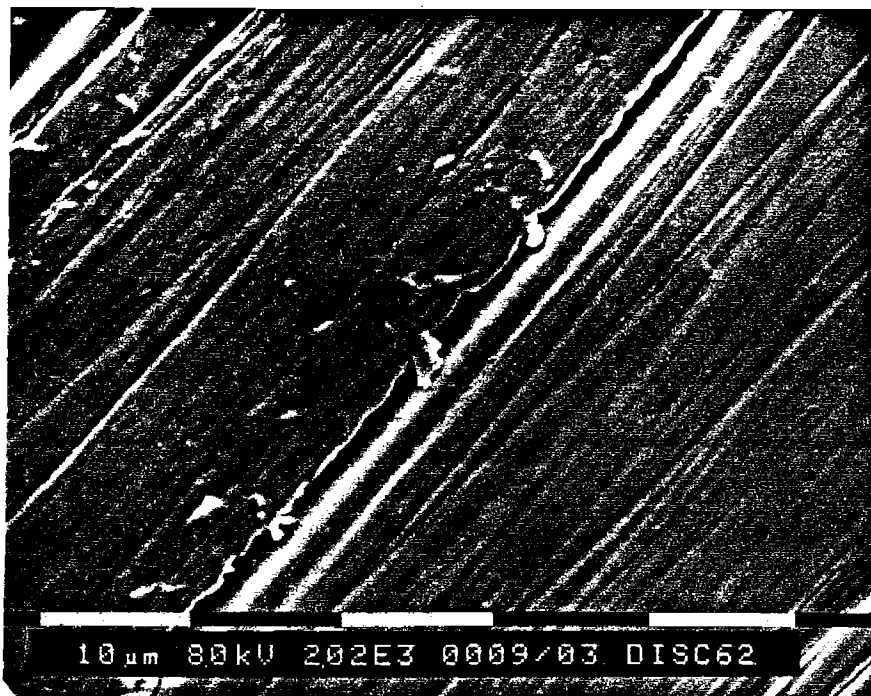
profiles measured for implanted ones are similar. Note that while most of the groove extends below the implanted layer, which is only  $\sim 0.1 \mu\text{m}$  deep, the pin is always in contact with and wearing away some nitrogen-implanted material. It is believed that nitrogen-bearing material drawn from this small contact zone at the top of the groove, which may combine with material from other locations in the groove, forms wear debris that is transferred mechanically throughout the wearing interface. The combination of the direct effect of the nitrogen in the implanted layer (at the edge of the wear track) and that distributed in the form of nitrogen-bearing wear debris is believed to be the cause of prolonged reduced wear rate observed in the fixed-pin case. It should be noted that the depth of the wear groove shown in Fig. 13 is sufficient to suggest that the effect of the nitrogen should be negligible. In the oscillating-pin case, on the other hand, nitrogen is present over the entire surface of the disc until the implanted layer is worn off the pin cannot find even the small amount of nitrogen-bearing material that comes from the edges of the wear groove in the fixed-pin case because the entire implanted layer has worn away nearly uniformly.

Many studies of nitrogen-implanted steels report reduced wear rates that persist to wear depths much beyond the implantation-modified layer. Several mechanisms for this behavior have been summarized (Hirvonen, [56]) including an early one (Hartley, [9]) that nitrides produced during implantation break up as a result of the wear process and allow nitrogen to diffuse as the wear proceeds. The process has been called tribo-enhanced-diffusion (Feller et al. [55]). Considerable evidence disputing this mechanism exists (Singer, [48]; Oliver et al., [50]; Hubler and Smidt, [57]; Fayeulle, [65]) but experimental studies in

support of it continue to appear (Dimigen et al., [53] and Korychi et al., [71]). Also, a recent theoretical treatment of this problem has been proposed (Iskanderova et al., [81]). Other models rely on the nitrogen-implanted layer as an initiator of improved wear (Oliver et al., [50]; Dearnaley et al., [18]; Fayeulle, [65]; Hale et al., [70] and Pollock et al., [72]). These models infer the wear mechanism is modified as a result of the nitrogen-implanted layer to one of low wear rate which then persists even though the original nitrogen disappears. The data of Figs. 7, 8, 9, 10, 12 and 13 and that of Williamson et al. [96,97] provide clear evidence that nitrogen break up and migration during wear does not occur under the conditions associated with the present tests.

The data presented in Fig. 13 and discussed in the preceding paragraph indicate that tests conducted using fixed-pin on disc machines could erroneously indicate that nitrogen diffuses through the bulk material, thereby producing prolonged wear resistant behavior. In reality, however, it could be the wear debris that carries the nitrogen over the surface of the wear track and/or the hard nitride layer at the edge of this fixed-pin wear track that sustains the apparent long-lasting reduced wear rate.

Additional evidence that nitrogen migrates mechanically over the surface of an implanted disc rather than within the bulk material is provided by EDS data associated with the SEM micrographs in Fig. 14. These pictures show a wear groove on a disc that has been implanted to a dose of  $4 \times 10^{17} \text{ N}_2/\text{cm}^2$  (Fe17) and then has been worn for 3 hr on the oscillating-pin machine. At this time, as seen in Fig. 7, the nitrogen did not totally disappear and the disc mass loss rate did not increase



a) GENERAL APPEARANCE



b) DETAIL OF WEAR GROOVE

Fig. 14 Typical Scanning Electron Micrographs of a Wear Groove in Nitrogen Implanted Iron. Points A-D Pertain to Table 5

up to the value for the unimplanted ones. The letters on the more magnified (lower) picture of Fig. 14 identify representative points on the wear track where nitrogen concentration measurements were made using EDS able to detect low atomic number elements. Point A is on the ridge of a wear groove, Point B is midway down the side of the groove, Point C is at the bottom of the groove and Point D is on the wear particle attached to the groove. Table 5 shows the nitrogen concentrations detected at each of these points as well as the mean concentration over the entire region of Fig. 14b.

The uncertainties associated with the quantitative analysis presented in Table 5, which are quite high, reflect the difficulties associated with detection of low energy x-rays from an ideal surface containing nitrogen. True uncertainties are even greater because the surfaces being examined are irregular (the emergence angle is variable). Nevertheless, the results of Table 5 and Figs. 7, 12, 13 and 14 taken together all suggest that the beneficial effects of nitrogen implantation might continue to be observed in a realistic wear environment after an assumed uniform layer with a depth significantly

Table 5

Results of Energy Dispersive X-ray Analysis  
of a Nitrogen Implanted Disc ( $4 \times 10^{17}$  N<sub>2</sub>/cm<sup>2</sup>)  
after 3 hr of Wear Testing

Location on Disc (Fig. 14b)	Atomic % of Iron	Atomic % of Nitrogen
Mean over Entire Region	34 ± 10	66 ± 18
A-Top of Ridge	55 ± 13	45 ± 17
B-Midway down Groove	72 ± 13	28 ± 13
C-Bottom of Groove	100 - 15	0 + 15
D-On Attached Particle	31 ± 8	69 ± 15

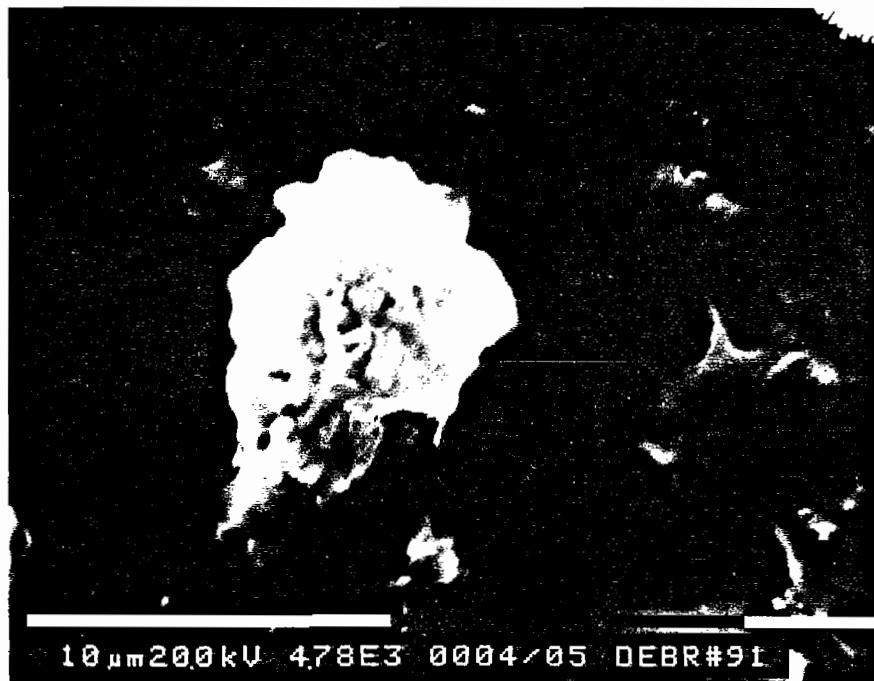
greater than the implanted layer depth had been removed. Nitrogen could still be present on the ridges of grooves and particles like D in Fig. 14 that could be forced into the valleys of the uneven, worn surface after an amount of material corresponding to an implanted layer had been removed. The modest beneficial effect of this mechanically transported nitrogen should, however, not persist substantially beyond the thickness of the implanted layer in a mild adhesive wear environment. This observation is consistent with those of Pollock et al., [72]; Fayeulle, [65] and Singer [49].

### **Wear Debris Study**

Typical scanning electron micrographs of debris obtained from wear tests of nitrogen-implanted and unimplanted iron are shown in Fig. 15. As these pictures indicate, the debris are typically irregular in shape. Although most debris seems to be somewhat ellipsoidal, long stringy shapes (Fig. 15c) and relatively flat, flake-like shapes (Fig. 15d) are also observed. Comparison of debris micrographs for tests of implanted and unimplanted discs suggests that the implanted samples have a more layered appearance. Further, the long, stringy shape has only been found in the tests that utilize implanted discs and it is assumed that such debris is produced as a result of an abrasive cutting or plowing process that could have produced the deep grooves observed in the early phases of implanted disc wear (10 and 30 min micrographs in Fig. 12). The general morphology of the debris is considered to be indicative of adhesive wear. In this case, debris would be formed from material that is typically transferred back and forth between the wearing surfaces of a pin and disc pair. It is also considered possible that the large (~20



a) NITROGEN ION IMPLANTED



b) UNIMPLANTED

Fig. 15 Scanning Electron Micrographs of Typical Wear Debris



c) NITROGEN IMPLANTED (w/LONG PARTICLE)



d) NITROGEN IMPLANTED (w/ FLAKE)

Fig. 15 (cont.) Scanning Electron Micrographs of Typical Wear Debris

$\mu\text{m}$ ) pieces of wear debris are produced as a result of the delamination mechanism (nucleation and growth of subsurface cracks) [100].

Surface analysis of typical wear debris using EDS has shown that they consist of iron particles and that many contained oxygen, but no evidence of significant concentrations of nitrogen has been found on them. Nitrogen has, however, been observed on what appear to be particles that are still attached to the disc. It is also noted at this point that EDS analysis of the discs reveals the presence of nitrogen but no oxygen while analysis of the pin shows oxygen is present but not nitrogen. The presence of oxygen on the pin is presumably related to the fact its surface is being worn continuously so it is hotter and its surface asperities tend to oxidize more readily than those on the disc.

#### **Microhardness Testing of Ferrite Discs**

Measurements have been made at Vickers indenter loads that range as low as 0.005 N on unimplanted, nitrogen-implanted and argon-implanted iron discs. They show that implantation of either nitrogen or argon ions induces a severalfold increase in surface hardness. It has not been possible, however, to relate hardness changes to the nitride constituents that are present as Fujihana et al. [80] have done because the substrate hardness perturbs the implanted surface hardness measurements substantially even at very light loads.

Microhardness measurements could be a useful indicator of the wear resistant potential of an implanted surface, but they would have to sense the hardness of the implanted layer rather than that of the bulk material beneath it to be meaningful. Figure 16 shows the variation in



Vickers microhardness of unimplanted, nitrogen-implanted and argon-implanted iron discs as a function of the load applied to indent the surfaces. They show that the indicated hardness of the implanted discs increases as the load is reduced. This occurs because the implanted layer has an increasingly greater influence on the depth to which the indenter penetrates as the load is reduced. The true hardness of the layer is, however, obviously not indicated even at the lowest load used (0.005 N).

In an effort to develop a way to estimate the true hardness of an implanted layer from data like those shown in Fig. 16 an experiment was conducted in which iron nitride layers of various thicknesses were sputtered-coated onto iron discs and the hardnesses of these layers were measured as a function of indenter load. The results of this experiment are shown in Fig. 17. It should be noted that two different microscopes were used to measure the sizes of indentations in this study. The indentations were so small at light loads in the hard iron nitride, that the scanning electron microscope had to be used to measure them. At greater indenter loads, however, both the optical and the SEM microscopes gave similar hardness values. The data of Fig. 17 suggest that the Vickers hardness of a nitrogen-implanted layer is in the range of  $2000 \text{ kgf/cm}^2$ , a value several times those measured at the lightest load level on typical implanted surfaces. The sputter-coated nitrides formed in this study (mostly  $\zeta\text{-Fe}_2\text{N}$ --as in the samples implanted at low temperature/high dose) were identified using CEMS.

One might consider the development of a technique that would utilize the shapes of curves like those in Fig. 16 coupled with hardness data for the various nitrides (like those in Fig. 17 for  $\zeta\text{-Fe}_2\text{N}$ ) to

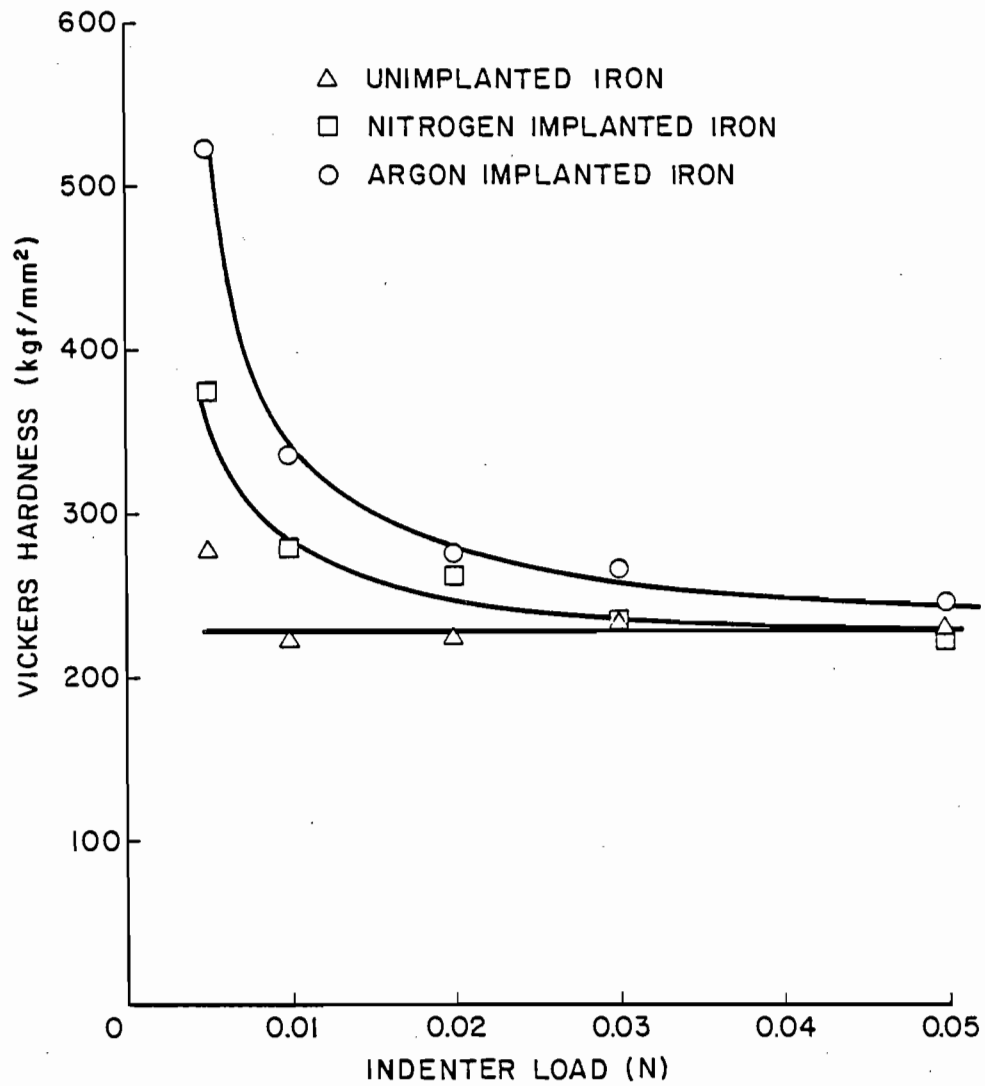


Fig. 16 The Effect of Indenter Load on the Vickers Hardness of Ion Implanted  $\alpha$ -Fe

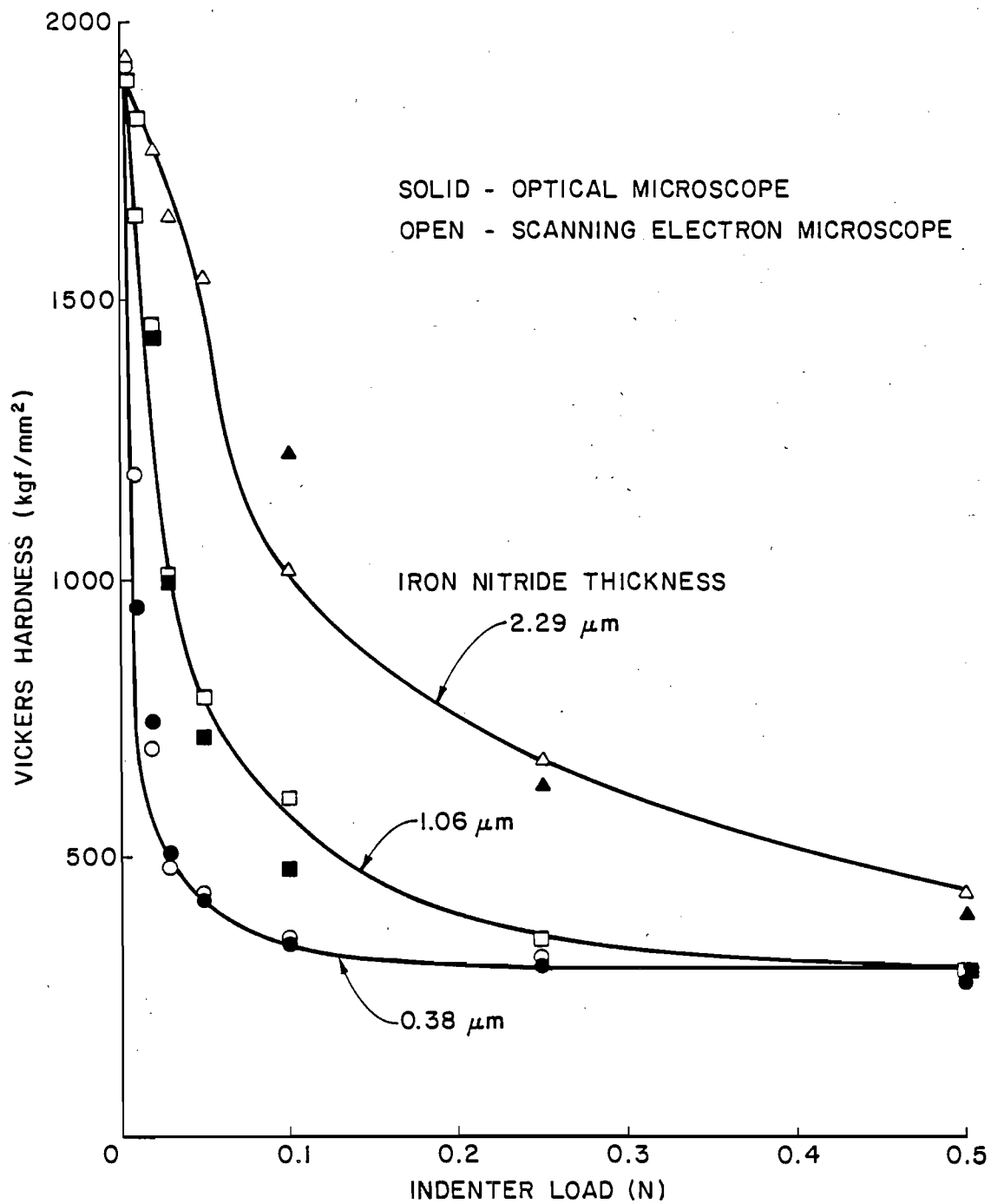


Fig. 17 The Effect of Indenter Load on the Vickers Hardness of Sputter-Coated Iron Nitride on  $\alpha$ -Fe

determine true layer hardnesses. Attempts to do this in the present study were unsuccessful, largely because of the great range over which the hardness data would have to be extrapolated to a near-zero indenter load and the difficulties associated with accurate indentation size measurement at the lightest loads, even when a scanning electron microscope was used.

## RESULTS AND DISCUSSION - STAINLESS STEELS

### Brief Summary

The effects of nitrogen implantation on the wear behavior of AISI 304 and 310 stainless steels (SS) were also investigated using the oscillating pin-on-disc wear tester. High dose implantation at elevated temperature increased the normal load at which the transition from mild to severe adhesive wear (galling) occurred in these steels by two to three orders of magnitude. At loads below the galling level where mild adhesive wear prevailed, the wear rates of nitrogen-implanted surfaces were found to be extremely low. Implantation also reduced the friction coefficients associated with these surfaces. Implantation at temperatures greater than 380 °C to dose levels of order  $4 \times 10^{17} \text{ N}_2/\text{cm}^2$  yielded the hardest, most durable surface layers. Implantation at these elevated temperatures to high doses yielded hard layers that were about a factor of 10 thicker than the ballistic range of the implanted ions. The beneficial effects of implanted nitrogen are related to nitrogen-induced solid solution hardening of the austenitic phase in these stainless steels. It is believed that this solid solution hardening increases both the ultimate strength and the stiffness of the implanted layer.

## Overview

Stainless steels have been implanted with various ions, including boron [10, 79] and titanium/carbon [33, 36, 64], but nitrogen is certainly the most widely used [10, 13, 21-14, 26-28, 30-32, 36-39, 42, 49-55, 58-63, 65-69, 73-78, 79, 82, 93-97]. Except for abrasive wear situations [24, 87], all of these implanted ions make the stainless steels more wear resistant than they were in the unimplanted state. The implantation conditions that are most beneficial and the mechanisms by which the improvements are induced, however, are not well understood. For example, researchers continue to disagree on the optimum implanted-nitrogen dose [53, 73].

Research conducted to date has not addressed, in a systematic way, the capacity for stainless steels to accept greater implanted ion doses if the substrate temperature is raised to the point where substantial nitrogen diffusion can occur. In this regard it is noted that N diffusion has been observed; this is illustrated by the fact that aging influences the wear behavior of nitrogen-implanted surfaces [67]. With regard to the mechanisms by which ion implantation induces a wear resistant surface, Fayeulle [75] recently reviewed the literature for AISI 304 SS and proposed two main reasons for improvements: (1) increased hardness and yield and fracture strengths via formation of martensite and nitrides in the superficial layers and (2) stabilization of the austenitic phase so that a brittle, strain-induced martensite does not form.

The objectives of this work are 1) to examine the influence of implanted nitrogen dose and substrate temperature history on the tribological performance of typical stainless steels and 2) to gain

further insight into the detailed mechanisms by which this enhancement occurs.

### **Nitrogen Concentration Profiles**

Results obtained on nitrogen-implanted iron showed that the most wear resistant surfaces were produced on discs held at a temperature near  $380 \pm 50$  °C while they were being implanted to doses as high as  $1 \times 10^{18}$   $\text{N}_2/\text{cm}^2$ . These conditions produced a thick nitride layer containing mostly  $\gamma'$ - $\text{Fe}_4\text{N}$ , which was the most wear-resistant nitride observed in the tests. It was assumed that the stainless steels might also exhibit good tribological performance if they were implanted under similar conditions. Figure 18 shows typical nitrogen concentration profiles in AISI 304 stainless steel implanted at temperatures ranging from  $340$  to  $380 \pm 50$  °C at doses ranging from  $1 \times 10^{17}$  to  $1 \times 10^{18}$   $\text{N}_2/\text{cm}^2$ . These AES data show that the disc implanted at low temperature to a low dose ( $1 \times 10^{17}$   $\text{N}_2/\text{cm}^2$  at  $340 \pm 50$ °C) contains nitrogen distributed in the distorted gaussian profile predicted by LSS theory [98] and observed previously in this thesis for similar implantation conditions in pure iron. When the implantation temperature is increased to  $380 \pm 50$  °C, for the same dose, the profile is distorted further, the peak concentration drops, and the profile extends deeper into the material. Increases in dose to  $4 \times 10^{17}$  and  $1 \times 10^{18}$   $\text{N}_2/\text{cm}^2$  while holding the same temperature ( $380 \pm 50$ °C) induce still deeper profiles extending in the latter case to a depth over 850 nm at a nitrogen concentration of ~20 at. %. It is noteworthy that this deep nitrogen penetration, which is an order of magnitude greater than the ballistic range of ions predicted by LSS theory, occurs at about the same temperature that induced deeper

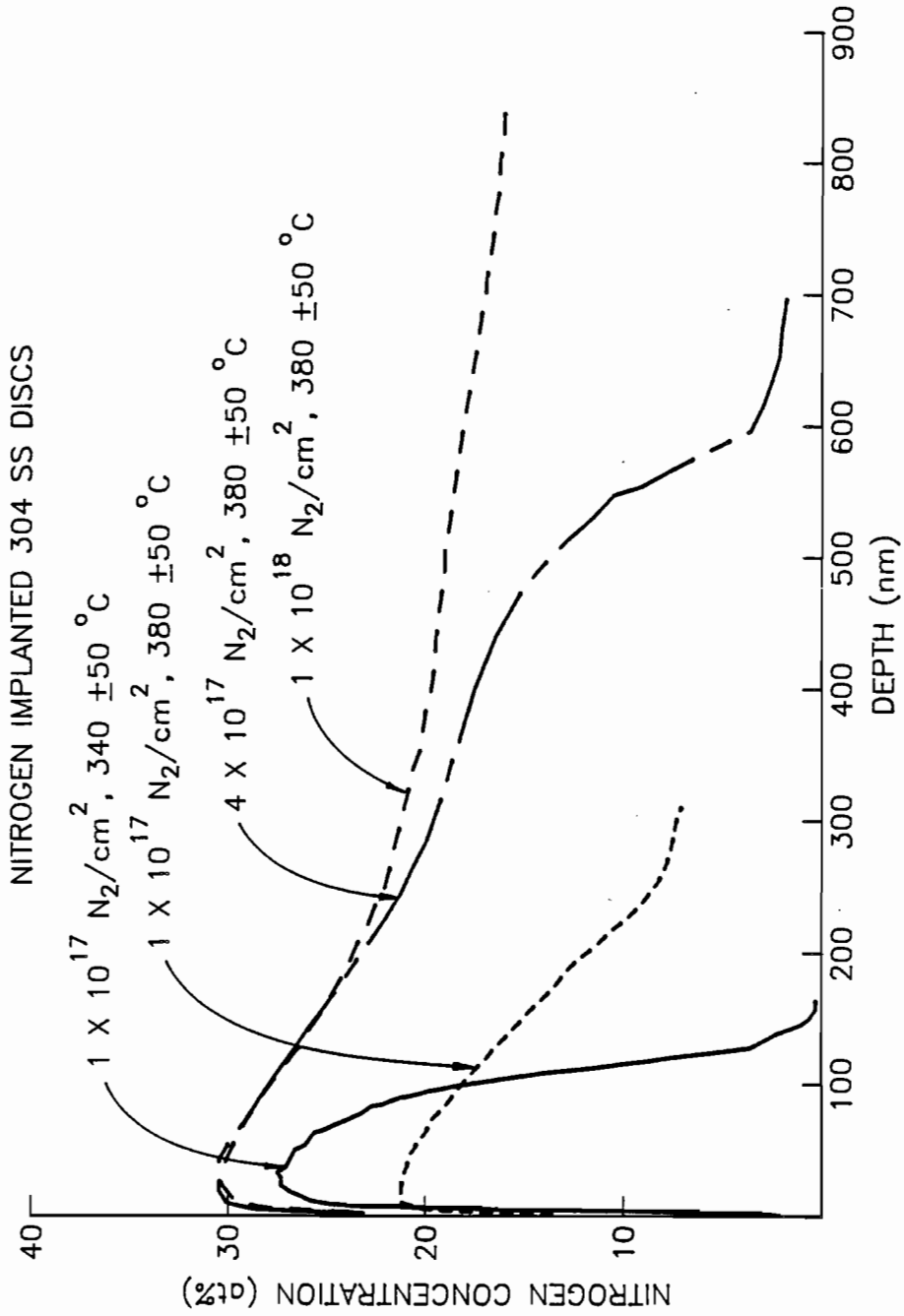


Fig. 18 Typical AES Profiles of Nitrogen Implanted 304 SS Discs



nitrogen penetration in pure iron. This is a striking result considering the fact that the composition and structure of these two materials are so different.

The data of Fig. 18 show very clearly that the proper combination of temperature and dose induce the same kind of deep nitrogen penetration that had a very beneficial tribological effect on the pure iron discs. It appears that the temperature assures the proper diffusion coefficient while the high dose assures both sufficient diffusion time and the amount of nitrogen needed to sustain concentrations at a high level. It should be pointed out that if the temperature is too high the nitrogen diffuses out of the free surface and concentrations can drop to low values where the tribological benefit of the implanted nitrogen would be expected to be minimal. It is also noted that the implantation temperatures cited in Fig. 18 are substantially higher than those used by most previous researchers.

#### **Mössbauer and XRD Analyses**

As with the pure iron, Mössbauer and XRD analyses enable one to track the formation and transformation of various phases and nitrogen compounds in stainless steels after implantation and throughout the wearing process. Thus, they facilitate identification of preferred phases and the implantation conditions that encourage their production. The typical CEMS data summarized in Fig. 19 pertain to 304 SS, but the results obtained for 310 SS are essentially the same (the only difference being that martensite formation is not induced in 310 SS during polishing). The details of the Mössbauer and XRD analyses are discussed in considerable detail elsewhere [101,102], but it is

important to note the following observations gleaned from this collective work:

1. Polishing of the 304 SS causes strains that induce an austenite-to-martensite transformation within a surface layer about 30 nm thick. The  $\alpha'$  indicated in Fig. 19a identifies the contribution of the martensite formed due to polishing in comparison to the  $\gamma$  peak produced by the austenite. The 310 SS spectrum is similar but its high nickel content stabilizes the austenite and prevents the formation of martensite.
2. Nitrogen implantation of 304 SS causes most of the martensite formed during polishing to revert back to austenite, as shown in Fig. 19b-e and observed previously [30].
3. When either 304 or 310 SS are implanted with nitrogen at a low temperature ( $<200$  °C) a paramagnetic nitride having the form  $\epsilon$ -(Fe, Cr, Ni)<sub>2</sub>N predominates, as shown in Fig. 19b. When the temperature is increased to 300 °C, a magnetic nitride [ $\epsilon$ -(Fe, Cr, Ni)<sub>x</sub>N (where  $x \approx 3$ )] is observed in addition to the paramagnetic phase, as shown in Fig. 19c. At much higher temperatures (500-600 °C) most of the nitrogen is in solution in the austenite, as indicated in Fig. 19e. On occasion low-Cr (or no Cr) ferrite or martensite is also present in 304 SS. At temperatures near 400 °C, the microstructure consists of a mixture of high nitrogen austenite (N in solid solution) and a small amount of  $\epsilon$ -(Fe, Cr, Ni)<sub>x</sub>N (and sometimes low-Cr ferrite in 304 SS), as shown in Fig. 19d.
4. Once an Fe-containing nitride (or nitrogen in solid solution), as shown in Fig. 19b-e, is formed in the implanted layer during

implantation, it remains in that form (i.e. no phase transformations occur) until it has been removed via the wearing process.

5. Even though polishing produces martensite in 304 SS, strain-induced martensite is not formed beneath the implanted layer as a result of wear process until the implanted layer is about to break.
6. When the implanted layer is removed as a consequence of wear, substantial martensitic transformation occurs in all 304 SS discs, as suggested by the data of Fig. 19f. This transformation does not occur in 310 SS because of its high Ni content.
7. Type 304 SS wear debris, collected on filter paper and analyzed by transmission Mössbauer spectroscopy, has a much higher ratio of martensite to austenite than the polished or worn surfaces do. This indicates a preferential removal of martensite or a transition to martensite as austenite is being strained and removed during the wearing process. If martensite is being removed preferentially this could be due to the more brittle nature of the martensitic phase and to the volume expansion associated with the austenite-to-martensite transformation. The latter is a likely mechanism for producing microcracks which propagate to the surface during wear and aid in material removal.

X-ray diffraction was used to confirm that the high nitrogen austenite phase (illustrated in Fig. 19 d and e) extends to a depth beyond  $1 \mu\text{m}$  for a surface implanted to a  $1 \times 10^{18} \text{ N}_2/\text{cm}^2$  dose at a

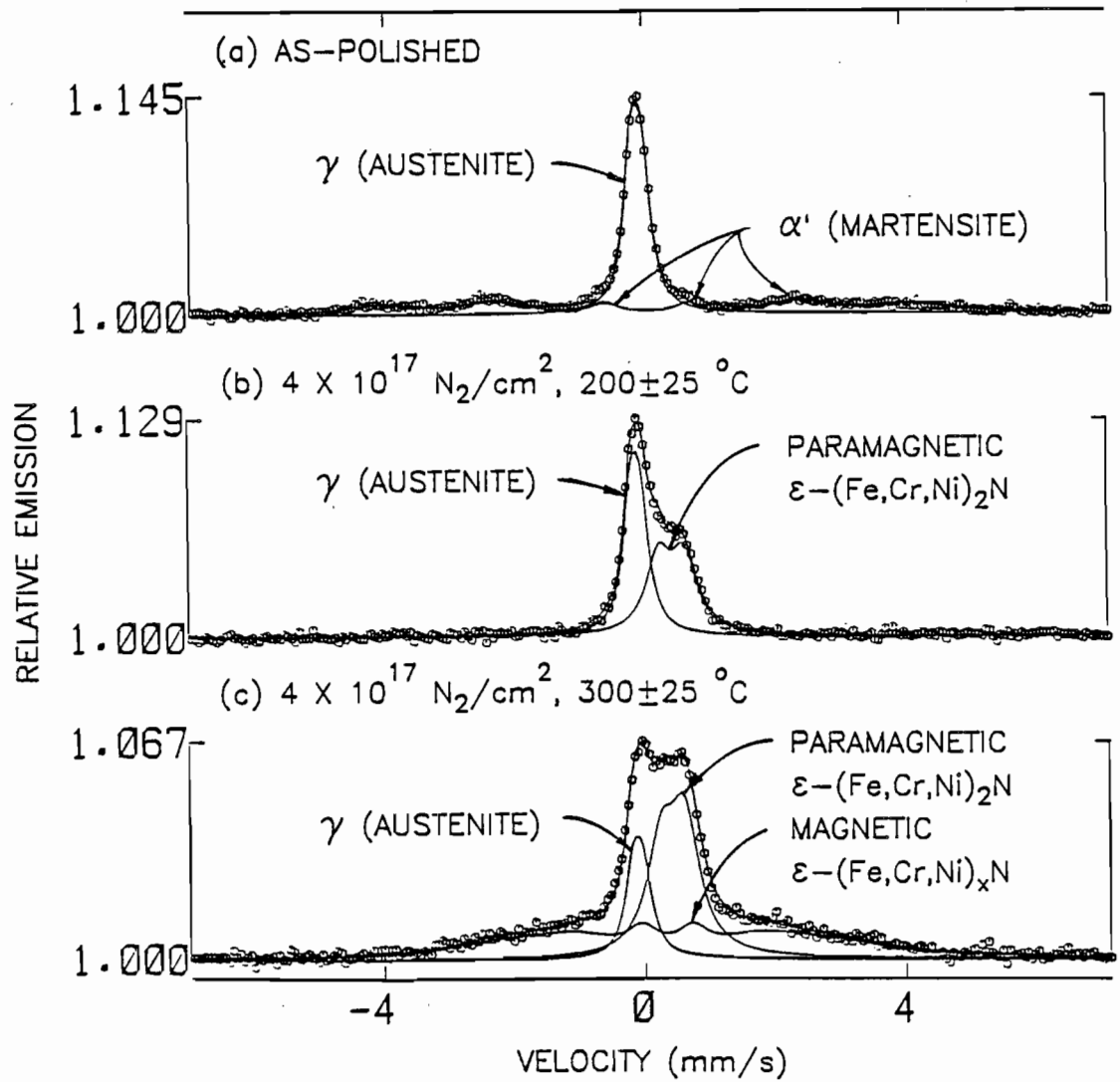


Fig. 19 Typical Conversion Electron Mössbauer Spectra of Nitrogen-Implanted 304 Stainless Steel, (a)-(c)

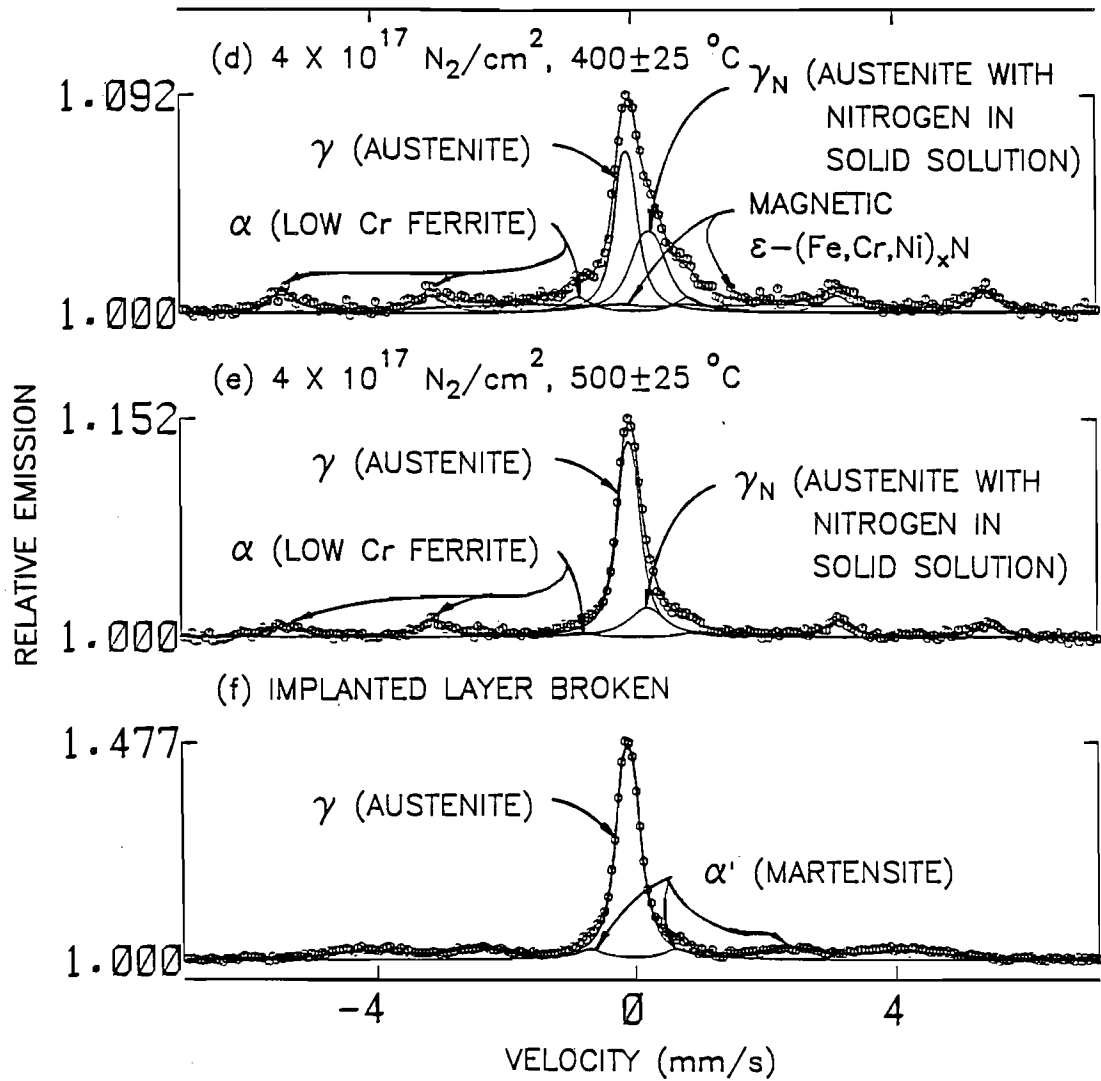


Fig. 19 (cont.) Typical Conversion Electron Mössbauer Spectra of Nitrogen-Implanted 304 Stainless Steel, (d)-(f)

temperature over  $\sim 400$  °C, in agreement with the AES data in Fig. 18. Because implantation above this temperature will be shown later to produce the most wear resistant surfaces, the observation of a thick layer of high-nitrogen austenite is considered to be important. It represents direct evidence that the mechanism of solid solution hardening and strengthening plays a major role in improving the tribological performance of ion-implanted stainless steels. It is noted that no CrN has been detected in this study, but it could be present in grain sizes below the detection limits of the test equipment ( $<10$  nm).

### **Oscillating Pin-On-Disc Wear Testing**

In a preliminary test, two AISI 304 SS discs (one unimplanted and the other implanted at 60 keV and  $100 \mu\text{A}/\text{cm}^2$  to a dose of  $1 \times 10^{17} \text{N}_2/\text{cm}^2$ ) were worn against 304 SS pins in the oscillating wear mode. Both were tested in the lubricated condition at a normal load of 1 N and an average sliding speed of 13 cm/s. The results of this test, which are shown in Fig. 20, reveal that the unimplanted disc wears away about 25 mg after a 25 hr test. This corresponds to a normalized wear rate near 2 mg/N/km while the implanted one exhibits a wear rate nearly three order of magnitude lower ( $\sim 0.006$  mg/N/km) during a 45 hr wear test. Examination of the worn surfaces of the two discs showed the unimplanted one was characterized by a roughness average ( $R_a$ ) an order of magnitude greater than that for the implanted one. Taken together these results indicated severe adhesive wear was occurring on the unimplanted disc while mild adhesive wear was occurring on the implanted one.

In view of the fact that different types of wear were occurring on the implanted and unimplanted discs, comparative tests were conducted to

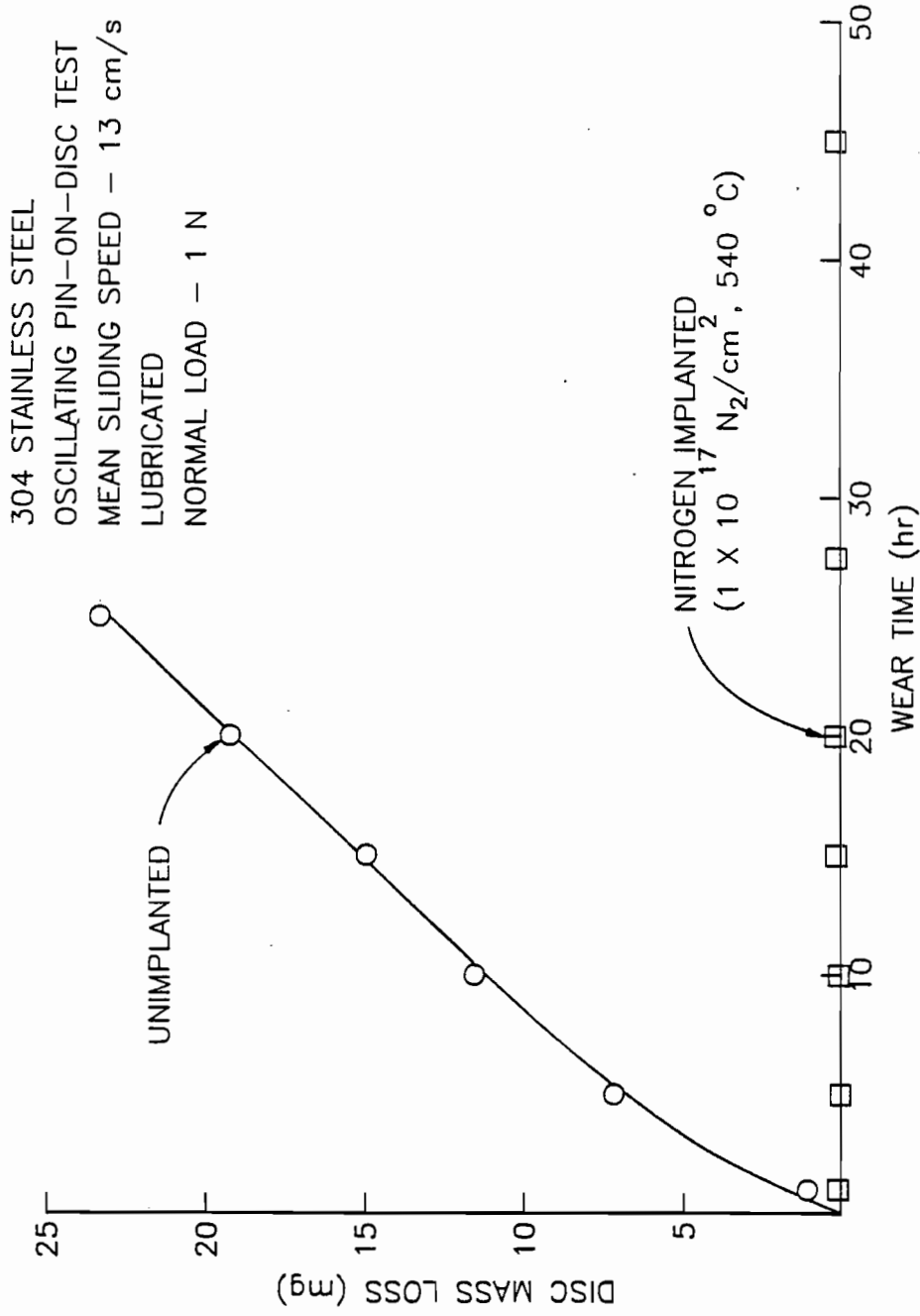


Fig. 20 Typical Sliding Wear Histories of Stainless Steel at 1 N Normal Load

determine the load at which the transition from mild to severe adhesive wear occurred in these two cases. Typical test results illustrating the nature of this transition are shown in Fig. 21. In the case of the disc implanted at the conditions identified on the figure, the wear rate was very low until a transition or critical load of 46 N was reached. For the unimplanted discs on the other hand, the high mass loss rate ( $\sim 2$  mg/N/km) and high roughness levels that characterize severe adhesive wear were observed down to the lowest load level indicated (0.1 N - the lowest load that could be applied reliably with the wear test machine). The unimplanted disc results exhibited substantial scatter, as suggested by the two sets of circular data points generated from separate but identical tests. The constancy of the disc mass loss rates associated with the data of Fig. 21a within each wear regime is appealing because it is consistent with the Archard wear model [104]. The tendency for the transition between wear modes to occur as a result of a small change in normal load (from 45 to 46 N for the implanted disc case) is particularly noteworthy.

Figure 21b shows roughness as a function of load for the discs that produced the wear test results of Fig. 21a. It can be seen that the roughness of the unimplanted discs increases with the load, while the roughness of the implanted one remains low below a 45 N normal load and then increases abruptly as the critical load, 46 N, is reached. The fact that a modest increase in normal load from 45 to 46 N caused the dramatic change in wear rate and roughness suggests that sudden implanted layer failure occurs at the critical load.

The changes in the disc and pin surface morphologies that accompany the mass loss rate and roughness changes shown in Fig. 21 are traced in



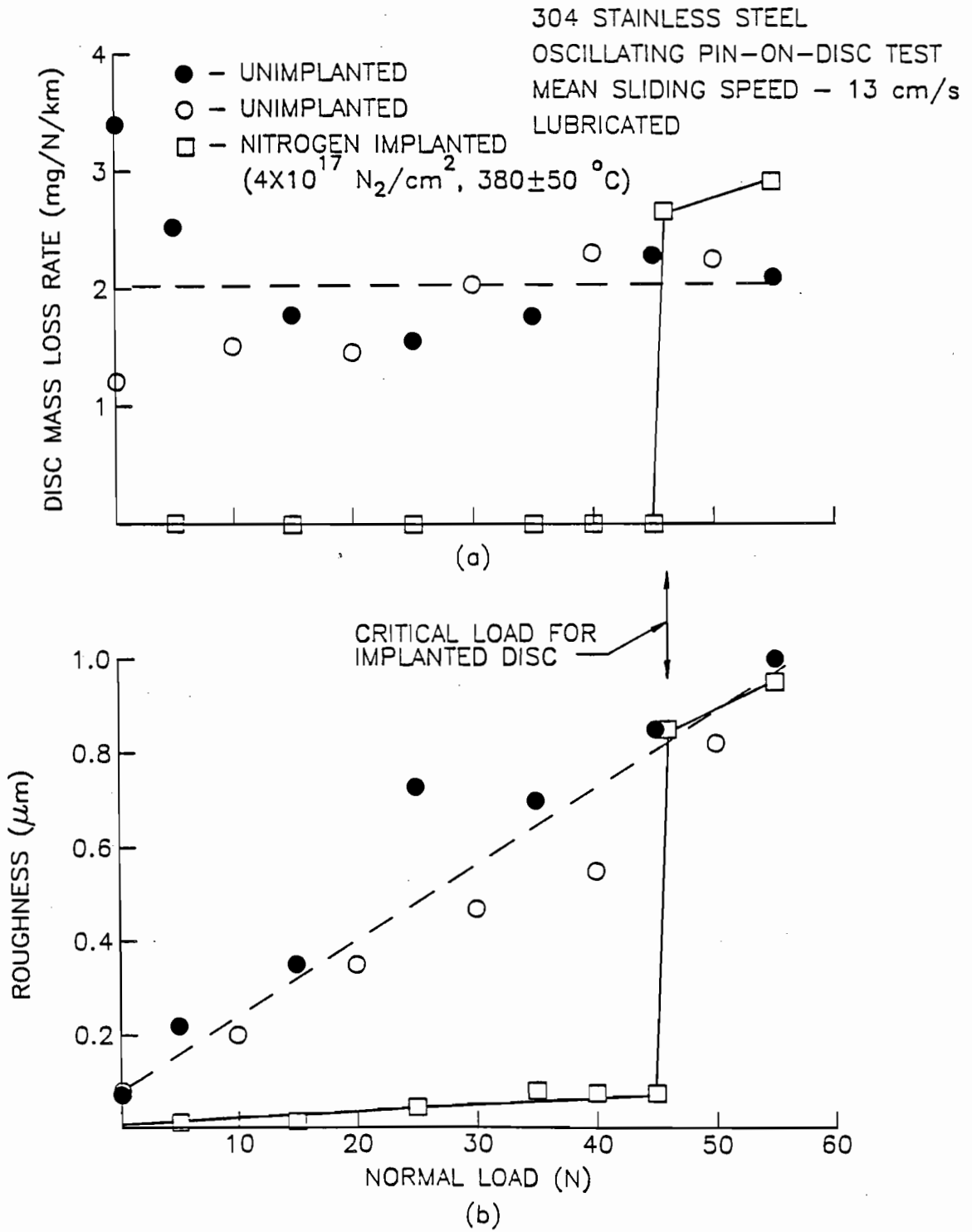


Fig. 21 Effect of Normal Load on Disc Mass Loss Rate (a) and Roughness (b)

304 STAINLESS STEEL  
 1 hr AT EACH LOAD, LUBRICATED  
 MEAN SLIDING SPEED - 13 cm/s

0.05 mm

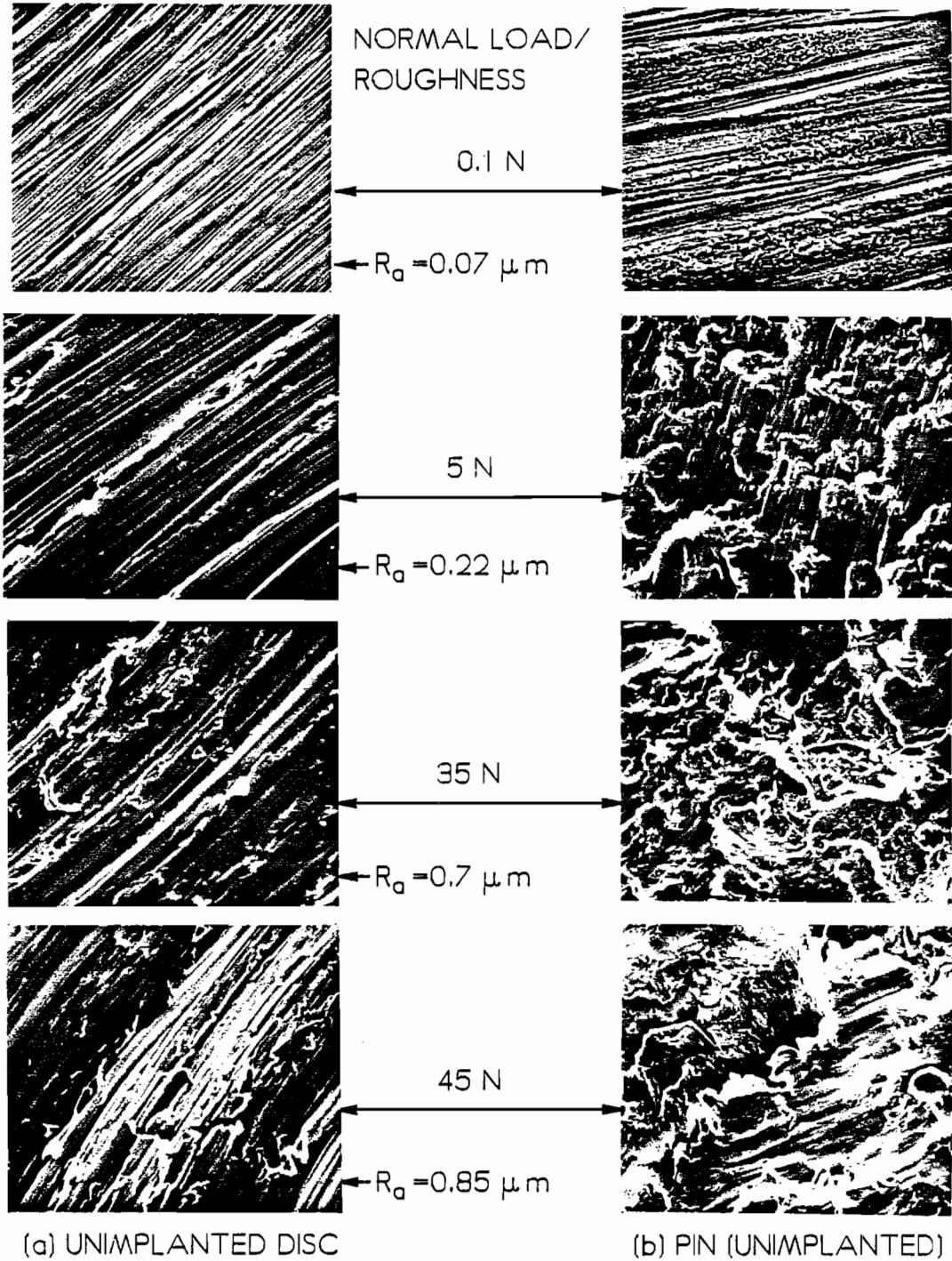


Fig. 22 Effect of Normal Load on the Surface Morphology of an Unimplanted 304 Stainless Steel Disc (a) and Pin (b) Pair

304 STAINLESS STEEL  
 1 hr AT EACH LOAD, LUBRICATED  
 MEAN SLIDING SPEED - 13 cm/s  
0.05 mm

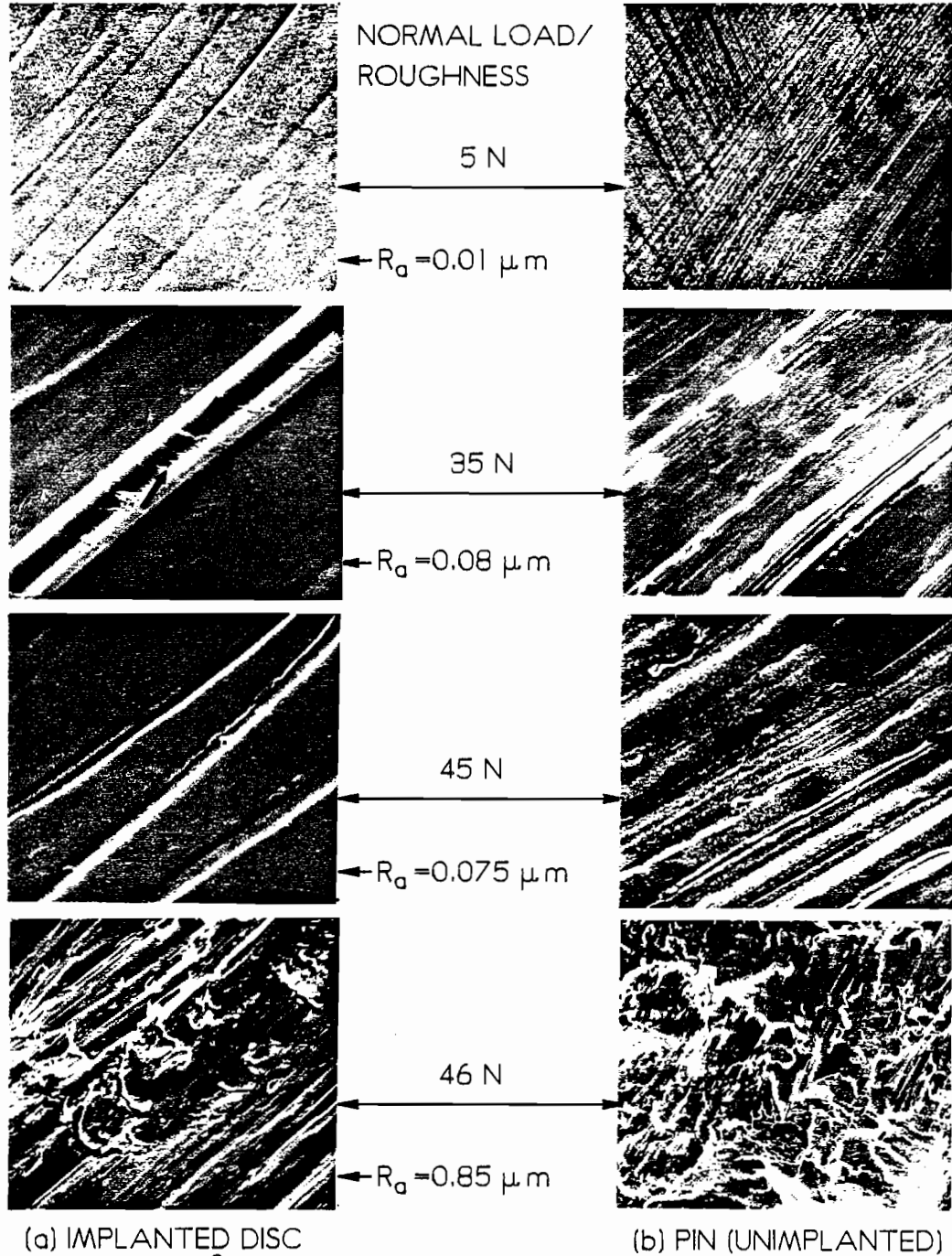


Fig. 23 Effect of Normal Load on the Surface Morphology of a Nitrogen-Implanted 304 Stainless Steel Disc (a) and Pin (b) Pair

the scanning electron micrograph sequences of Figs. 22 and 23 for the unimplanted and implanted discs, respectively. In Fig. 22 one observes a plowed appearance on the 304 stainless steel disc (a) at the lowest load (0.1 N). The pin (b) on the other hand shows evidence of wear involving asperity welding and tearing at even this low load. As the load is increased the asperity welding and tearing for the unimplanted case becomes more severe (torn junction size increases) on the pin, and this same appearance becomes apparent on the disc surface. In contrast, the implanted disc and pin show a totally different morphology in Fig. 23. Both the disc and pin have relatively shallow and sparse plowed grooves at all loads below the critical one (46 N for the case associated with Figs. 21 and 23). At and beyond this critical load the severely torn appearance characteristic of the unimplanted pins and discs develops.

Based on the results given in Figs. 21 through 23, the critical load is defined as the one at which the wear state changes from a mild one characterized by shallow plowing to a severe one characterized by asperity junction welding and tearing. Mössbauer and EDS studies also show that the nitrogen concentration and bonding states in the disc remain relatively unchanged until the critical load is exceeded. At this point, the nitrogen rapidly disappears from the surface. Figures 21 through 23 pertain to AISI 304 SS, but 310 SS discs exhibited the same behavior.

Careful examination of implanted disc wear tracks in Fig. 23 after 35 N load test reveals that small transverse cracks develop across wear tracks, as indicated by the arrow, at a load that is substantial but still below the critical value. It is believed that these cracks

initiate beneath the implanted layer as a consequence high stresses induced by pin [105] and that they propagate to the surface. At the critical load it is suggested that the implanted layer shears between adjacent cracks thereby allowing the pin to come into direct contact with material beneath the implanted layer.

Results like those in Figs. 21 through 23 demonstrate that nitrogen implantation improves the sliding wear resistance of the stainless steels under study by increasing the normal load required to induce the transition from mild to severe adhesive wear. Hence, the focus of the research can be properly directed at identifying the implantation conditions that will maximize this critical load. In order to do this, a number of AISI 304 and 310 SS discs were implanted to different doses and at different temperature. They were then tested using the procedures that yielded the critical load data of Fig. 21. Typically, the implanted discs were subjected to oscillating pin wear tests for 1 hour at a 1 N normal load. If the wear rate did not jump to a high value, the load was increased in 1 to 5 N increments depending on how close to the critical load the disc appeared to be. The 1 h wear test was then repeated. This process of increasing the normal load and wear testing was continued until the implanted layer failed and the critical load was established.

Data obtained on AISI 304 and 310 SS showing the effects of implanted ion dose and the temperature at which the implantation was carried out on the critical load are shown in Table 6. Some of these data are also presented in Fig. 24 to summarize the important trends. All of these data show that nitrogen ion implantation increases the critical load dramatically and therefore enhances the wear resistance of

both of these stainless steels in an equally dramatic way. As the data of Fig. 24a indicate, increases in dose induce substantial increases in

Table 6

## Critical Loads for Stainless Steel Discs

(Lubricated, Oscillating SS Pin Used Unless Noted Otherwise)

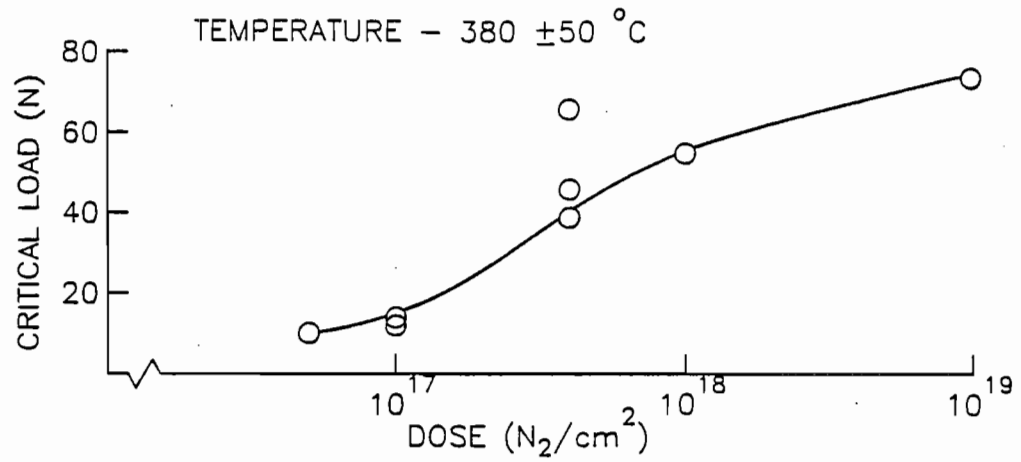
Disc No.	Implantation Conditions			Critical Load (N)
	Dose ( $\times 10^{17}$ N <sub>2</sub> /cm <sup>2</sup> )	Temp. (°C)	Time Held Over 330 °C	
S1	0	-		<0.1
S2	0	-		<0.1
S3	0	-		<0.1
S4	0	-		<0.1
S5	0.5	280		<5
S6	0.5	400		10
S7	1	320 ±50		5
S8	1	340 ±50		5
S9	1	380 ±50	2 min	12
S10	1	380 ±50	3 min	14
S11	1	500		11
S12	1	540		7.5
S13	4	350		15
S14	4	380 ±50	13 min	39
S15	4	380 ±50	18 min	46
S16	4	380 ±50	22 min	66
* S17	4	100 ±25		6
* S18	4	220		4
* S19	4	300 ±25		22
* S20	4	400 ±25		50
* S21	4	500 ±25		51
* S22	4	600 ±25		72
S23	10	380 ±50	50 min	55
S24	100	380 ±50	110 min	73
** S25	0	-		-
** S26	1	380 ±50		22
T1	0	-		<0.1
T2	0.5	380 ±50		9
T3	1	380 ±50		27
T4	4	380 ±50		24
T5	10	380 ±50		52

S--304 Stainless Steel

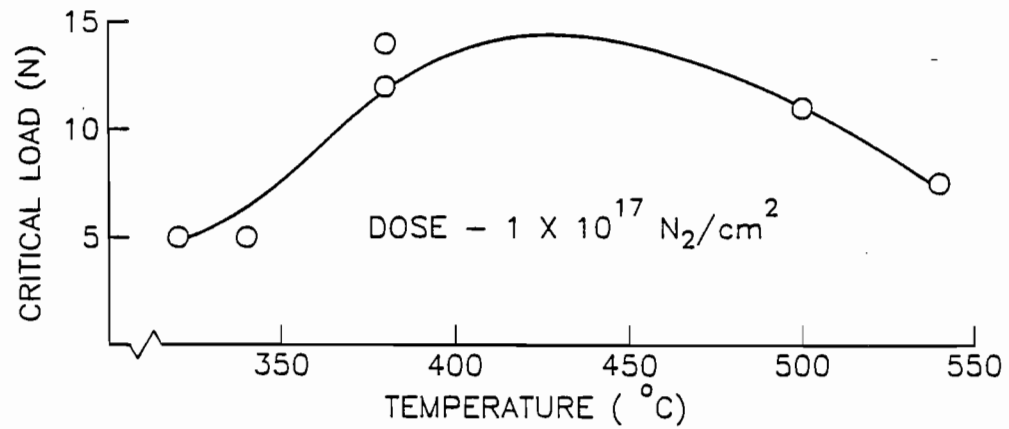
T--310 Stainless Steel

\* WC Pin Test.

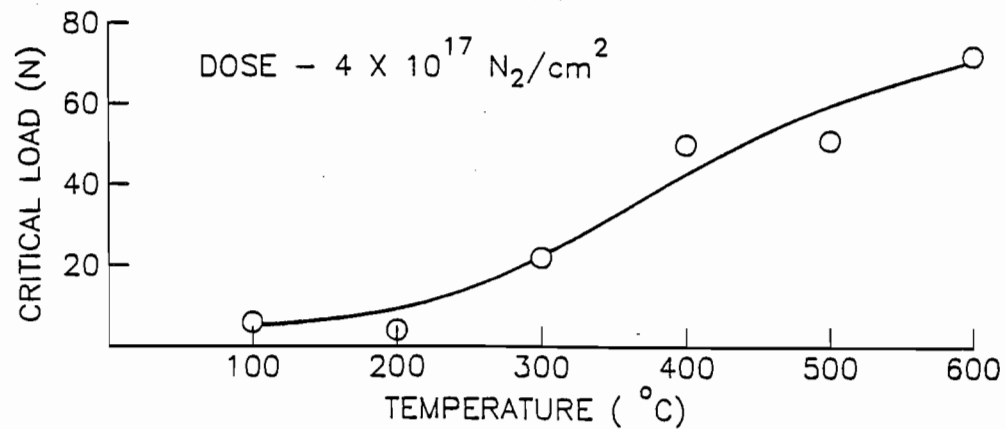
\*\* Fixed Pin Wear Test



(a)



(b)



(c)

Fig. 24 Effects of Implanted Nitrogen Dose and Implantation Temperature on the Critical Loads for 304 Stainless Steel

the critical load at an implantation temperature near  $380 \pm 50^\circ\text{C}$ . At the highest dose ( $100 \times 10^{17} \text{ N}_2/\text{cm}^2$ ) the critical load is over 700 times that for the unimplanted material (the critical load for unimplanted stainless steel is less than 0.1 N, as mentioned previously). The capacity to realize continued increases in critical load with increased dose levels is, however, realized only when the implantation temperature is sufficiently high to facilitate nitrogen diffusion. The three data points on Fig. 24a at a dose of  $4 \times 10^{17} \text{ N}_2/\text{cm}^2$  are worthy of special mention. At first glance, they suggest substantial data scatter, but they actually represent three cases (S14, S15, and S16) where the same dose and temperature were maintained but the times the discs were at moderate temperatures ( $>330^\circ\text{C}$ ) were different as shown in Table 6. It is argued therefore that the critical loads associated with these discs increase with implantation (and therefore diffusion) times. This same trend is also observed at the lower dose of  $1 \times 10^{17} \text{ N}_2/\text{cm}^2$  (discs S9 and S10 in Table 6).

The effect of implantation temperature on critical load for the samples implanted to a dose of  $1 \times 10^{17} \text{ N}_2/\text{cm}^2$  is shown in Fig. 24b. It shows results consistent with those obtained using pure iron (Figs. 8 and 9) that indicate the preferred implantation temperature is near  $380^\circ\text{C}$  for this dose. This result is also consistent with AES results that suggest implantation at higher temperatures facilitates formation of a thicker nitrogen-containing layer. At sufficiently high temperatures, one might expect substantial nitrogen loss because it would diffuse too rapidly. In spite of this effect, the data of Fig. 24c show that higher temperatures ( $500 - 600^\circ\text{C}$ ) do have a beneficial effect on the critical load provided a higher dose is



implanted ( $4 \times 10^{17} \text{ N}_2/\text{cm}^2$ ). In this case the higher dose must be sufficient to sustain a high concentration of nitrogen in the layer in spite of more rapid diffusion. On the basis of the data in Table 6 and Fig. 24 it is argued that higher doses coupled with higher temperatures should result in greater nitrogen retention in thick layers and even more wear-resistant (higher critical load) surfaces.

It is noted that the data of Fig. 24c were obtained using a tungsten carbide (WC) pin rather than the SS ones that were used in the other tests. This was done because the WC pin wore very little during the tests while flat spots of order 1 mm in dia. could be worn on the heads of the SS ones during a test. By changing the pin material, the effect of pin contact area on measured critical loads was investigated. Comparisons made during this study showed that changes in the pins and/or pin contact area induced no significant changes in the test results.

Taken together, the critical load, AES, Mössbauer and XRD data suggest the high critical loads are realized when temperatures and doses are sufficiently high so nitride dissolution coupled with significant nitrogen diffusion occurs and a solid solution of nitrogen in austenite at concentration levels in the 10 to 20 at.% range develops within a relatively thick layer ( $>1 \mu\text{m}$ ) [101]. The observed increase in layer strength induced by nitrogen solid solution hardening compares favorably with the observations of Werner [105] on bulk nitrogen-alloyed steels.

#### **Fixed Pin-on-Disc Tests**

In order to provide points of comparison with the oscillating pin-on-disc tests, a few fixed pin-on-disc tests were also conducted. In

one test, unimplanted and nitrogen implanted 304 SS discs were worn in a lubricated environment with a normal load of 1 N and a sliding velocity of 9 cm/s for 20 h. It was found that the mass loss rate from the implanted disc was within the measurement uncertainty of zero while that for the unimplanted one was large. Hence, tests similar to those conducted using the oscillating pin apparatus were conducted to determine the critical loads for both unimplanted and implanted stainless steels. Figure 25 shows typical results obtained in these fixed pin-on-disc tests. The results are qualitatively similar to those observed in the oscillating pin-on-disc tests (Fig. 21). Careful comparison of the fixed and oscillating pin data shows, however, that the wear rates are lower and critical loads are higher for the fixed pin tests than they were for the oscillating pin tests (S9 and S10 in Table 6). As with the iron samples, these differences are related to the fact that plastic deformation of the disc surface causes shoulders to form on each side of a plowing track formed by the pin and an oscillating pin removes these shoulders more rapidly and, therefore, induces more rapid wear than that measured in the fixed pin tests.

### **Frictional Effects**

The coefficients of friction for both unimplanted and implanted AISI 304 and 310 SS discs were measured at a sliding speed of 3 cm/s using the fixed pin apparatus with WC and 304 SS pins under both lubricated and unlubricated conditions. The implanted discs used in this test were given a dose of  $1 \times 10^{17} \text{ N}_2/\text{cm}^2$  at a temperature of  $380 \pm 50 \text{ }^\circ\text{C}$ . Figure 26a shows the variation in coefficient of friction with normal load for both unimplanted and implanted AISI 304 SS discs under lubricated

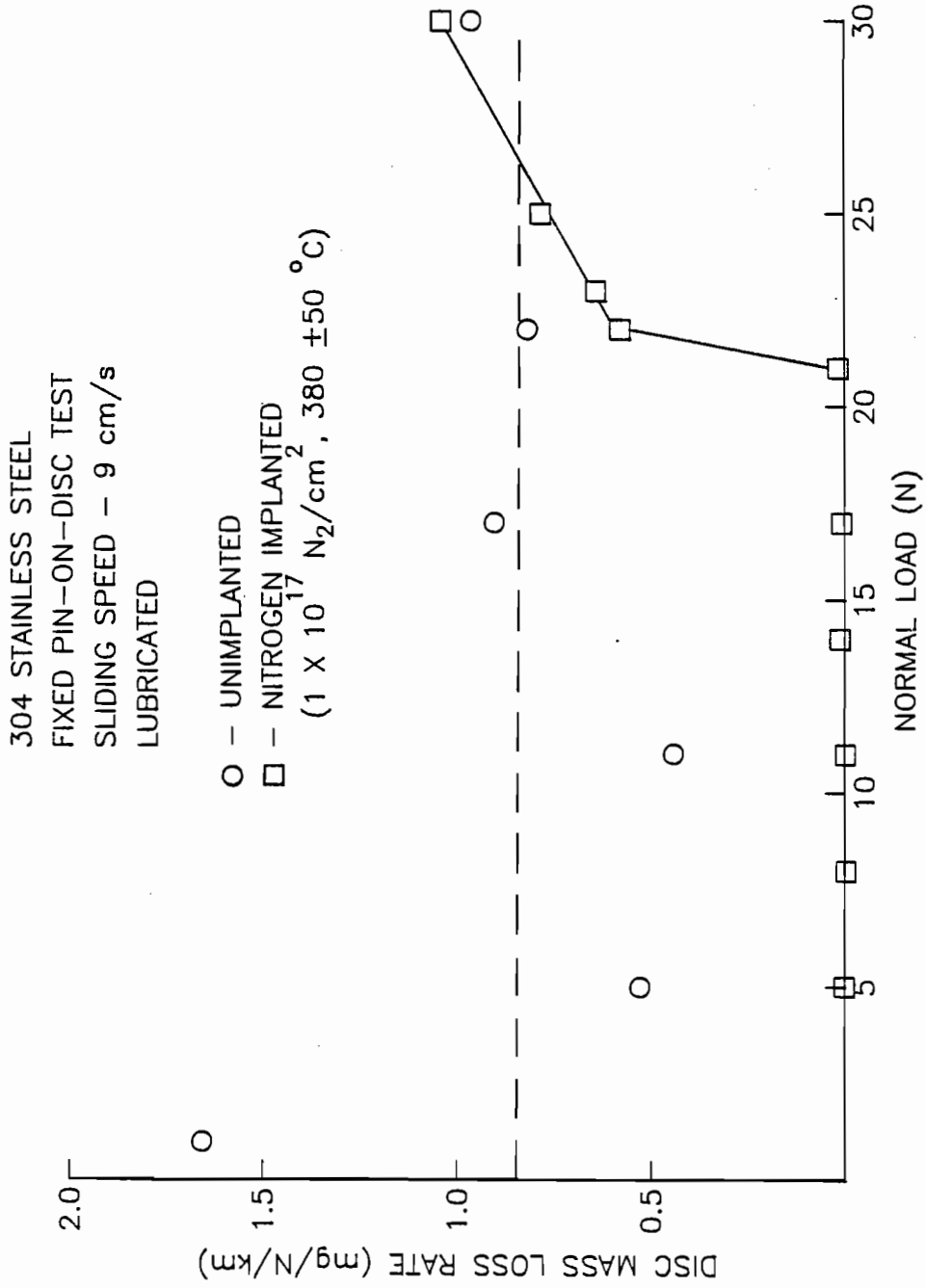


Fig. 25 Effect of Normal Load on Disc Mass Loss Rate - Fixed Pin Test

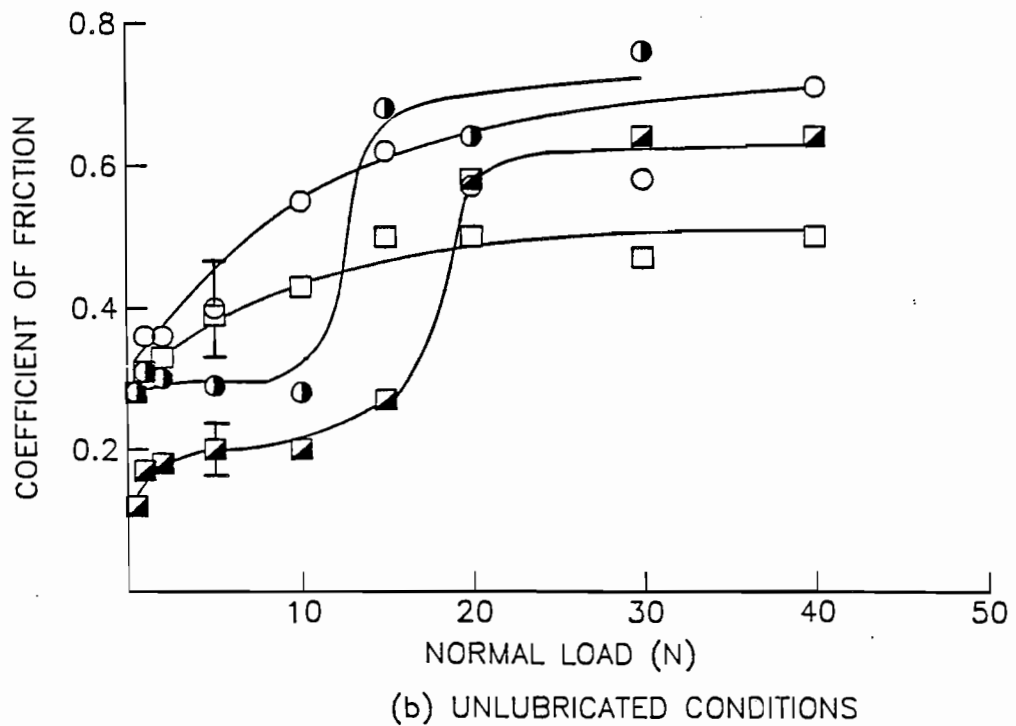
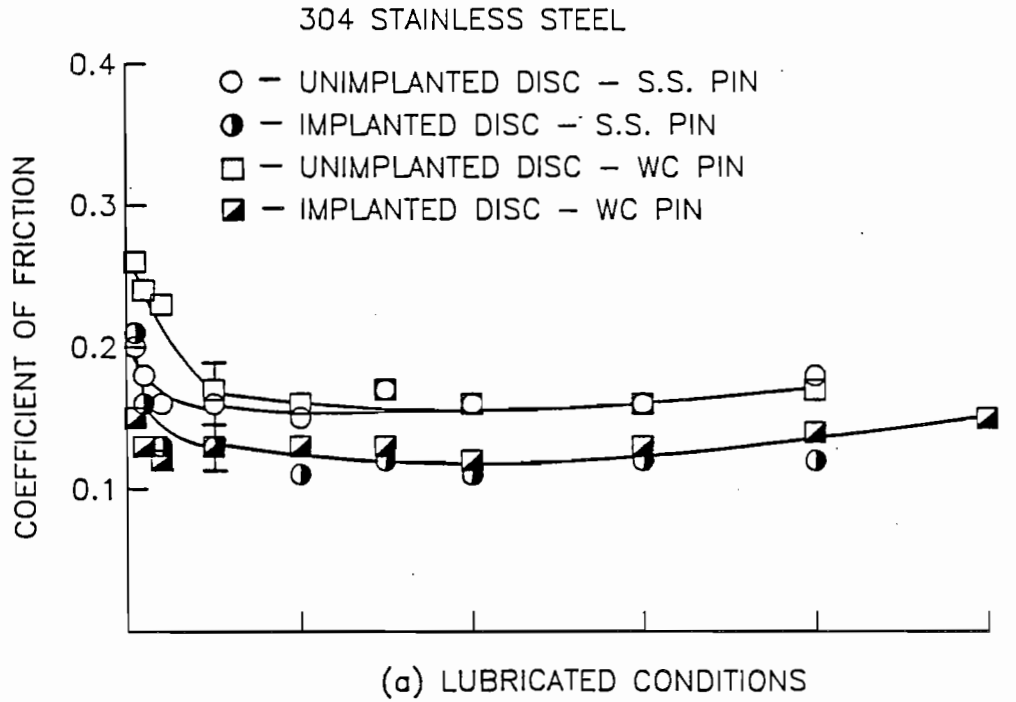


Fig. 26 Effects of Normal Load, Pin Material and Lubrication on Friction Coefficient - Fixed Pin Test

conditions. It can be seen that nitrogen ion implantation reduces the coefficient of friction by about 25%. The increase in coefficient of friction observed as the normal load is reduced to very low values is believed to be related to the viscous drag associated with the lubricant, which could become significant at these loads.

When tests are conducted under unlubricated conditions generally higher friction coefficients are measured as the data of Fig. 26b show. The friction coefficients also exhibit the following dependencies on applied normal load that differ from those observed in the lubricated tests.

1. The friction coefficient increases with load in the low load range. This is believed to be an effect related to removal of a lubricating oxide layer from the disc.
2. Lower coefficients of friction are related with the WC pins (possibly because adhesive forces are lower).
3. A sudden increase in the coefficients of friction of the implanted discs to values greater than those for unimplanted discs are observed when critical loads are exceeded.

Note that the error bars on each curve in Fig. 26 indicate the typical range of data scatter for the tests associated with that curve. The data given in Fig. 26 were all measured using AISI 304 SS discs, but results obtained using 310 SS are essentially identical.

The reduction in coefficient of friction for nitrogen-implanted stainless steels is believed to be due to the fact that the implanted layer prevents asperity welding and the high shear forces required to break them. It is noted that a transition to severe adhesive wear did not occur in the lubricated tests (Fig. 26a) even though loads exceeded

the critical values measured in the fixed pin tests (Fig. 25). The transition probably didn't occur because friction tests were conducted for only a few minutes rather than the hour periods used for the wear tests. The transitions would probably have been observed if times and/or normal loads had been increased.

### **Microhardness Measurements**

The Vickers microhardness values ( $H_V$ ) of typical AISI 304 SS discs used in these tests were also measured using the ultralight load microhardness tester. Typical results of these measurements showing the effects of polishing and implantation on disc hardness are given in Fig. 27. These results, shown in the form of a plot of microhardness as a function of indenter load, illustrate the fact that the bulk material hardness is sensed at loads above  $\sim 0.1$  N. Even at the lowest load levels, the hardness is affected by the bulk and is not truly representative of the implanted layer. In spite of this deficiency, the following observations can be made on the basis of the data:

1. The slight increase in hardness as indenter load is reduced on the as-received material from which the discs were made is probably due to an oxide layer or the formation of hard martensite during indenter loading.
2. Polishing increases the disc hardness slightly, probably because of the austenite-to-martensite transformation this polishing induces.
3. Nitrogen ion implantation induces an increase in surface hardness. As the implanted ion dose is increased and the

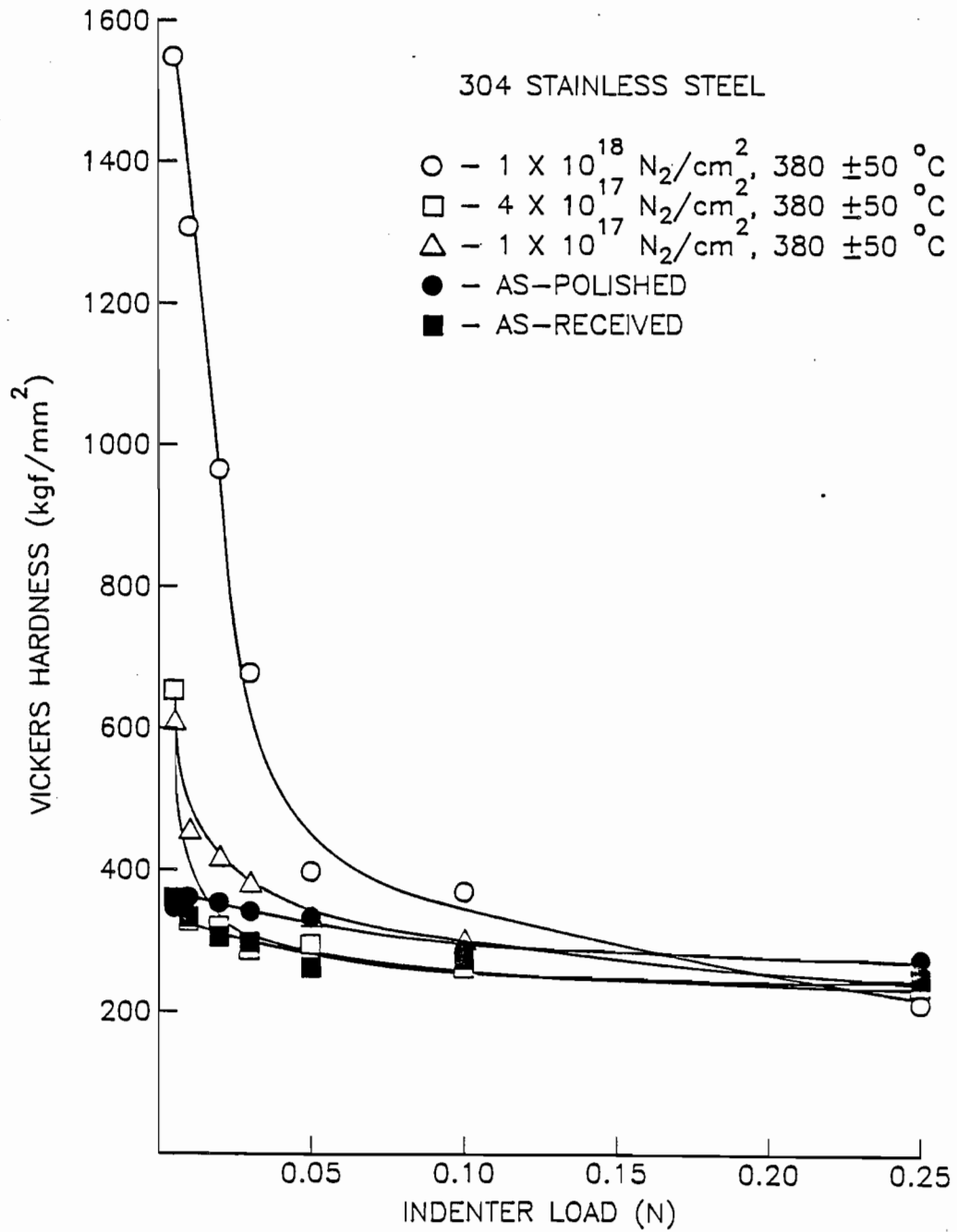


Fig. 27 Effects of Ion Implantation on the Microhardness for 304 Stainless Steel

implanted layers grow in thickness (Fig. 18), the indicated hardness at low loads increases dramatically.

It is noteworthy that the highest hardness measured in the tests reached  $\sim 1600 \text{ kgf/mm}^2$ , which is over four times the bulk material hardness. This increase exceeds the hardness measurement uncertainty (generally 20 - 30%) by an amount sufficient to demonstrate that the effect is real. In order to hold the measurement uncertainty at this level when light loads were applied to the high dose implanted surfaces, it was again necessary to measure the size of the indentations using an SEM. This was required because the small indentation diagonals ( $0.7 \mu\text{m}$  at  $H_V = 1600 \text{ kgf/mm}^2$  for instance) are beyond the capability of an optical microscope.



## CONCLUSIONS

Nitrogen ion implantation into  $\alpha$ -Fe and stainless steels induces great improvements in the mild adhesive wear behavior and the transition to severe adhesive wear, respectively. Deep penetration of implanted nitrogen ( $\sim 1 \mu\text{m}$ ) can be achieved when the implantation is accomplished at low ion energies provided a sufficiently high dose is delivered and the surface being implanted is maintained at a temperature that facilitates significant nitrogen diffusion. Such deep penetration prolongs the mild adhesive wear lifetime for  $\alpha$ -Fe ferrite and induces a dramatic (100 to 1000 fold) increase in the critical load at which adhesive wear undergoes a transition from mild to severe conditions for austenitic stainless steels.

The wear resistance of nitrogen-implanted ferrite is determined by the nitride formed. Ranked from most to least wear resistant the nitrides observed are  $\gamma'$ -Fe<sub>4</sub>N (20 at.% N),  $\epsilon$ -Fe<sub>3</sub>N (25 at.% N), and  $\zeta$ -Fe<sub>2</sub>N (33 at.% N). On the other hand, the most wear resistant surfaces are produced in austenitic stainless steels when the nitrogen is in solid solution. The fact that implantation temperatures near 380 °C induce rapid layer growth in both ferrite and the stainless steels suggests that this is the temperature at which near-surface nitrides undergo the thermal decomposition that precedes nitrogen diffusion.

High dose, rapid implantation at the elevated temperatures readily realized in a high beam current density implanter facilitate production

of thick layers of both the preferred  $\gamma'$  phase in ferrite and a solid solution of nitrogen in austenite. The commercial implications of this finding are considered to be great, especially when it is recognized that the processing was effected rapidly and inexpensively in these tests because the implantation was accomplished at high current densities.

Wear tests conducted using the oscillating pin-on-disc wear tester demonstrate that nitrides do not break up during the wearing process so it is unlikely that significant nitrogen diffusion occurs as a surface is being worn. Data collected in both the fixed and oscillating pin-on-disc modes suggest that tests conducted using the fixed pin device can be interpreted erroneously to suggest wear-induced nitrogen migration is occurring when it is not. Thus, it is concluded that the oscillating pin wear tester should be used to study the tribology of ion implanted surfaces and possibly surfaces covered with thin coatings. Tests conducted on the oscillating pin device indicate the wear rate stabilizes at the steady-state value for unimplanted iron and evidence of nitrogen on or near the surface disappears when the mass worn from the surface is equal to the thickness of the implanted layer.

## REFERENCES

- [1]. J. K. Hirvonen, C. A. Carosella, R. A. Kant, I. Singer, R. Vardiman and B. B. Rath, "Improvement of Metal Properties by Ion Implantation," Thin Solid Films, 63 (1979) 5.
- [2]. S. T. Picraux, "Ion Implantation Metallurgy," Phys. Today, Nov. (1984) 38-44.
- [3]. A. j. Perry and D. J. Rowcliffe, "Friction Changes in Ion-Implanted Steel," J. Mater. Sci., 8 (1973) 900.
- [4]. N. E. W. Hartley, "Ion Implantation and Surface Modification in Tribology," Wear, 34 (1978) 427.
- [5]. G. Dearnaley and N. E. W. Hartley, "Ion Implantation into Metals and Carbides", Thin Solid Films, 54 (1978) 215.
- [6]. N. E. W. Hartley, "Applications for Ion Implantation as a Surface Treatment Process in Production Engineering," Radiat. Eff., 44 (1979) 19.
- [7]. G. Dearnaley, "Application of Ion Implantation in Metals," Thin Solid Films, 107 (1983) 315.
- [8]. J. K. Hirvonen, "Ion Implantation in Tribological and Corrosion Science," J. Vac. Sci. Technol., 15 (5) (1978) 1662.
- [9]. N. E. W. Hartley, "Friction and Wear of Ion-Implanted Metals-A Review," Thin Solid Films, 64 (1979) 177-190.
- [10]. A. K. Suri, R. Nimmagadda and R. F. Bunshah, "Influence of Ion Implantation and Overlay Coatings on Various Physico-Mechanical and Wear Properties of Stainless Steel, Titanium and Aluminum," Thin Solid Films, 64 (1979) 191-203.
- [11]. H. Herman, W. W. Hu, C. R. Clayton, J. K. Hirvonen, R. Kant and R. K. Maccrone, "Modification of Mechanical Properties by Ion Implantation," Thin Solid Films, 73 (1980) 189.
- [12]. H. T. Li, P. S. Liu, S. C. Chang, H. C. Lu, H. H. Wang and K. Tao, "Some Experimental Studies on Metal Implantation," Nucl. Instrum. Meth., 182-183 (1981) 915.
- [13]. H. Bakhru, W. Gibson, C. Burr, A. J. Kumnick and G. E. Welsch, "Modification of the Fatigue Behavior of Copper and Stainless

- Steel by Ion Implantation," Nucl. Instrum. Meth., 182/183 (1981) 959-964.
- [14]. Z.-Y. Xie, Y.-M. Qiao-Yong and C.-R. Lin, "Ion Implantation for Improving Wear Resistance of Metals," in V. Ashworth, W. A. Grant and R. P. M. Procter (eds.), Proc. Conf. on Ion Implantation into Metals, Manchester, 1981, Pergamon, Oxford, (1982), 117.
- [15]. S. Saritas, R. P. M. Procter, V. Ashworth and W. A. Grant, "The Effect of Ion Implantation on the Friction and Wear Behavior of a Phosphor Bronze", Wear, 82 (1982) 233.
- [16]. S. A. Dillich and I. L. Singer, "Effect of Titanium Implantation on the Friction and Surface Chemistry of a Co-Cr-W Alloy," Thin Solid Films, 108 (1983) 219.
- [17]. R. Hutchings and W. C. Oliver, "A Study of the Improved Wear Performance of Nitrogen-Implanted Ti-6Al-4V," Wear, 92 (1983) 143
- [18]. G. Dearnaley, F. J. Minter, P. K. Rol, A. Saint and V. Thompson, "Microhardness and Nitrogen Profiles in Ion Implanted Tungsten Carbides and Steels," Nucl. Instrum. and Meth. Phys. Res., B7/8 (1985) 88-94.
- [19]. R. Wei, W. S. Sampath and P. J. Wilbur, "Cross-Sectional Transmission Electron Microscopy Studies on Ultrahigh Dose Rate Ion Implanted Aluminum," Proceedings of the Shanghai Workshop on Ion Implantation, ed. by Zou Shichang Hangzhou, China, (1988) 244.
- [20]. D. S. Grummon, J. W. Jones and G. S. Was, "Fatigue Damage Accumulation in Nickel Modified by Ion Beam Surface Microalloying," Metall. Trans., 19 A (1988) 2775-2787.
- [21]. S. L. Russo, P. Mazzoldi, I. Scotoni, C. Tosello and S. Tosto, "Effect of Nitrogen-Ion Implantation on the Unlubricated Sliding Wear of Steel," Appl. Phys. Lett., 34 (1979) 627.
- [22]. R. N. Bolster and I. L. Singer, "Surface Hardness and Abrasive Wear Resistance of Ion Implanted Steels," ASTL Paper, 80-LC-8B-3, (1980) 6.
- [23]. I. L. Singer and R. N. Bolster, "Surface Hardness and Abrasive Wear Resistances of Nitrogen-Implanted Steels," in C. M. Preece and J. K. Hirvonen (eds.) Ion Implantation Metallurgy, Proc. 2nd Int. Conf. , Metallurgical Society of AIME, Warrendale, PA, (1980) 116.
- [24]. R. N. Bolster and I. L. Singer, "Surface Hardness and Abrasive Wear Resistance of Nitrogen-implanted Steels," Appl. Phys. Lett., 36 (1980) 208-209.
- [25]. T. Varjoranta, J. Hirvonen and A. Anttila, "Measuring the Wear of Nitrogen-Implanted Steel," Thin Solid Films, 75 (1981) 241.

- [26]. I. L. Singer and J. S. Murday, "Chemical State of Ion-Implanted Nitrogen in Fe18Cr8Ni Steel," J. Vac. Sci. Technol., 17 (1980) 327-329.
- [27]. M. Baron, A. L. Chang, J. Schreurs and R. Koszowski, "Nitrogen Distribution and Nitride Precipitation in  $^{14}\text{N}^+$  Ion Implanted 304 and 316 Steels," Nucl. Instrum. Meth., 182/183 (1981) 531-538.
- [28]. P. D. Goode and I. J. R. Baumvol, "The Influence of Ion Implantation Parameters on the Surface Modification of Steels," Nucl. Instrum. Meth., 189 (1981) 161-168.
- [29]. G. Dearnaley and P. D. Goode, "Techniques and Equipment for Non-Semiconductors Applications of Ion Implantation, Part III, Nucl. Instrum. Meth., 189 (1981) 117.
- [30]. R. G. Vardiman, R. N. Bolster and I. L. Singer, "The Effect of Nitrogen Implantation on Martensite in 304 Stainless Steel," in Metastable Materials Formation by Ion Implantation, eds. S. T. Picraux and W. J. Choyke, Elsevier Science Pub. Co., Inc., (1982) 269-274.
- [31]. J. L. Whitton, M. M. Ferguson, G. T. Ewan, I. V. Mitchell and H. H. Plattner, "Rutherford Backscattering Nuclear Reaction and Channeling Studies of Nitrogen Implanted Single-Crystal Stainless Steel," Appl. Phys. Lett., 41 (1982) 150-152.
- [32]. H. Herman, "Modification of the Surface Mechanical Properties of Ferrous Alloy by Nitrogen Ion Implantation," in V. Ashworth, W. A. Grant and R. P. M. Procter (eds.), Proc. Conf. on Ion Implantation into Metals, Manchester, 1981, Pergamon, Oxford, (1982) 102.
- [33]. F. G. Yost, L. E. Pope, D. M. Follstaedt, J. A. Knapp and S. T. Picraux, "Friction and Wear of Stainless Steels Implanted With Ti and C," in S. T. Picraux and W. J. Choyke (eds.), Metastable Materials Formation by Ion Implantation, Material Res. Soc. Symp. Proc., 7 (1982) 261.
- [34]. J. Ferrante and W. R. Jones, Jr., "Friction, Wear, and Auger Analysis of Iron Implanted with 1.5 MeV Nitrogen Ions," NASA Tech. Paper 1989, (1982).
- [35]. F. G. Yost, S. T. Picraux, D. M. Follstaedt, L. E. Pope and J. A. Knapp, "The Effects of N<sup>+</sup> Implantation on the Wear and Friction of Type 304 and 15-5 PH Stainless Steels," Thin Solid Films, 107 (1983) 287-295.
- [36]. D. M. Follstaedt, L. E., Pope, J. A., Knapp, S. T., Picraux, and F. G. Yost, F.G., "The Microstructure of Type 304 Stainless Steel Implanted With Titanium and Carbon and Its Relation to Friction and Wear Tests," Thin Solid Films, 107 (1983) 259-267.

- [37]. F.-Z. Cui, H.-L. Li and X.-Z. Zhang, "Modification of Tribological Characteristics of Metals After Nitrogen Implantation," Nucl. Instrum. Meth., 209/210 (1983) 881-887.
- [38]. G. Welsch and J. J. Wang, "Fatigue Deformation Behavior of Nitrogen-Ion Implanted Surface Layers of Type 304 Stainless Steel," Solid Thin Films, 107 (1983) 305-314.
- [39]. L. E. Pope, F. G. Yost, D. M. Follstaedt, J. A. Knapp and S. T. Picraux, "Effects of Ion Implantation on Friction and Wear of Stainless Steels," Proc. Intl. Conf. on Wear of Materials, Reston, VA, 1983, American Society of Mechanical Engineers, New York, (1983) 280-287.
- [40]. W. R. Jones Jr. and J. Ferrante, "Tribological Characteristics of Nitrogen ( $N^+$ ) Implanted Iron," ASLE Trans., 26 (1983) 351-359.
- [41]. I. L. Singer and R. A. Jeffries, "Effects of Implantation Energy and Carbon Concentration on the Friction and Wear of Titanium Implanted Steel," Appl. Phys. Lett., 43 (10) (1983) 925.
- [42]. C. A. Dos Santos, M. Behar, J. P. De Souza and I. J. R. Baumvol, "Composition and Thermal Evolution of Nitrogen Implanted Steels," Nucl. Instrum. Meth., 209/210 (1983) 907-912.
- [43]. B. Rauschenbach and A. Kolitsch, "Formation of Compounds by Nitrogen Ion Implantation in Iron," Phys. Status Solidi, A 80 (1983) 211.
- [44]. A. Kolitsch, B. Rauschenbach and E. Richter, "Formation of Compositions by Implantation in Iron," Radiat. Eff. Lett., 76 (1983) 193.
- [45]. T. Barnavon, J. Tousset, S. Fayeulle, P. Guiraldenq, D. Treheux and M. Robelt, "Distribution of Nitrogen as a Function of Fluence," Radiat. Eff., 77 (1983) 249.
- [46]. E. Ramous, G. Principi, L. Giordano, S. L. Russo and C. Tosello, "Thermal Effect of Nitrogen Implantation on High Carbon Steels," Thin Solid Films, 102 (1983) 97.
- [47]. U. Ebersbach, F. Henny, U. Winckler, G. Reisse and C. Weissmantel, "Ion Beam Nitriding of High Purity Iron Surfaces," Thin Solid Films, 112 (1984) 29.
- [48]. I. L. Singer, "Tribomechanical Properties of Ion Implanted Metals," Mat. Res. Soc. Symp. Proc., 27 (1984) 585-595.
- [49]. I. L. Singer and R. A. Jeffries, "Friction, Wear and Deformation of Soft Steels Implanted with Ti and N," Mat. Res. Soc. Symp. Proc., 27 (1984) 667-672.
- [50]. W. C. Oliver, R. Hutchings and J. B. Pethica, "The Wear Behavior of Nitrogen-Implanted Metals," Met. Trans., 15A (1984) 2221-2229.

- [51]. F. M. Kustas, M. S. Misra and P. Sioshansi, "Effect of Ion Implantation on the Rolling Contact Fatigue of 440C Stainless Steel," Mat. Res. Soc. Symp. Proc., 27 (1984) 685-690.
- [52]. I. L. Singer, "Surface Analysis, Ion Implantation and Tribological Processes Affecting Steels," Appl. Surf. Sci., 18 (1984) 28-62.
- [53]. H. Dimigen, K. Kobs, R. Leutenecker, H., Ryssel and P. Eichinger, "Wear Resistance of Nitrogen Implanted Steels," Mat. Sci. Engr., 69 (1985) 181-190.
- [54]. B. L. Doyle, D. M. Follstaedt, S. T. Picraux, F. G. Yost, L. E. Pope and J. A. Knapp, "Nuclear Microprobe Analysis of Wear Tracks on  $^{14}\text{N}$ -Implanted Steels," Nucl. Instrum. Meth. Phys. Res., B7/8 (1985) 166-170.
- [55]. H. G. Feller, R. Kingler and W. Benecke, "Tribo-Enhanced Diffusion of Nitrogen Implanted into Steel," Mat. Sci. Engr., 69 (1985) 173-180.
- [56]. J. K. Hirvonen, "Summary Abstract: Nitrogen Ion Implantation for Wear Applications: A Review," J. Vac. Sci. Technol. A3 (1985) 2691-2692.
- [57]. G. K. Hubler, and F. A. Smidt, "Application of Ion Implantation to Wear Protection of Materials," Nucl. Instrum. Meth. Phys. Res., B7/8 (1985) 151-157.
- [58]. J. Hirvonen and A. Anttila, "Annealing Behavior of Implanted Nitrogen in AISI 316 Stainless Steel," Appl. Phys. Lett., 46 (1985) 835-836.
- [59]. C. G. Dodd, G. P. Meeker, S. M. Baumann, J. C. Norberg and K. O. Legg, "Surface Microanalytical Studies of Nitrogen Ion-Implanted Steel," Nucl. Instrum. Meth. Phys. Res., B7/8 (1985) 219-227.
- [60]. J. L. Whitton, G. T. Ewan, M. M. Ferguson, T. Laursen, I. V. Mitchell, H. H. Plattner, M. L. Swanson, A. V. Drigo, G. Celotti and W. A. Grant, "Chromium Nitride and Martensite Formation in Nitrogen-implanted Single-crystal Stainless Steel," Mat. Sci. Engr., 69 (1985) 111-116.
- [61]. D. C. Kothari, M. R. Nair, A. A. Rangwala, K. B. Lai, P. D. Prabhawalkar and P. M. Raole, "XPS Studies at Various Temperatures of Nitrogen Implanted 304 Stainless Steel," Nucl. Instrum. Meth. Phys. Res., B7/8 (1985) 235-241.
- [62]. S. Fayeulle, D. Treheux and C. Esnouf, "TEM Characterization of A Nitrogen Implanted Austenitic Stainless Steel," App. Surf. Sci., 25 (1986) 288-304.
- [63]. A. Cavalleri, L. Guzman, P. M. Ossi and I. Rossi, "On the Wear Behavior of Nitrogen Implanted 304 Stainless Steel," Scripta Metallurgica, 20 (1986) 37-42.

- [64]. F. M. Kustas, M. S. Misra and W. T. Tack, "Ion Implantation of Ti and C in 440C Steel for Enhanced Resistance to Lubricated Sliding Wear," J. Vac. Sci. Technol., A4 (1986) 2885-2891.
- [65]. S. Fayeulle, "Tribological Behavior of Nitrogen-Implanted Materials," Wear, 107 (1986) 61-70.
- [66]. J.-P. Hirvonen and J. W. Mayer, "Fretting Wear of Nitrogen-Implanted AISI 304 Stainless Steel," Materials Letters, 4 (1986) 404-408.
- [67]. S. Shrivastava, A. Jain, A. Sethuramiah, V. D. Vankar and K. L. Chopra, "Wear Behavior of Nitrogen Implanted Stainless Steel," Nucl. Instrum. Meth. Phys. Res., B21 (1987) 591-594.
- [68]. L. O. Daniels, and P. J. Wilbur, "Effects of Nitrogen Ion Implantation on Load-Bearing Capacity and Adhesive Wear Behavior in Steels," Nucl. Instrum. and Meth. Phys. Res., B19/20 (1987) 221-226.
- [69]. S. Fayeulle, "TEM Microstructural Study of the Friction and Wear Behavior of a Nitrogen Implanted Austenitic Stainless Steel," in Wear of Materials 1987, edited by K.C. Ludema, ASME, New York, (1987) 13-22.
- [70]. E. B. Hale, R. Reibold and R. A. Kohser, "Nitrogen Implantation of Steels: A Treatment which can Initiate Sustained Oxidative Wear," Mater. Sci. Engr., 90 (1987) 273-80.
- [71]. J. Korychi, A. Dygo, R. Pietrak, A. Turos, G. Gawlik and J. Jagielski, "Relocation of Nitrogen Implanted into Steel due to Tribological Processes," Nucl. Instrum. and Meth. Phys. Res., B19/20 (1987) 177-179.
- [72]. J. T. A. Pollock, R. A. Clissold, P.J. Paterson and C. J. Veitch, "Nitrogen Implanted Steels-Aspects of Oxidation and Diffusion during Wear," Nucl. Instrum. and Meth. Phys. Res., B19/20 (1987) 263-267.
- [73]. S. Fayeulle and D. Treheux, "Friction and Wear of a Nitrogen Implanted Austenitic Stainless Steel," Nucl. Instrum. Meth. Phys. Res., B19/20 (1987) 216-220.
- [74]. S. Shrivastava, R. D. Tarey, A. Jain and K. L. Chopra, "Surface Modification in Nitrogen-Ion-Implanted Stainless Steel," Thin Solid Films, 163 (1988) 359-363.
- [75]. S. Fayeulle, "Ion Implantation in Stainless Steels: Microstructures and Mechanical Properties," Ion Implantation 1988, ed. by F. H. Wohlbiel, Trans. Tech. Pub., Switzerland, (1988) 327-358.
- [76]. G. Wagner, R. Leutenecker, T. Louis and U. Gonser, "CEMS Study of a Nitrogen Implanted CrNi18.9 Steel," Hyperfine Interactions, 42 (1988) 1017-1020.



- [77]. F. M. Kustas, M. S. Misra and D. L. Williamson, "Microstructural Characterization of Nitrogen Implanted 440C Steel," Nucl. Instrum. Meth. Phys. Res., B31 (1988) 393-401.
- [78]. M. R. Nair, S. Venkatraman, D. C. Kothari, K. B. Lal and R. Roman, "Pitting and EPR Studies of Ion Implanted Plain and Sensitized 304 Stainless Steel," Nucl. Instrum. Meth. Phys. Res., B34 (1988) 53-61.
- [79]. L. Palmetshofer, J. Faderl and F. Lehner, "Dry Wear Behavior of Boron-and Nitrogen-implanted Steels," Mat. Sci. Engr., A114 (1989) 173-178.
- [80]. T. Fujihana, Y. Okabe and I. Masaya, "The Relationship between Crystal Structure and Hardness of Nitrogen Implanted Iron Surface Layers," Mat. Res. Soc. Symp. Proc., 128 (1989) 415-420.
- [81]. Z. A. Iskanderova, T. D. Radjabov, G. R. Rokhimova, F. K. Tukfatullin and O. A. Glozman, "Influence of Some Bulk and Surface Processes on Strengthening and Wear Resistance Under Ion Implantation," Nucl. Instrum. Meth. Phys. Res., B42 (1989) 193-204.
- [82]. R. Wei, P. J. Wilbur, W. S. Sampath, D. L. Williamson, Y. Qu and L. Wang "Tribological Studies of Ion-Implanted Steel Constituents Using an Oscillating Pin-on-Disc Wear Tester," J. Trib., 112 (1990) 27-34.
- [83]. J. R. Conrad and J. L. Radtke, "Plasma Source Ion-Implantation Technique for Surface Modification of Materials," J. Appl. Phys., 62 (11) (1987) 4591.
- [84]. P. J. Wilbur and L. O. Daniels, "The Development and Application of Ion Implanter Based on Ion Thruster Technology," Vacuum, 36 (1986) 5-9.
- [85]. W. S. Sampath, R. Wei and P. J. Wilbur, "Ultrahigh Current Density Ion Implantation," J. of Metals, 39 (1987) 17-19.
- [86]. Z. Y. Yang, M. G. S. Naylor and D. A. Rigney, "Sliding Wear of 304 and 310 Stainless Steels," Wear, 105 (1985) 73-86.
- [87]. I. L. Singer, R. G. Vardiman and R. N. Bolster, "Polishing Wear Resistance of Ion-Implanted 304 Steel," J. Mater. Res., 3 (1988) 1134-1143.
- [88]. R. Leutenecker, "Phase Transformations of a Nitrogen Implanted Austenitic Stainless Steel," Mat. Sci. Engr. (in press).
- [89]. G. Longworth and R. Atkinson, "The Use of Conversion Electron Mössbauer Spectroscopy to Study Ion Implanted Alloys and Archaeological Materials," in Mössbauer Spectroscopy and its Chemical Application, edited by J. G. Stevens and G. K. Shenoy, Published by ACS, Washington DC, (1981) 101-116.

- [90]. S. R. Shepard and N. P. Suh, "The Effects of Ion Implantation on Friction and Wear of Metals," J. Lubr. Technol., 104 (1982) 29-38.
- [91]. P. D. Goode, A. T. Peacock and J. Asher, "A Study of the Wear Behavior of Ion Implanted Pure Iron," Nucl. Instrum. Meth., 209/210 (1983) 925.
- [92]. S. M. Lim and M. F. Ashby, "Wear Mechanism Maps," Acta. Metall., 35 (1987) 1-24.
- [93]. J. A. Kiek, G. W. Egerton and B. D. Sartwell, "Wear and Friction of Nitrogen Ion Implanted Steel," J. Lubric. Technol., 105 (1983) 239.
- [94]. M. Carbucicchio and L. Bardani, "Surface Mössbauer Analysis of 38NCd4 Steel Ion Implanted with Nitrogen," J. Appl. Phys., 52 (7) (1981) 4589.
- [95]. E. Johnson, A. Johansen, L. Sarholt-Kristensen and L. Graabaek, "Mössbauer and TEM Study of Martensitic Transformations in Ion Implanted 17/7 Stainless Steel," Nucl. Instrum. Meth. Phys. Res., B19/20 (1987) 171.
- [96]. D. L. Williamson, Y. Qu, R. Wei, W. S. Sampath and P. J. Wilbur, "Tribology and Mössbauer Studies of Ion-Implanted Iron," Matr. Res. Soc. Symp. Proc., 128 (1989) 409-414.
- [97]. Y. Qu, "Mössbauer and Tribological Studies of Ion-Implanted Iron," M. S. Thesis, Phys. Dept., Colorado School of Mines, August, 1988.
- [98]. J. Lindhard, M. Scharff and H. E. Schiott, Mat. Fys. Medd. Dan. Vid. Selsk., 33 (14) (1963).
- [99]. G. Terwagne and M. Piette, "Temperature and Dose Dependences of Nitrogen Implantation into Iron," Mat. Sci. Engr., B2 (1989) 195.
- [100]. N. P. Suh, "Update on the Delamination Theory of Wear," in Fundamentals of friction and Wear of Materials, ed. by D. A. Regney, American Society for Metals, (1980) 43.
- [101]. D. L. Williamson, L. Wang, R. Wei and P. J. Wilbur, "Solid Solution Strengthening of Stainless Steel Surface Layers by Rapid, High-Dose, Elevated Temperature Nitrogen Ion Implantation" (to be published).
- [102]. L. Wang, "Mössbauer and Tribological Studies of Nitrogen Implanted Stainless Steels Austenitic," M. S. Thesis, Phys. Dept., Colorado School of Mines, August, 1989.
- [103]. J. F. Archard and W. Hirst, "The Wear of Metals under Unlubricated Conditions," Proc. Royal Soc., London, A236 (1956) 397.

- [104]. A. D. Sarkar, Friction and Wear, Academic Press, London, 1980.
- [105]. E. Werner, "Solid Solution and Grain Size Hardening of Nitrogen-Alloyed Austenitic Steels," Mat. Sci. Engr., 101A (1988) 93.

